SCATTERING MATRIX ELEMENTS FOR THE NONADIABATIC COLLISION

$$B\left({}^{2}P_{j_a}\right)+H_2\left({}^{1}\Sigma_g^{+},\nu,j\right)\leftrightarrow B\left({}^{2}P_{j_a'}\right)+H_2\left({}^{1}\Sigma_g^{+},\nu',j'\right)$$

DISSERTATION

Luke A. Barger, Captain, USAF
AFIT/DS/ENP/10-S02

DEPARTMENT OF THE AIR FORCE
AIR UNIVERSITY

Air Force Institute of Technology

Wright-Patterson Air Force Base, Ohio

Report Documentation Page	*Form Approved* *OMB No. 0704-0188*

1. REPORT DATE **01 DEC 2010**	2. REPORT TYPE	3. DATES COVERED **00-00-2010 to 00-00-2010**

4. TITLE AND SUBTITLE **SCATTERING MATRIX ELEMENTS FOR THE**	5a. CONTRACT NUMBER 5b. GRANT NUMBER 5c. PROGRAM ELEMENT NUMBER
6. AUTHOR(S)	5d. PROJECT NUMBER 5e. TASK NUMBER 5f. WORK UNIT NUMBER
7. PERFORMING ORGANIZATION NAME(S) AND ADDRESS(ES) **Air Force Institute of Technology,2950 Hobson Way,WPAFB,OH,45433-7765**	8. PERFORMING ORGANIZATION REPORT NUMBER
9. SPONSORING/MONITORING AGENCY NAME(S) AND ADDRESS(ES)	10. SPONSOR/MONITOR’S ACRONYM(S) 11. SPONSOR/MONITOR’S REPORT NUMBER(S)

12. DISTRIBUTION/AVAILABILITY STATEMENT

Approved for public release; distribution unlimited

13. SUPPLEMENTARY NOTES

14. ABSTRACT

Scattering matrix elements are calculated for the nonadiabatic inelastic collision . This calculation utilizes the effective potential energy surfaces for this collision generated by Garvin along with a correction to the asymptotic H2 potential. Wavepackets are propagated on these surfaces using a split-operator propagator. This propagation yields correlation functions between reactant and product M?ller states which are used to calculate the scattering matrix elements with the channel packet method. These scattering matrix elements represent probability amplitudes for the collision to result in changes to the electronic fine structure and to the rotational and vibrational eigenstates of the H2 molecule over a range of energies, and are presented, discussed and compared to previous work in which the hydrogen bond length was fixed at its equilibrium value. A method for approximating probability for the reaction B+H2-BH+H as a function of collisional energy is presented.

15. SUBJECT TERMS

16. SECURITY CLASSIFICATION OF:			17. LIMITATION OF ABSTRACT	18. NUMBER OF PAGES	19a. NAME OF RESPONSIBLE PERSON
a. REPORT	b. ABSTRACT	c. THIS PAGE			
unclassified	**unclassified**	**unclassified**	**Same as Report (SAR)**	**132**	

AFIT/DS/ENP/10-S02

SCATTERING MATRIX ELEMENTS FOR THE NONADIABATIC COLLISION $B\left({}^{2}P_{j_a}\right)+H_2\left({}^{1}\Sigma_g^+,\nu,j\right)\leftrightarrow B\left({}^{2}P_{j_a'}\right)+H_2\left({}^{1}\Sigma_g^+,\nu',j'\right)$

DISSERTATION

Presented to the Faculty

Graduate School of Engineering and Management

Air Force Institute of Technology

Air University

Air Education and Training Command

In Partial Fulfillment of the Requirements for the

Degree of Doctor of Philosophy

Luke A. Barger, BSE, MS

Captain, USAF

December 2010

APPROVED FOR PUBLIC RELEASE; DISTRIBUTION UNLIMITED

AFIT/DS/ENP/10-S02

SCATTERING MATRIX ELEMENTS FOR THE NONADIABATIC COLLISION

$$B\left({}^{2}P_{j_a}\right)+H_2\left({}^{1}\Sigma_g^{+},\nu,j\right)\leftrightarrow B\left({}^{2}P_{j_a'}\right)+H_2\left({}^{1}\Sigma_g^{+},\nu',j'\right)$$

Luke A. Barger, BSE, MS
Captain, USAF

Approved:

_____**Signed**_________________________ ____________
David E. Weeks, PhD (Chairman) Date

_____ **Signed** _________________________ ____________
Kevin C. Gross, PhD (Member) Date

_____ **Signed** _________________________ ____________
Michael J. Havrilla, PhD (Member) Date

Accepted:

_____ **Signed** _________________________ ____________
M. U. Thomas Date
Dean, Graduate School of
Engineering and Management

AFIT/DS/ENP/10-S02

Abstract

Scattering matrix elements are calculated for the nonadiabatic inelastic collision $B\left({}^2P_{j_a}\right)+H_2\left({}^1\Sigma_g^+,\nu,j\right)\leftrightarrow B\left({}^2P_{j_a'}\right)+H_2\left({}^1\Sigma_g^+,\nu',j'\right)$. This calculation utilizes the effective potential energy surfaces for this collision generated by Garvin [1] along with a correction to the asymptotic H_2 potential. Wavepackets are propagated on these surfaces using a split-operator propagator. This propagation yields correlation functions between reactant and product Møller states which are used to calculate the scattering matrix elements with the channel packet method [2]. These scattering matrix elements represent probability amplitudes for the collision to result in changes to the electronic fine structure and to the rotational and vibrational eigenstates of the H_2 molecule over a range of energies, and are presented and discussed. They are also compared to previous work in which the hydrogen bond length was fixed at its equilibrium value. A method for approximating probability for the reaction $B+H_2\rightarrow BH+H$ as a function of collisional energy is presented.

To my family

Acknowledgements

Dr. David Weeks contributed immeasurably to this work both in inspiring wonder at the physical universe and in guidance of how to manage a research project. For both of those things, the arcane and the mundane, I am grateful. I also wish to thank Dr. Kevin Gross and Dr. Michael Havrilla for their service on my committee.

Luke A. Barger

Table of Contents

Page

Abstract iv

Acknowledgements vi

List of Figures ix

List of Tables xiii

I. Introduction 1

The $B+H_2$ System 1

Statement of Objectives 3

II. Theory 4

Schrödinger's Equations 4

The Hamiltonian 5

The Born-Oppenheimer Approximation 6

The Asymptotic Representation 12

The Effective Diabatic Potential Energy Surfaces for $B+H_2$ 21

Structure of the Effective Diabatic Potential Energy Matrix 22

The Split-Operator Propagator 24

Scattering Theory 31

The Channel Packet Method 37

Absorbing Boundary Conditions 42

Other Practical Grid Considerations 44

III. Results and Discussion 49

The $B+H_2$ Effective Potential Energy Surfaces 49

Propagation 72

The Scattering Matrix Elements 91

Comparison to One Dimensional Calculation 106

IV. Conclusion 111

  Summary of Key Contributions....113
  Recommendations for Future Work....114

Bibliography....115

Vita....117

List of Figures

Figure Page

1. DPAL Transition for Rubidium 2

2. Space and Body Fixed Coordinate System for B+H_2 13

3. Angular Momentum Coupling Scheme 15

4. Structure of the $J = 1/2$ Block of the Effective Potential Energy Matrix 22

5. Diabatic Effective Potential Energy Surface $\left\langle \begin{matrix} 0 & \frac{1}{2} \\ 0, & \frac{1}{2} \end{matrix} \right| V_{eff}^{D}\left(r,R\right) \left| \begin{matrix} 0 & \frac{1}{2} \\ 0, & \frac{1}{2} \end{matrix} \right\rangle$ 50

6. Diabatic Effective Potential Energy Surface $\left\langle \begin{matrix} 0 & \frac{1}{2} \\ 0, & \frac{1}{2} \end{matrix} \right| V_{eff}^{D}\left(r,R\right) \left| \begin{matrix} 0 & \frac{1}{2} \\ 0, & \frac{1}{2} \end{matrix} \right\rangle$ Contour Plot 51

7. Diabatic Effective Potential Energy Surface $\left\langle \begin{matrix} 2 & \frac{3}{2} \\ 0, & \frac{1}{2} \end{matrix} \right| V_{eff}^{D}\left(r,R\right) \left| \begin{matrix} 2 & \frac{3}{2} \\ 0, & \frac{1}{2} \end{matrix} \right\rangle$ 52

8. Diabatic Effective Potential Energy Surface $\left\langle \begin{matrix} 2 & \frac{3}{2} \\ 0, & \frac{1}{2} \end{matrix} \right| V_{eff}^{D}\left(r,R\right) \left| \begin{matrix} 2 & \frac{3}{2} \\ 0, & \frac{1}{2} \end{matrix} \right\rangle$ Contour Plot 53

9. The Coupling Surface $\left\langle \begin{matrix} 0 & \frac{1}{2} \\ 0, & \frac{1}{2} \end{matrix} \right| V_{eff}^{D}\left(r,R\right) \left| \begin{matrix} 0 & \frac{3}{2} \\ 0, & \frac{1}{2} \end{matrix} \right\rangle$ 54

10. The Coupling Surface $\left\langle \begin{matrix} 0 & \frac{1}{2} \\ 0, & \frac{1}{2} \end{matrix} \right| V_{eff}^{D}\left(r,R\right) \left| \begin{matrix} 0 & \frac{3}{2} \\ 0, & \frac{1}{2} \end{matrix} \right\rangle$ Contour Plot 55

11. The Coupling Surface $\left\langle \begin{matrix} 0 & \frac{3}{2} \\ 0, & \frac{1}{2} \end{matrix} \right| V_{eff}^{D}\left(r,R\right) \left| \begin{matrix} 1 & \frac{1}{2} \\ 1, & -\frac{1}{2} \end{matrix} \right\rangle$ 56

12. The Coupling Surface $\left\langle \begin{matrix} 0 & \frac{3}{2} \\ 0, & \frac{1}{2} \end{matrix} \right| V_{eff}^{D}\left(r,R\right) \left| \begin{matrix} 1 & \frac{1}{2} \\ 1, & -\frac{1}{2} \end{matrix} \right\rangle$ Contour Plot 57

13. First Adiabatic Surface with Basis Size $n = 2$ Contour Plot 59

14. First Adiabatic Surface with Basis Size $n = 8$ Contour Plot 60

15. First Adiabatic Surface with Basis Size $n = 14$ Contour Plot 61

16. First Adiabatic Surface with Basis Size $n = 20$ Contour Plot 62

17. First Adiabatic Surface with Basis Size $n = 26$ Contour Plot 62

18. First Adiabatic Surface with Basis Size $n = 32$ Contour Plot 63

19. Diabatic Potential Energy Surfaces Cross-section at r_{eq} 64

20. Correction to Asymptotic H_2 Potential 65

21. Cross-sections of the Diabatic PESs for $j = 0, 2, 4$ at Limit of Large R 66

22. Detail of Diabatic PES Cross-sections for $j = 0, 2, 4$ Around $r = 1.402$ au Showing Spin-Orbit Splitting 66

23. Cross-section of First Diabatic PES with First Two Vibrational Eigenstates 70

24. Initial Wavepacket on the Ground State at $t = 0$ au 73

25. P_R Cross-section of Initial Wavepacket 75

26. Barrier to Reaction in Lowest Adiabatic Potential Energy Surface 76

27. Wavepacket on the First Two Surfaces at $t = 0$ au 82

28. Wavepacket on the First Two Surfaces at $t = 5000$ au 83

29. Wavepacket on the First Two Surfaces at $t = 12500$ au 84

30. Wavepacket on the First Two Surfaces at $t = 20000$ au 85

31. Wavepacket on the First Two Surfaces at $t = 27500$ au 86

32. Wavepacket on the First Two Surfaces at $t = 35000$ au 87

33. Wavepacket on the First Two Surfaces at $t = 42500$ au 88

34. Wavepacket on the First Two Surfaces at $t = 50000$ au 89

35. Wavepacket on the First Two Surfaces at $t = 65000$ au 90

36. Probability to Transition from $\left|\begin{matrix}0 & \tfrac{1}{2}\\ 0 & \tfrac{1}{2}\end{matrix}, 0\right\rangle$ to $\left|\begin{matrix}0 & \tfrac{1}{2}\\ 0 & \tfrac{1}{2}\end{matrix}, 0\right\rangle$ and $\left|\begin{matrix}0 & \tfrac{3}{2}\\ 0 & \tfrac{1}{2}\end{matrix}, 0\right\rangle$ 92

37. Probability to Transition from $\left|\begin{matrix}0 & \frac{1}{2} \\ 0 & \frac{1}{2}\end{matrix},0\right\rangle$ to the Six Allowed $\left|\begin{matrix}2 & j_a \\ j & \omega\end{matrix},0\right\rangle$ States........ 92

38. Probability to Transition from $\left|\begin{matrix}0 & \frac{1}{2} \\ 0 & \frac{1}{2}\end{matrix},0\right\rangle$ to the Six Allowed $\left|\begin{matrix}4 & j_a \\ j & \omega\end{matrix},0\right\rangle$ States........ 93

39. Probability to Transition from $\left|\begin{matrix}0 & \frac{1}{2} \\ 0 & \frac{1}{2}\end{matrix},0\right\rangle$ to the Six Allowed $\left|\begin{matrix}6 & j_a \\ j & \omega\end{matrix},0\right\rangle$ States........ 93

40. Probability to Transition from $\left|\begin{matrix}0 & \frac{1}{2} \\ 0 & \frac{1}{2}\end{matrix},0\right\rangle$ to the Six Allowed $\left|\begin{matrix}8 & j_a \\ j & \omega\end{matrix},0\right\rangle$ States........ 94

41. Probability to Transition from $\left|\begin{matrix}0 & \frac{1}{2} \\ 0 & \frac{1}{2}\end{matrix},0\right\rangle$ to the Six Allowed $\left|\begin{matrix}10 & j_a \\ j & \omega\end{matrix},0\right\rangle$ States 94

42. Comparison of Reflection Probability for $j_{\max} = 0,2,4,6,8,10$ 96

43. Comparison of Fine Structure Probability for $j_{\max} = 0,2,4,6,8,10$ 97

44. Sum of Scattering Matrix Elements.. 98

45. Probability to React to Form *BH+H*.. 99

46. Probability to Transition from $\left|\begin{matrix}0 & \frac{1}{2} \\ 0 & \frac{1}{2}\end{matrix},0\right\rangle$ to $\left|\begin{matrix}0 & \frac{1}{2} \\ 0 & \frac{1}{2}\end{matrix},1\right\rangle$ and $\left|\begin{matrix}0 & \frac{3}{2} \\ 0 & \frac{1}{2}\end{matrix},1\right\rangle$ 100

47. Probability to Transition from $\left|\begin{matrix}0 & \frac{1}{2} \\ 0 & \frac{1}{2}\end{matrix},0\right\rangle$ to the Six Allowed $\left|\begin{matrix}2 & j_a \\ j & \omega\end{matrix},1\right\rangle$ States 100

48. Probability to Transition from $\left|\begin{matrix}0 & \frac{1}{2} \\ 0 & \frac{1}{2}\end{matrix},0\right\rangle$ to the Six Allowed $\left|\begin{matrix}4 & j_a \\ j & \omega\end{matrix},1\right\rangle$ States 101

49. Probability to Transition from $\left|\begin{matrix}0 & \frac{1}{2} \\ 0 & \frac{1}{2}\end{matrix},0\right\rangle$ to the Six Allowed $\left|\begin{matrix}6 & j_a \\ j & \omega\end{matrix},1\right\rangle$ States 101

50. Cross-section of First Three Adiabatic Surfaces at $r = 1.402$ au Showing Shallow Wells 102

51. Detail of Feshbach Resonances in Reflection Scattering Matrix Element 103

52. Feshbach Resonance Detail for Transition from $\left|\begin{matrix}0 & \frac{1}{2} \\ 0 & \frac{1}{2}\end{matrix},0\right\rangle$ to $\left|\begin{matrix}0 & \frac{1}{2} \\ 0 & \frac{1}{2}\end{matrix},1\right\rangle$ and $\left|\begin{matrix}0 & \frac{3}{2} \\ 0 & \frac{1}{2}\end{matrix},1\right\rangle$ 104

53. Cross-section of First Three Adiabatic Surfaces at $R = 7$ au 105

54. Detail of Feshbach Resonances for $T_{\max} = 2,3,4\ \times 10^6$ au 106

55. 1-D and 2-D Results for the Transition from $\left|\begin{matrix}0 & \frac{1}{2} \\ 0 & \frac{1}{2}\end{matrix},0\right\rangle$ to $\left|\begin{matrix}0 & \frac{1}{2} \\ 0 & \frac{1}{2}\end{matrix},0\right\rangle$ 107

56. 1-D and 2-D Results for the Transition from $\left|\begin{matrix}0 & \frac{1}{2} \\ 0 & \frac{1}{2}\end{matrix},0\right\rangle$ to $\left|\begin{matrix}0 & \frac{3}{2} \\ 0 & \frac{1}{2}\end{matrix},0\right\rangle$ 108

57. 1-D and 2-D Feshbach Resonances for the Transition from $\left|\begin{matrix}0 & \frac{1}{2} \\ 0 & \frac{1}{2}\end{matrix},0\right\rangle$ to $\left|\begin{matrix}0 & \frac{1}{2} \\ 0 & \frac{1}{2}\end{matrix},0\right\rangle$ 109

58. 1-D and 2-D Feshbach Resonances for the Transition from $\left|\begin{matrix}0 & \frac{1}{2} \\ 0 & \frac{1}{2}\end{matrix},0\right\rangle$ to $\left|\begin{matrix}0 & \frac{3}{2} \\ 0 & \frac{1}{2}\end{matrix},0\right\rangle$ 110

List of Tables

Table Page

1. Summary of Internal Energies …………………………………………………… 71

2. Propagation Parameters ……………………………………………...………...… 79

3. Summary of Steps for Calculating Scattering Matrix Elements ……..…………..... 112

SCATTERING MATRIX ELEMENTS FOR THE NONADIABATIC COLLISION

I. Introduction

The $B+H_2$ System

The $B+H_2$ system became of particular interest when boron was proposed as an energetic additive to solid molecular hydrogen (SMH) for use as a novel rocket propellant. Realization of this technology would require complete characterization of the chemical, physical, and transport properties of boron doped SMH [3]. These early studies prompted additional theoretical interest in the $B+H_2$ system. Specifically challenging, and hence interesting, is the unpaired electron in the $2p$ orbital of atomic boron. This electron creates a ${}^2P$ spectroscopic term consisting of three degenerate orbitals. When in proximity of a hydrogen molecule this degeneracy is slightly lifted resulting in three orbitals whose energy levels are very similar. As a result, the electronic eigenstates exhibit strong dependence of nuclear coordinates, causing the system to behave nonadiabatically [4]. Given the ${}^2P$ electronic character of the $B+H_2$ system [3] [5] [6] [7], it can also serve as an accessible means to understand other atomic systems that exhibit ${}^2P$ electronic behavior. Of particular interest is the insight the $B+H_2$ system lends to collisional de-excitation in the operation of diode-pumped alkali lasers

(DPALs). The Air Force is currently very interested in the development of DPAL systems.

During operation of a DPAL this electron is pumped to the ${}^2P_{3/2}$ states are collisionally de-excited to the ${}^2P_{1/2}$ states. This process is shown for rubidium [8]

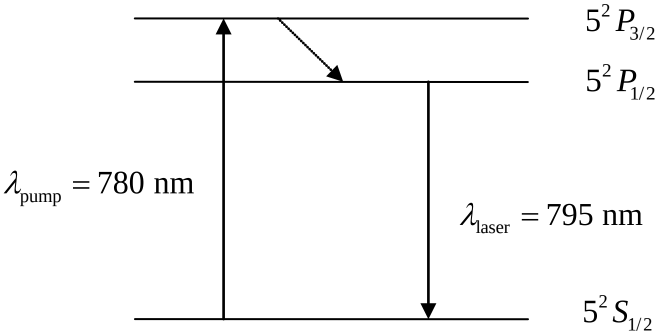

Figure 1. DPAL Transition for Rubidium

For practical operation, electron population excited to the ${}^2P_{3/2}$ level must transition to the ${}^2P_{1/2}$ level at a sufficient rate. Specifically it must be much faster than the ${}^2P$ spontaneous emission rate of $:\ 3\times10^{7}\ \text{sec}^{-1}$ [8]. Ground-state boron also has a ${}^2P$ spectroscopic term. Since it shares the same valence electron configuration with alkalis in the first excited state it will behave similarly. The fine-structure collisional de-excitation from ${}^2P_{3/2}$ to ${}^2P_{1/2}$ is among the transitions examined when studying the collision of boron with molecular hydrogen and will provide insight into the behavior of alkali atoms in DPAL systems.

Statement of Objectives

This work will investigate the nonadiabatic effects of the collision of a boron atom with molecular hydrogen, given by the equation

$$B\left({}^{2}P_{j_a}\right)+H_2\left({}^{1}\Sigma_g^{+},\nu,j\right)\leftrightarrow B\left({}^{2}P_{j_a^{'}}\right)+H_2\left({}^{1}\Sigma_g^{+},\nu^{'},j'\right) \qquad (1)$$

Effective potential energy surfaces for this interaction are provided by Garvin [1], extending initial *ab initio* calculations performed by Dr. David Yarkony at Johns Hopkins University.

By propagating wavepackets on these surfaces, scattering matrix elements can be obtained using the channel packet method [2]. These represent energy-resolved probability amplitudes for scattering from an incoming state to an outgoing state, both of which are selected prior to the calculation. As shown by eq. (1), the collision may involve changes to the hydrogen vibrational and/or rotational states and the fine-structure of the boron electronic state. The objectives of this research are to: 1) characterize the $B+H_2$ effective potential energy surfaces; 2) propagate wavepackets on these surfaces; and 3) compute $B+H_2$ scattering matrix elements and present analysis.

II. Theory

Schrödinger's Equations

Fundamental to much of quantum mechanics, and this research in particular, is determining the time-evolution of a system. The governing equation is the time-dependent Schrödinger equation

$$i\hbar\frac{\partial}{\partial t}\left|\psi\right\rangle = \hat{H}\left|\psi\right\rangle \tag{2}$$

where $\left|\psi\right\rangle$ is the wavefunction and $\hat{H}$ is the Hamiltonian.

The time-dependent Schrödinger equation is most easily solved when the wavefunction is chosen to be a superposition of eigenstates of the Hamiltonian

$$\left|\psi\right\rangle = \sum_i a_i\left|\phi_i\right\rangle \tag{3}$$

where the eigenstates $\left|\phi\right\rangle$ are solutions to the equation

$$\hat{H}\left|\phi\right\rangle = E\left|\phi\right\rangle \tag{4}$$

Eq. (4) is known as the time-independent Schrödinger equation. The eigenvalue E corresponding to each eigenstate is the energy of that eigenstate. The set of all eigenstates of the Hamiltonian is complete, allowing any wavefunction to be constructed as a superposition of eigenstates of the Hamiltonian. Solving the time-independent Schrödinger equation is often the first and most important step in understanding a quantum mechanical system.

The Hamiltonian

The Hamiltonian for a system is the sum of the kinetic and potential energy operators of the system,

$$\hat{H} = \hat{T} + \hat{V} \tag{5}$$

where $\hat{T}$ is the kinetic energy operator and $\hat{V}$ is the potential energy operator. If the system is made up of interacting nuclei and electrons, it may be represented as

$$\hat{H} = \hat{T}_N + \hat{T}_e + \hat{V}_{NN} + \hat{V}_{eN} + \hat{V}_{ee} \tag{6}$$

In eq. (6) the subscripts identify the particle types – *N* for nuclei and *e* for electrons. The kinetic energy operators are simply the sum of the kinetic energy operators of their respective particle type, while the potential operators are the sum of the Coulomb potentials for all the particles – among nuclei, between nuclei and electrons, and among electrons, respectively. If the system contains n_N nuclei and n_e electrons, the Hamiltonian is

$$\hat{H} = \sum_{\alpha=1}^{n_N} \frac{\hat{p}_\alpha^2}{2m_\alpha} + \sum_{i=1}^{n_e} \frac{\hat{p}_i^2}{2m_e} + \sum_{\alpha=1}^{n_N} \sum_{\beta>\alpha}^{n_N} \frac{Z_\alpha Z_\beta e^2}{\left|\hat{q}_\alpha - \hat{q}_\beta\right|} - \sum_{\alpha=1}^{n_N} \sum_{i=1}^{n_e} \frac{Z_\alpha e^2}{\left|\hat{q}_\alpha - \hat{q}_i\right|} + \sum_{i=1}^{n_e} \sum_{j>i}^{n_e} \frac{e^2}{\left|\hat{q}_i - \hat{q}_j\right|} \tag{7}$$

where $\hat{p}$ is the momentum operator, *m* is the mass of the particle, *Ze* is the charge of the particle (given by its atomic number multiplied by the charge of the electron), and $\hat{q}$ is the position operator of the particle. The Greek letters α and β index nuclei, while *i* and *j* index electrons.

The total number of terms in the Hamiltonian increases rapidly as the number of interacting particles increases. The $B + H_2$ system has 3 nuclei and 7 electrons, giving a total of 55 terms in the Hamiltonian. The time-independent Schrödinger equation for the

Hamiltonian given in eq. (7) cannot be solved analytically, prompting the use of approximations and numerical methods.

The Born-Oppenheimer Approximation

Since nuclei are much more massive than electrons, it is expected that they will move very slowly relative to the electrons' motion. The electrons move under the influence of nuclei which are approximately fixed in space. In turn, nuclei move under the influence of an average electron 'cloud'. This suggests an approximation for solving the molecular time-independent Schrödinger equation by separating nuclear and electronic motion.

The nuclei are fixed in place by setting their kinetic energy operators to zero in the Hamiltonian. The remaining terms are known as the electronic Hamiltonian.

$$H_{elec} = \sum_{i=1}^{n_e} \frac{\hat{p}_i^2}{2m_e} + \sum_{\alpha=1}^{n_N} \sum_{\beta>\alpha}^{n_N} \frac{Z_\alpha Z_\beta e^2}{\left|q_\alpha - q_\beta\right|} - \sum_{\alpha=1}^{n_N} \sum_{i=1}^{n_e} \frac{Z_\alpha e^2}{\left|q_\alpha - \hat{q}_i\right|} + \sum_{i=1}^{n_e} \sum_{j>i}^{n_e} \frac{e^2}{\left|\hat{q}_i - \hat{q}_j\right|} \tag{8}$$

In eq. (8) the nuclear coordinates are parameters rather than operators, and the second term $V_{NN}\left(q_N\right) = \sum_{\alpha=1}^{n_N} \sum_{\beta>\alpha}^{n_N} \frac{Z_\alpha Z_\beta e^2}{\left|q_\alpha - q_\beta\right|}$ is a constant for a given set of nuclear coordinates $q_N = \left\{q_1, q_2, ...\right\}$.

The electronic time-independent Schrödinger equation is

$$\hat{H}_{elec} \left| j\left(q_N\right)\right\rangle = E_{elec}^j\left(q_N\right) \left| j\left(q_N\right)\right\rangle \tag{9}$$

where both the electronic eigenstates $\left| j \right\rangle$ and their associated energy eigenvalues E_{elec}^j are explicitly shown to depend parametrically on the nuclear coordinates q_N. This equation may be solved using *ab initio* numerical techniques such as the Hartree-Fock approximation, configuration interaction or multi-configuration self-consistent field methods. These techniques are described by Szabo and Ostlund [9], and are generally applied through the use of mature software packages developed specifically for large quantum chemistry applications to yield E_{elec}^{j} over a range of nuclear coordinates. The result is a potential energy surface (PES) $E_{elec}^{j}\left(q_N\right)$, which has a dimensionality given by the number of nuclear degrees of freedom, as well as the associated electronic eigenstates $\left|j\left(q_N\right)\right\rangle$.

The set of electronic eigenstates is complete and the eigenstates of the full system $\left|\psi\right\rangle$ can therefore be represented in the basis of the electronic eigenstates.

$$\left|\psi\left(q_N\right)\right\rangle = \sum_j F_j\left(q_N\right)\left|j\left(q_N\right)\right\rangle \tag{10}$$

Substituting this into the full time-independent Schrödinger equation gives

$$\left(\hat{T}_N + \hat{H}_{elec}\right)\sum_j F_j\left(q_N\right)\left|j\left(q_N\right)\right\rangle = E\sum_j F_j\left(q_N\right)\left|j\left(q_N\right)\right\rangle \tag{11}$$

This expression is simplified by noting that E is a constant and the electron eigenstates are orthonormal. Multiplying from the left by $\left\langle i\left(q_N\right)\right|$ and integrating over electronic coordinates gives

$$\left\langle i\left(q_N\right)\right|\left(\hat{T}_N + \hat{H}_{elec}\right)\sum_j F_j\left(q_N\right)\left|j\left(q_N\right)\right\rangle = EF_i\left(q_N\right) \tag{12}$$

Additionally the electronic Hamiltonian does not operate on nuclear coordinates, allowing this to be simplified as

$$\left\langle i\left(q_N\right)\right|\hat{T}_N\sum_j F_j\left(q_N\right)\left|j\left(q_N\right)\right\rangle + \left\langle i\left(q_N\right)\right|\sum_j F_j\left(q_N\right)\hat{H}_{elec}\left|j\left(q_N\right)\right\rangle = EF_i\left(q_N\right)$$

$$\left\langle i\left(q_N\right)\right|\hat{T}_N\sum_j F_j\left(q_N\right)\left|j\left(q_N\right)\right\rangle + E_{elec}^{i}F_i\left(q_N\right) = EF_i\left(q_N\right) \tag{13}$$

where $\hat{H}_{elec}\left|j\left(q_N\right)\right\rangle = E_{elec}^{j}\left|j\left(q_N\right)\right\rangle$ and $\left\langle i\left(q_N\right)\right|\left.j\left(q_N\right)\right\rangle = \delta_{ij}$. The nuclear kinetic energy operator $\hat{T}_N$ does operate on nuclear coordinates. Expressing eq. (13) in the coordinate representation with $\left|j\right\rangle \to \phi_j$ and $\hat{T}_N \to \sum_\alpha -\frac{\hbar^2}{2m_\alpha}\nabla_{q_N}^2$ gives

$$-\frac{\hbar^2}{2}\sum_\alpha\sum_j\frac{1}{m_\alpha}\int\phi_i^*\left(q_N,q_e\right)\nabla_{q_N}^2F_j\left(q_N\right)\phi_j\left(q_N,q_e\right)dq_e + E_{elec}^{i}F_i\left(q_N\right) = EF_i\left(q_N\right) \tag{14}$$

The dependence of the various functions on nuclear coordinates q_N and electronic coordinates q_e is shown explicitly. The subscript $\nabla_{q_N}^2$ indicates which coordinates the derivatives are with respect to. Applying the product rule eq. (14) becomes

$$\begin{aligned}&-\frac{\hbar^2}{2}\sum_{\alpha,j}\frac{1}{m_\alpha}\Big\{\delta_{ij}\nabla_{q_N}^2 + 2\int\phi_i^*\left(q_N,q_e\right)\vec{\nabla}_{q_N}\phi_j\left(q_N,q_e\right)dq_e\cdot\vec{\nabla}_{q_N}\\&+\int\phi_i^*\left(q_N,q_e\right)\nabla_{q_N}^2\phi_j\left(q_N,q_e\right)dq_e\Big\}F_j\left(q_N\right)\\&=\left(E-E_{elec}^{i}\right)F_i\left(q_N\right)\end{aligned} \tag{15}$$

This expression is simplified by defining two terms. The first is a vector quantity known as the derivative coupling term (DCT):

$$\vec{\tau}_{ij} = \int\phi_i^*\left(q_N,q_e\right)\vec{\nabla}_{q_N}\phi_j\left(q_N,q_e\right)dq_e \tag{16}$$

The second is a scalar quantity known as the kinetic coupling term:

$$\kappa_{ij} = \frac{1}{2}\int\phi_i^*\left(q_N,q_e\right)\nabla_{q_N}^2\phi_j\left(q_N,q_e\right)dq_e \tag{17}$$

Using eqs. (16) and (17) gives

$$-\frac{\hbar^2}{2}\sum_\alpha\sum_j\frac{1}{m_\alpha}\left\{\delta_{ij}\nabla_{q_N}^2 + 2\vec{\tau}_{ij}\cdot\vec{\nabla}_{q_N} + 2\kappa_{ij}\right\}F_j\left(q_N\right) = \left(E-E_{elec}^{i}\right)F_i\left(q_N\right) \tag{18}$$

When the derivative and kinetic coupling terms are small they can be ignored, and the system is said to behave adiabatically. This is the Born-Oppenheimer approximation. Eliminating those terms from eq. (18) gives the simpler form

$$\left\{-\frac{\hbar^2}{2}\sum_{\alpha}\frac{1}{m_{\alpha}}\nabla_{q_N}^2+E_{elec}^i\right\}F_i\left(q_N\right)=EF_i\left(q_N\right) \tag{19}$$

Here eq. (19) has been cast in the form of the time-independent Schrödinger equation where $F_i\left(q_N\right)$ is interpreted as the nuclear wavefunction. This wavefunction only depends on one adiabatic PES, E_{elec}^i. If the derivative and kinetic coupling terms cannot be ignored, the system is said to behave nonadiabatically, and the coupling in eq. (18) cannot be neglected. For this reason the derivative and kinetic coupling terms are collectively known as nonadiabatic coupling terms (NACTs).

The Adiabatic to Diabatic Transformation

Many polyatomic systems behave nonadiabatically [10], that is, they contain nonnegligible NACTs when expressed in the adiabatic representation as in eq. (18). The clearest predictor of nonadiabatic behavior is when the adiabatic electronic PESs E_{elec}^i are close together [11]. This is seen in the generalized Hellman-Feynman theorem which gives the derivative coupling terms in the adiabatic representation [12]:

$$\vec{\tau}_{ij}=\frac{\left\langle i\left(q_N\right)\middle|\vec{\nabla}_{q_N}\hat{H}_{elec}\middle|j\left(q_N\right)\right\rangle}{E_{elec}^j-E_{elec}^i} \tag{20}$$

The $B+H_2$ system is an example of a system with nonnegligible NACTs. The unpaired $2p$ electron in ground-state boron gives rise to a ^2P spectroscopic term involving three degenerate atomic orbitals. This degeneracy is slightly lifted when in the presence of a hydrogen molecule, but they remain energetically very close. Eq. (20) predicts that these three orbitals will be strongly coupled to each other, but only weakly coupled to the other atomic orbitals from when they are separated energetically.

The problem in solving the coupled set of equations on the adiabatic basis is handled by transforming to the diabatic basis in which the NACTs are negligible [13]. This is accomplished via a unitary transformation and results in a form of the time-independent Schrödinger equation where the wavefunction is coupled by the diabatic PES.

In the interest of computational efficiency, the basis of electronic eigenstates is truncated to only include those states that are strongly coupled. These are the three adiabatic PESs corresponding to the three ${}^2P$ states. These PESs are labeled $V_{1^2A'}$, $V_{2^2A'}$ and $V_{A''}$, where the subscripts are inherited from the C_s symmetry displayed by the $B+H_2$ system [1]. For this calculation the $V_{1^2A'}$, $V_{2^2A'}$ and $V_{A''}$ PESs were calculated by Dr. David Yarkony using a multi-reference configuration interaction calculation.

The adiabatic time-independent Schrödinger equation (18) is represented in the truncated basis consisting of these three states.

$$\begin{aligned}&\left\{-\frac{\hbar^2}{2}\begin{pmatrix}\sum_\alpha \frac{\nabla^2_{q_N}}{m_\alpha} & 0 & 0\\ 0 & \sum_\alpha \frac{\nabla^2_{q_N}}{m_\alpha} & 0\\ 0 & 0 & \sum_\alpha \frac{\nabla^2_{q_N}}{m_\alpha}\end{pmatrix} - \begin{pmatrix}0 & \sum_\alpha \frac{1}{m_\alpha}\left[\vec{\tau}^{A}_{12}\cdot\vec{\nabla}_{q_N}+\kappa^{A}_{12}\right] & 0\\ \sum_\alpha \frac{1}{m_\alpha}\left[\vec{\tau}^{A}_{12}\cdot\vec{\nabla}_{q_N}+\kappa^{A}_{12}\right] & 0 & 0\\ 0 & 0 & 0\end{pmatrix}\right. \qquad (21)\\ &\left.+\begin{pmatrix}V_{1^2A'} & 0 & 0\\ 0 & V_{2^2A'} & 0\\ 0 & 0 & V_{A''}\end{pmatrix}\right\}\begin{pmatrix}F_{1^2A'}\\ F_{2^2A'}\\ F_{A''}\end{pmatrix} = \begin{pmatrix}E & 0 & 0\\ 0 & E & 0\\ 0 & 0 & E\end{pmatrix}\begin{pmatrix}F_{1^2A'}\\ F_{2^2A'}\\ F_{A''}\end{pmatrix}\end{aligned}$$

Since the basis has been truncated to include three PES, the adiabatic to diabatic transformation matrix is 3×3. The restriction that the electronic wavefunctions are real, along with the fact that states with A'' symmetry type will not mix with those with A' symmetry means the transformation matrix may be represented by an orthogonal matrix parameterized by a single angle [14], [15]:

$$U_{AD}(q_N)=\begin{pmatrix}\cos(\gamma(q_N)) & -\sin(\gamma(q_N)) & 0\\ \sin(\gamma(q_N)) & \cos(\gamma(q_N)) & 0\\ 0 & 0 & 1\end{pmatrix} \tag{22}$$

This transformation matrix relates the adiabatic wavefunctions to the diabatic wavefuctions as

$$\begin{aligned}\phi^A_{1^2A'}(q_n,q_e)&=\phi^D_{1^2A'}(q_n,q_e)\cos(\gamma(q_n))+\phi^D_{2^2A'}(q_n,q_e)\sin(\gamma(q_n))\\ \phi^A_{2^2A'}(q_n,q_e)&=-\phi^D_{1^2A'}(q_n,q_e)\sin(\gamma(q_n))+\phi^D_{2^2A'}(q_n,q_e)\cos(\gamma(q_n))\end{aligned} \tag{23}$$

Substituting eq. (23) into the definition of the derivative coupling terms in eq. (16) gives an expression for the derivative coupling terms in the diabatic representation in terms of the derivative coupling terms in the adiabatic representation and the mixing angle γ. The derivative coupling terms may be shown to be antihermitian, which simplifies this relation to

$$\vec{\tau}^{\,D}_{12}=\vec{\nabla}_{q_n}\gamma(q_n)+\vec{\tau}^{\,A}_{12} \tag{24}$$

The requirement that the mixing angle causes the diabatic coupling terms to be zero gives

$$\vec{\tau}^{\,A}_{12}=-\vec{\nabla}_{q_n}\gamma(q_n) \tag{25}$$

and the mixing angle $\gamma(q_N)$ may be calculated by performing a line integral through the vector space of the derivative coupling terms at each nuclear configuration:

$$\gamma\left(R,\theta,r\right)=\int_{R_0}^{R}\tau_{R,12}^{A}\Big|_{r_0\theta_0}dR+\int_{\theta_0}^{\theta}\tau_{\theta,12}^{A}\Big|_{Rr_0}d\theta+\int_{r_0}^{r}\tau_{r,12}^{A}\Big|_{R\theta}dr+\gamma_0 \tag{26}$$

The adiabatic to diabatic transformation is applied to the truncated basis representation in eq. (21) to give the diabatic representation

$$\left\{-\frac{1}{2}\begin{pmatrix}\sum_\alpha\frac{\hat{p}_\alpha^2}{m_\alpha} & 0 & 0\\ 0 & \sum_\alpha\frac{\hat{p}_\alpha^2}{m_\alpha} & 0\\ 0 & 0 & \sum_\alpha\frac{\hat{p}_\alpha^2}{m_\alpha}\end{pmatrix}+\begin{pmatrix}V_{xx} & V_{xz} & 0\\ V_{xz} & V_{zz} & 0\\ 0 & 0 & V_{yy}\end{pmatrix}\right\}\begin{pmatrix}F_{zz}\\ F_{xx}\\ F_{yy}\end{pmatrix}=\begin{bmatrix}E & 0 & 0\\ 0 & E & 0\\ 0 & 0 & E\end{bmatrix}\begin{pmatrix}F_{zz}\\ F_{xx}\\ F_{yy}\end{pmatrix} \tag{27}$$

where the NACTs have been eliminated and the diabatic wavefunctions are coupled by the diabatic PES.

The Asymptotic Representation

To facilitate wavepacket propagation as required by the channel-packet method (described in a later section), the Hamiltonian can be represented in an asymptotic basis. Before introducing this basis it is necessary to establish a new coordinate system.

Body Fixed and Space Fixed Coordinates

The coordinates used by Weeks et al [16] are shown in Figure 2.

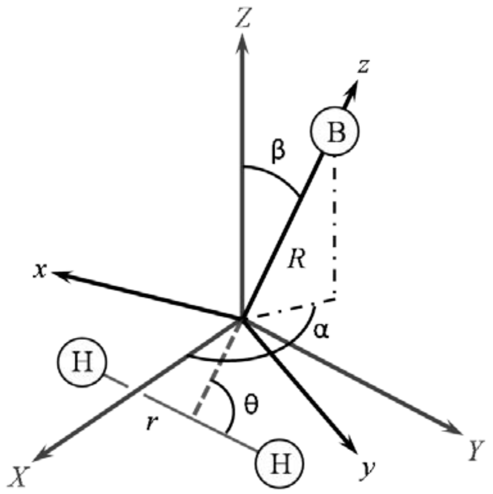

Figure 2. Space and Body Fixed Coordinate System for B+H$_2$

The $B+H_2$ system is described using the Jacobi coordinates: *R* is the distance from the boron atom to the center of mass of the hydrogen molecule; *r* is the hydrogen bond length; θ is the angle formed between the hydrogen axis and the line connecting the boron atom to the hydrogen center of mass. The space fixed axes are labeled X, Y, Z while the body fixed axes are labeled x, y, z. Both have their origin at the $B+H_2$ center of mass, which in the figure is displaced away from the boron atom for visualization purposes. The body fixed *z* axis contains both the boron atom and the hydrogen molecule center of mass. The azimuthal angle ϕ is formed between the body fixed *x* axis and the projection of the hydrogen molecule's axis onto the *xy* plane, and is omitted from the figure for clarity. The body fixed *y* axis is constrained to lie in the *XY* plane. The body fixed axis system is oriented in the space fixed coordinate axes using the Euler angles α and β. The angle α is defined between the projection of the *z* axis onto the *XY* plane and the *X* axis. β is the polar angle formed between the body fixed *z* axis and the space fixed *Z* axis.

Using these space fixed and body fixed coordinates, the Hamiltonian may be rewritten in the center of mass frame [17] as

$$\hat{H} = \frac{\hat{p}_R^2}{2\mu_{B,H_2}} + \frac{\hat{p}_r^2}{2\mu_{H_2}} + \frac{\hat{j}^2}{2\mu_{H_2} r^2} + \frac{\hat{L}^2}{2\mu_{B,H_2} R^2} + \hat{H}_{el}^{H_2} + \hat{H}_{el}^{B} + \hat{V}_{el} + \hat{H}_{so} + E_{off} \qquad (28)$$

The first four terms in eq. (28) represent the nuclear kinetic energy operators using the reduced mass of the nuclei $\mu_{B,H_2} = \frac{2m_B m_H}{m_B + 2m_H}$, the reduced mass of the hydrogen molecule $\mu_{H_2} = \frac{m_H}{2}$, and the momentum operators for their respective coordinates, $\hat{p}_R$ and $\hat{p}_r$. The angular momentum operator $\hat{j}$ describes the H_2 rigid rotor, while $\hat{L}$ corresponds to the rigid rotor composed of the boron atom and the hydrogen molecule center of mass. $\hat{H}_{el}^{H_2}$ and $\hat{H}_{el}^{B}$ represent the kinetic energy and coulomb potential of the electrons in the molecule and the atom, while $\hat{V}_{el}$ represents the coulomb potential between the boron atom and the hydrogen molecule. $\hat{H}_{so}$ is the spin-orbit Hamiltonian for the boron atom, and E_{off} is an arbitrary energy offset.

A complete basis for this system is given by $\left| \begin{matrix} J \\ MP \end{matrix}, \begin{matrix} j \\ k \end{matrix}, l, s, \begin{matrix} j_a \\ \omega \end{matrix}, r, R \right\rangle$ where the coupling scheme is identified as “case 1A” by Dubernet and Hutson [17].

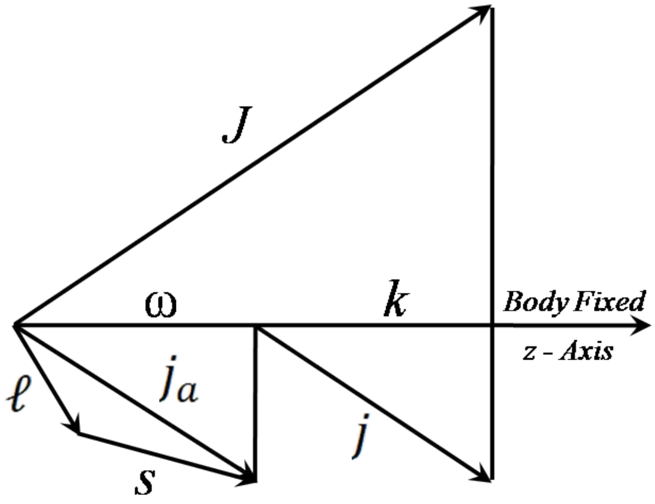

Figure 3. Angular Momentum Coupling Scheme

The electronic orbital angular momentum l and spin s of the boron's unpaired outer electron couple to give j_a with projection ω onto the body fixed z axis. The angular momentum of the H_2 rigid rotor is j with a projection k onto the body fixed z axis, and there is assumed to be no coupling between j and j_a. The total angular momentum is $J = L + j + j_a$, which in the centrifugal sudden approximation [18] has a projection onto the body fixed z axis of $P = k + \omega$ and a projection onto the space fixed z axis of M.

This basis $\left| \begin{matrix} J \\ MP \end{matrix}, \begin{matrix} j \\ k \end{matrix}, l, s, \begin{matrix} j_a \\ \omega \end{matrix}, r, R \right\rangle$ has an infinite number of states, but may be truncated to include only the range of states accessible as determined by the kinetic energy of the $B + H_2$ system. The electronic basis has been truncated to only include the boron ${}^2P$ states, which gives $l = 1,\ s = 1/2$ which limits j_a to the values $1/2, 3/2$. Additionally the hydrogen molecule is restricted to the ground electronic state. This work considers only a total angular momentum $J = 1/2$. A more concise notation for the basis is obtained by including only those labels which are not constant.

$$\left|\begin{matrix}J\\M\end{matrix}\ P,\begin{matrix}j\\k\end{matrix},l,s,\begin{matrix}j_a\\\omega\end{matrix},r,R\right\rangle \rightarrow \left|\begin{matrix}j\\k\end{matrix},\begin{matrix}j_a\\\omega\end{matrix},r,R\right\rangle$$

Representing the Hamiltonian

The Hamiltonian in eq. (28) is now represented in this basis. The details behind the results presented here are covered in more detail by Weeks [16] and again by Garvin [1]. The matrix elements of the first three terms in eq. (28) are diagonal in this basis. They are

$$\left\langle\begin{matrix}j'\\k'\end{matrix},\begin{matrix}j_a'\\\omega'\end{matrix},r',R'\right|\frac{\hat{p}_R^2}{2\mu_{B,H_2}}\left|\begin{matrix}j\\k\end{matrix},\begin{matrix}j_a\\\omega\end{matrix},r,R\right\rangle = \frac{-\hbar^2}{2\mu_{B,H_2}}\frac{1}{R}\frac{\partial^2}{\partial R^2}R\delta_{x'x} \tag{29}$$

$$\left\langle\begin{matrix}j'\\k'\end{matrix},\begin{matrix}j_a'\\\omega'\end{matrix},r',R'\right|\frac{\hat{p}_r^2}{2\mu_{H_2}}\left|\begin{matrix}j\\k\end{matrix},\begin{matrix}j_a\\\omega\end{matrix},r,R\right\rangle = \frac{-\hbar^2}{2\mu_{H_2}}\frac{1}{r}\frac{\partial^2}{\partial r^2}r\delta_{x'x} \tag{30}$$

$$\left\langle\begin{matrix}j'\\k'\end{matrix},\begin{matrix}j_a'\\\omega'\end{matrix},r',R'\right|\frac{\hat{j}^2}{2\mu_{H_2}r^2}\left|\begin{matrix}j\\k\end{matrix},\begin{matrix}j_a\\\omega\end{matrix},r,R\right\rangle = \frac{\hbar^2 j(j+1)}{2\mu_{H_2}r^2}\delta_{x'x} \tag{31}$$

where $\delta_{x'x} = \delta_{M'M}^{J'J}\delta_{P'P}\delta_{k'k}^{j'j}\delta_{\omega'\omega}^{j_a'j_a}\delta(r-r')\delta(R-R')$. The remainder of the terms are not diagonal.

The fourth term is obtained by solving for $\hat{L}$ in terms of the total angular momentum $\hat{J}$, then expanding using raising and lowering operators.

$$\begin{gathered}\hat{L}^2 = \left(\hat{J} - j - j_a\right)^2 = \\ \hat{J}^2 + \hat{j}^2 + \hat{j}_a^2 - \hat{J}^+\hat{j}_- - \hat{J}^-\hat{j}_+ - 2\hat{J}_z\hat{j}_z - \hat{J}^+\hat{j}_{a_-} - \hat{J}^-\hat{j}_{a_+} - 2\hat{J}_z\hat{j}_{a_z} + \hat{j}_+\hat{j}_{a_+} + 2\hat{j}_z\hat{j}_{a_z}\end{gathered} \tag{32}$$

Each term in eq. (32) is evaluated to give the full expression

$$\begin{aligned}
&\left\langle \begin{matrix} j' & j_a' \\ k', & \omega', \end{matrix} r', R' \right| \frac{\hat{L}^2}{2\mu_{B,H_2} R^2} \left| \begin{matrix} j & j_a \\ k, & \omega \end{matrix}, r, R \right\rangle = \left\langle \begin{matrix} j' & j_a' \\ k', & \omega', \end{matrix} r', R' \right| \frac{\left(\hat{J} - \hat{j} - \hat{j}_a\right)^2}{2\mu_{B,H_2} R^2} \left| \begin{matrix} j & j_a \\ k, & \omega \end{matrix}, r, R \right\rangle \\
&= \frac{\hbar^2}{2\mu_{B,H_2} R^2} \Big[\left\{ J(J+1) + j(j+1) + j_a(j_a+1) - 2(k+\omega)^2 + 2k\omega \right\} \delta_{x'x} \\
&+ \left\{ \left(J(J+1) - P(P\mp 1)\right)\left(j(j+1) - k(k\mp 1)\right) \right\}^{1/2} \delta^{J'J}_{M'M} \delta_{j'j} \delta_{k'k\mp 1} \delta_{j_a' j_a} \delta_{\omega'\omega} \delta(R-R') \\
&+ \left\{ \left(J(J+1) - P(P\mp 1)\right)\left(j_a(j_a+1) - \omega(\omega\mp 1)\right) \right\}^{1/2} \delta^{J'J}_{M'M} \delta_{j'j} \delta_{k'k} \delta_{j_a' j_a} \delta_{\omega'\omega\mp 1} \delta(R-R') \\
&+ \left\{ \left(J(J+1) - k(k\pm 1)\right)\left(j_a(j_a+1) - \omega(\omega\mp 1)\right) \right\}^{1/2} \delta^{J'J}_{M'M} \delta_{P'P} \delta_{j'j} \delta_{k'k\pm 1} \delta_{j_a' j_a} \delta_{\omega'\omega\mp 1} \delta(R-R')
\end{aligned} \qquad (33)$$

The second and third terms in eq. (33) are neglected under the centrifugal sudden approximation.

The spin-orbit Hamiltonian is given by $\hat{H}_{so} = \zeta \hat{l} \cdot \hat{s}$, where ζ is treated as a constant under the pure precession approximation [6], and when represented in the angular momentum basis is given by

$$\left\langle \begin{matrix} j' & j_a' \\ k', & \omega', \end{matrix} r', R' \right| \hat{H}_{so} \left| \begin{matrix} j & j_a \\ k, & \omega \end{matrix}, r, R \right\rangle = \frac{\zeta}{2} \left\{ j_a(j_a+1) - l(l+1) - s(s+1) \right\} \delta_{x'x} \qquad (34)$$

The remaining terms are $\hat{H}^{H_2}_{el} + \hat{V}_{el} + \hat{H}^{B}_{el} + E_{off}$. These are represented in the asymptotic electronic basis $\left|\Sigma, \Lambda\right\rangle \equiv \left|{}^1\Sigma_g^+\right\rangle \otimes \left|l, \Lambda\right\rangle$ consisting of the ground state of the hydrogen molecule electronic Hamiltonian $\left|{}^1\Sigma_g^+\right\rangle$ and the three ${}^2P$ states of the boron electronic Hamiltonian, given by $\left|l, \Lambda\right\rangle$ with possible values $l = 1, \Lambda = -1, 0, 1$. In the asymptotic limit the term $\left\langle \Sigma', \Lambda \right| \hat{H}^B_{el} \left| \Sigma, \Lambda \right\rangle$ is constant, and $E_{off} = -\left\langle \Sigma', \Lambda \right| \hat{H}^B_{el} \left| \Sigma, \Lambda \right\rangle$ is chosen to eliminate these terms.

The representation of the remaining terms $\left\langle \begin{matrix} j' & j_a' \\ k', & \omega', \end{matrix} r', R' \middle| \hat{H}_{el}^{H_2} + \hat{V}_{el} \middle| \begin{matrix} j & j_a \\ k, & \omega, \end{matrix} r, R \right\rangle$ is accomplished using the numerically determined diabatic electronic potential energy surfaces from equation (27). These are cast in a new form by expanding in terms of reduced rotation matrix elements which are related to the associated Legendre polynomials $P_m^l(\cos\theta)$ by $d_{m0}^l(\theta) = \left[(l-m)!/(l+m)!\right]^{1/2} P_m^l(\cos\theta)$. This expansion takes the form

$$\begin{aligned}
V_{zz}^D(r,R,\theta) &= \sum_{\lambda_r=0} V_{zz}^{\lambda_r}(r,R)\, d_{00}^{\lambda_r}(\theta) \\
V_{xz}^D(r,R,\theta) &= \sum_{\lambda_r=1} V_{xz}^{\lambda_r}(r,R)\, d_{10}^{\lambda_r}(\theta) \\
V_{xx}^D(r,R,\theta) &= \sum_{\lambda_r=0} V_{s}^{\lambda_r}(r,R)\, d_{00}^{\lambda_r}(\theta) + \sum_{\lambda_r=2} V_{d}^{\lambda_r}(r,R)\, d_{20}^{\lambda_r}(\theta) \\
V_{yy}^D(r,R,\theta) &= \sum_{\lambda_r=0} V_{s}^{\lambda_r}(r,R)\, d_{00}^{\lambda_r}(\theta) - \sum_{\lambda_r=2} V_{d}^{\lambda_r}(r,R)\, d_{20}^{\lambda_r}(\theta)
\end{aligned} \tag{35}$$

The expansion coefficients $V_{zz}^{\lambda_r}, V_{xz}^{\lambda_r}, V_{s}^{\lambda_r}, V_{d}^{\lambda_r}$ in equation (35) are obtained by performing a multipole expansion of $\langle \Sigma', \Lambda' | \hat{V}_{el} + \hat{H}_{el}^{H_2} | \Sigma, \Lambda \rangle$. Integrating over molecular and atomic electronic coordinates, with the exception of the polar and azimuthal angles of boron’s outer 2*p* electron, gives the matrix elements [6]

$$\begin{aligned}
&V_{\Lambda'\Lambda}^D(r,R,\theta) = \langle \Sigma', \Lambda' | \hat{V}_{el} + \hat{H}_{el}^{H_2} | \Sigma, \Lambda \rangle \\
&= \langle \Sigma', \Lambda' | \textstyle\sum_{i,j} \frac{q_{mi}\, q_{aj}}{|\vec{r}_{mi} - \vec{r}_{aj}|} | \Sigma, \Lambda \rangle + \langle \Sigma', \Lambda' | \hat{H}_{el}^{H_2} | \Sigma, \Lambda \rangle \\
&= \sum_{\lambda_r \lambda_a \mu} V_{\lambda_r \lambda_a \mu}(r,R)\, C_{\mu}^{\lambda_r}(\theta,\phi) \langle \Lambda' | C_{-\mu}^{\lambda_a}(\theta_a,\phi_a) | \Lambda \rangle \delta_{\Sigma'\Sigma} + V_{H_2}(r)\, \delta_{\Sigma'\Sigma} \delta_{\Lambda'\Lambda} \qquad (36) \\
&= 3 \sum_{\lambda_r \lambda_a \mu} \Bigg\{ V_{\lambda_r \lambda_a \mu}(r,R)\, C_{\mu}^{\lambda_r}(\theta,\phi) \left[(-1)^{2-\Lambda'} \begin{pmatrix} 1 & \lambda_a & 1 \\ -\Lambda' & -\mu & \Lambda \end{pmatrix} \begin{pmatrix} 1 & \lambda_a & 1 \\ 0 & 0 & 0 \end{pmatrix} \right] \\
&+ V_{H_2}(r)\, C_0^0(\theta,\phi)\, \delta_{\Sigma'\Sigma} \delta_{\Lambda'\Lambda} \Bigg\}
\end{aligned}$$

Here the terms indicated by $\begin{pmatrix} \cdot & \cdot & \cdot \\ \cdot & \cdot & \cdot \end{pmatrix}$ are the Wigner 3j symbols and $C_{\mu}^{\lambda_r}\left(\theta,\phi\right)$ are modified spherical harmonics. Collisional energies considered here will not allow an H_2 electronic transition so $\delta_{\Sigma'\Sigma}$ may be removed. The value λ_a is restricted to $\lambda_a = 0,1,2$ by the triangle inequality $\left|1-\lambda_a\right| \le 1 \le \left|1+\lambda_a\right|$. This reduces equation (36) to

$$\begin{aligned} V_{\Lambda'\Lambda}^{D}\left(r,R,\theta\right) = \sum_{\lambda_r\ \mu} C_{\mu}^{\lambda_r}(\theta,\phi)\Bigg[& V_{\lambda_r\,0\,0}\left(r,R\right)(-1)^{3-\Lambda'}(3)^{1/2}\begin{pmatrix} 1 & 0 & 1 \\ -\Lambda' & 0 & \Lambda \end{pmatrix}\delta_{\Lambda'\Lambda}^{\mu,0} \quad + \\ & V_{\lambda_r\,2\,\mu}\left(r,R\right)(-1)^{2-\Lambda'}\left(\frac{6}{5}\right)^{1/2}\begin{pmatrix} 1 & 2 & 1 \\ -\Lambda' & -\mu & \Lambda \end{pmatrix}\delta_{\mu,\Lambda'-\Lambda} + \\ & V_{H_2}\left(r\right)C_0^0\left(\theta,\phi\right)\delta_{\Lambda'\Lambda}\Bigg] \end{aligned} \tag{37}$$

A further restriction $\mu = \Lambda - \Lambda'$ is obtained by considering the bottom row of the Wigner 3j symbols, where it is required that $-\Lambda' - \mu - \Lambda = 0$. Defining a new form of expansion coefficients $V_{\lambda_a\mu} = \sum_{\lambda_r} C_{\mu}^{\lambda_r}\left(\theta,0\right)V_{\lambda_r\lambda_a\mu}\left(r,R\right)$ the μ matrix elements are

$$V^{D}\left(r,R,\theta\right) = \begin{array}{c|ccc} & \left|\,1\right\rangle & \left|\,0\right\rangle & \left|\,-1\right\rangle \\ \hline \left\langle 1\,\right| & \begin{array}{l} V_{00}-\frac{1}{5}V_{20} \\ +V_{H_2}\delta_{\lambda_r 0} \end{array} & -\frac{\sqrt{3}}{5}V_{21} & -\frac{\sqrt{6}}{5}V_{22} \\ \left\langle 0\,\right| & -\frac{\sqrt{3}}{5}V_{21} & \begin{array}{l} V_{00}+\frac{2}{5}V_{20} \\ +V_{H_2}\delta_{\lambda_r 0} \end{array} & \frac{\sqrt{3}}{5}V_{21} \\ \left\langle -1\,\right| & -\frac{\sqrt{6}}{5}V_{22} & \frac{\sqrt{3}}{5}V_{21} & \begin{array}{l} V_{00}-\frac{1}{5}V_{20} \\ +V_{H_2}\delta_{\lambda_r 0} \end{array} \end{array} \tag{38}$$

Transforming to a Cartesian basis $\left|x\right\rangle = \frac{1}{\sqrt{2}}\left(-\left|1\right\rangle + \left|-1\right\rangle\right), \left|y\right\rangle = \frac{i}{\sqrt{2}}\left(\left|1\right\rangle + \left|-1\right\rangle\right)$, $\left|z\right\rangle = \left|0\right\rangle$

gives

$$V^{D}\left(r,R,\theta\right)=$$

$$\begin{array}{c|ccc} & \left| z \right\rangle & \left| x \right\rangle & \left| y \right\rangle \\ \hline \left\langle z \right| & V_{00}+\frac{2}{5}V_{20}+V_{H_2}\delta_{\lambda_r 0} & \frac{\sqrt{6}}{5}V_{21} & 0 \\ \left\langle x \right| & \frac{\sqrt{6}}{5}V_{21} & V_{00}-\frac{1}{5}V_{20}+\frac{\sqrt{6}}{5}V_{22}+V_{H_2}\delta_{\lambda_r 0} & 0 \\ \left\langle y \right| & 0 & 0 & V_{00}-\frac{1}{5}V_{20}-\frac{\sqrt{6}}{5}V_{22}+V_{H_2}\delta_{\lambda_r 0} \end{array} \tag{39}$$

Each matrix element in equation (39) is compared to the expansion of the numerical diabatic potential energy surfaces in equation (35), for which the fit process has given expansion coefficients $V_{zz}^{\lambda_r}, V_{xz}^{\lambda_r}, V_{s}^{\lambda_r}, V_{d}^{\lambda_r}$ as a function of *r* and *R*. These are related to the expansion coefficients $V_{\lambda_r\lambda_a\mu}\left(r,R\right)$ by

$$\begin{aligned} V_{\lambda_r 00}\left(r,R\right) &= \tfrac{1}{3}\left[V_{zz}^{\lambda_r}\left(r,R\right)+2V_{s}^{\lambda_r}\left(r,R\right)\right]-V_{H_2}\left(r\right)\delta_{\lambda_r 0} \\ V_{\lambda_r 20}\left(r,R\right) &= \tfrac{5}{3}\left[V_{zz}^{\lambda_r}\left(r,R\right)-V_{s}^{\lambda_r}\left(r,R\right)\right] \\ V_{\lambda_r 21}\left(r,R\right) &= \tfrac{5}{\sqrt{6}}V_{xz}^{\lambda_r}\left(r,R\right) \\ V_{\lambda_r 22}\left(r,R\right) &= \tfrac{5}{\sqrt{6}}V_{d}^{\lambda_r}\left(r,R\right) \end{aligned} \tag{40}$$

Having obtained the expansion coefficients the interaction electronic potential $\hat{V}_{el}+\hat{H}_{el}^{H_2}$ is represented in the angular momentum basis. This is given by [16]

$$\begin{aligned} &\left\langle \begin{matrix} j' & j_a' \\ k', & \omega' \end{matrix}, r', R' \right| \hat{H}_{el}^{H_2}+\hat{V}_{el} \left| \begin{matrix} j & j_a \\ k, & \omega \end{matrix}, r, R \right\rangle = \\ &\sum_{\lambda_r\lambda_a\mu} V_{\lambda_r\lambda_a\mu}\left(r,R\right)\left(-1\right)^{k+\omega-s}\left(2l+1\right)\left\{\left(2j'+1\right)\left(2j+1\right)\right\}^{1/2}\left\{\left(2j_a'+1\right)\left(2j_a+1\right)\right\}^{1/2} \\ &\times\begin{pmatrix} j' & \lambda_r & j \\ -k' & \mu & k \end{pmatrix}\begin{pmatrix} j' & \lambda_r & j \\ 0 & 0 & 0 \end{pmatrix}\begin{Bmatrix} j_a' & \lambda_a & j_a \\ l & s & l \end{Bmatrix}\begin{pmatrix} j_a & \lambda_a & j_a' \\ \omega & -\mu & -\omega' \end{pmatrix}\begin{pmatrix} l & \lambda_a & l \\ 0 & 0 & 0 \end{pmatrix}\delta_{M'M}^{J'J}\delta_{P'P}\delta_{v^{\gamma'}v^{\lambda}}\delta\left(R'-R\right) \end{aligned} \tag{41}$$

where terms of the form $\begin{pmatrix} \mathsf{L} \\ \mathsf{L} \end{pmatrix}$ are $3-j$ symbols and those of the form $\begin{Bmatrix} \mathsf{L} \\ \mathsf{L} \end{Bmatrix}$ are $6-j$ symbols.

The Effective Diabatic Potential Energy Surfaces for B+H_2

Taken together, eqs. (31), (33), (34) and (41) give the effective diabatic potential energy matrix elements

$$V_{eff}^{D}\left(r,R\right)_{\gamma'\gamma} = \left\langle \begin{matrix} j' & j_a' \\ k', & \omega', \end{matrix} r', R' \right| \frac{\hat{j}^2}{2\mu_{H_2} r^2} + \frac{\hat{L}^2}{2\mu_{B,H_2} R^2} + \hat{H}_{el}^{H_2} + \hat{V}_{el} + \hat{H}_{so} \left| \begin{matrix} j & j_a \\ k, & \omega, \end{matrix} r, R \right\rangle \tag{42}$$

where the label γ represents appropriate values of *J, M, P, j, k,* j_a and ω. These represent surfaces for which the time-dependent Schrödinger equation can be solved. The surfaces are two dimensional (for *r* and *R*) and each is labeled by the choice of γ. The diabatic effective potential energy surfaces used in this work were calculated by Garvin [1].

The full Hamiltonian is obtained by adding the nuclear kinetic energy terms from eqs. (29) and (30) to the effective potential in eq. (42). Reduced wavefunctions $\Phi\left(r,R,t\right) = rR\Psi\left(r,R,t\right)$ are introduced to simplify the radial form of the kinetic energy operators, giving the time-dependent Schrödinger equation as

$$\begin{aligned} i\hbar\frac{\partial}{\partial t}\begin{pmatrix} \Phi_1\left(r,R,t\right) \\ \Phi_2\left(r,R,t\right) \\ \vdots \end{pmatrix} &= \begin{pmatrix} H_{11} & H_{12} & \cdots \\ H_{21} & H_{22} & \cdots \\ \vdots & \vdots & \ddots \end{pmatrix}\begin{pmatrix} \Phi_1\left(r,R,t\right) \\ \Phi_2\left(r,R,t\right) \\ \vdots \end{pmatrix} \\ &= \left[\left\{-\frac{\hbar^2}{2\mu_{B,H_2}}\frac{\partial^2}{\partial R^2} - \frac{\hbar^2}{2\mu_{H_2}}\frac{\partial^2}{\partial r^2}\right\}\begin{pmatrix} 1 & 0 & \cdots \\ 0 & 1 & \cdots \\ \vdots & \vdots & \ddots \end{pmatrix}\right. \\ &\quad \left. + \begin{pmatrix} V_{eff}^{D}\left(r,R\right)_{11} & V_{eff}^{D}\left(r,R\right)_{12} & \cdots \\ V_{eff}^{D}\left(r,R\right)_{21} & V_{eff}^{D}\left(r,R\right)_{22} & \cdots \\ \vdots & \vdots & \ddots \end{pmatrix}\right]\begin{pmatrix} \Phi_1\left(r,R,t\right) \\ \Phi_2\left(r,R,t\right) \\ \vdots \end{pmatrix} \end{aligned} \tag{43}$$

Eq. (43) shows that each wavepacket is dependent on more than one effective diabatic PES $V_{eff}^{D}\left(r,R\right)_{\gamma'\gamma}$ as it evolves in time.

Structure of the Effective Diabatic Potential Energy Matrix

The effective diabatic potential energy matrix $V_{eff}^{D}\left(r,R\right)_{\gamma'\gamma}$ is block diagonal as governed by the Kronecker deltas in eqs. (31), (33), (34) and (41). These give the matrix a structure of infinite dimensional blocks arranged in a hierarchy. The largest are labeled by their value of total rotational energy *J*. Each *J* block is subdivided into identical blocks labled by *M*. This study is restricted to $J=1/2$. This block is shown in Figure 4.

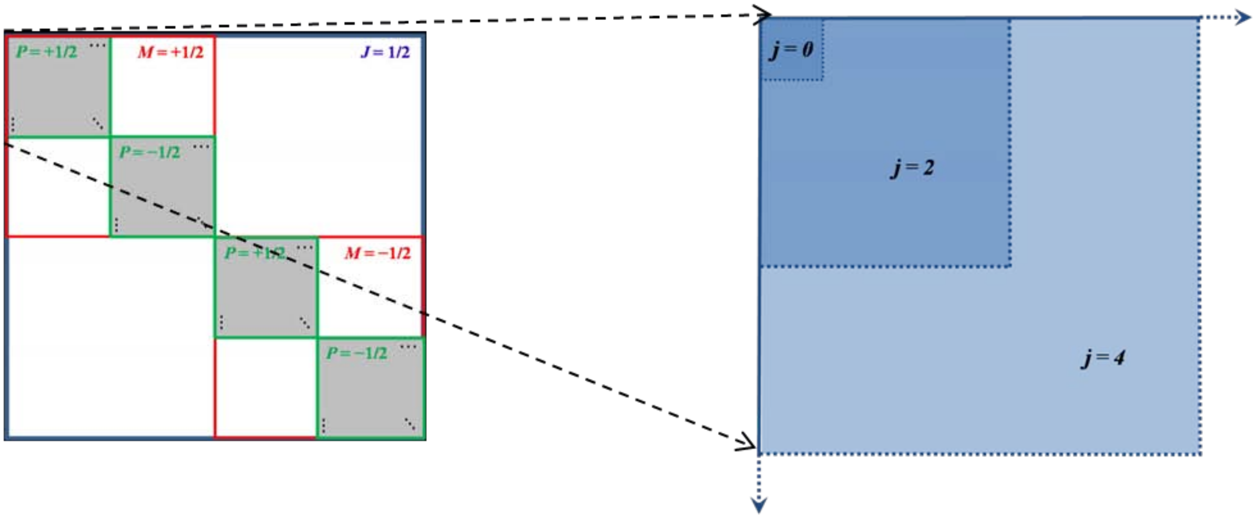

Figure 4. Structure of the *J* = 1/2 Block of the Effective Potential Energy Matrix

Since the *M* blocks are identical, only $M=1/2$ is considered. Under the centrifugal sudden approximation [18] $\Delta P=0$, so we may consider only the $P=1/2$ block.

The $J = 1/2, M = 1/2, P = 1/2$ block is further divided into orthohydrogen and parahydrogen blocks. In this work only transitions from the ground rotational state $j = 0$ are considered, so only the even valued *j* states corresponding to the parahydrogen block are considered. The requirement $k + \omega = P = 1/2$ along with $j_a = \frac{1}{2}, \frac{3}{2}$ restricts the number of states available for each value if *j*. Specifically they are

$$\begin{aligned} j = 0 &\rightarrow \left| \begin{matrix} j & j_a \\ k & \omega \end{matrix} \right\rangle = \left| \begin{matrix} 0 & \frac{1}{2} \\ 0 & \frac{1}{2} \end{matrix} \right\rangle, \left| \begin{matrix} 0 & \frac{3}{2} \\ 0 & \frac{1}{2} \end{matrix} \right\rangle \\ j = 2, 4, \ldots &\rightarrow \left| \begin{matrix} j & j_a \\ k & \omega \end{matrix} \right\rangle = \left| \begin{matrix} j & \frac{3}{2} \\ 2 & -\frac{3}{2} \end{matrix} \right\rangle, \left| \begin{matrix} j & \frac{3}{2} \\ 1 & -\frac{1}{2} \end{matrix} \right\rangle, \left| \begin{matrix} j & \frac{1}{2} \\ 1 & -\frac{1}{2} \end{matrix} \right\rangle, \left| \begin{matrix} j & \frac{1}{2} \\ 0 & \frac{1}{2} \end{matrix} \right\rangle, \left| \begin{matrix} j & \frac{3}{2} \\ 0 & \frac{1}{2} \end{matrix} \right\rangle, \left| \begin{matrix} j & \frac{3}{2} \\ -1 & \frac{3}{2} \end{matrix} \right\rangle \end{aligned} \tag{44}$$

The total number of these states is infinite but may be truncated to only include those states which are energetically accessible as determined by the total energy of the wavepacket being considered. Truncating to only include values up to $j_{\max}$ results in the effective potential energy matix having a dimension given by

$$n = 2 + 3 j_{\max} \tag{45}$$

This *n* is also referred to as the basis size, since the effect of truncating is to restrict the number of basis states in which we represent the Hamiltonian to *n*.

As seen in Eq. (43) the off-diagonal terms of $V_{eff}^{D}\left(r, R\right)_{\gamma'\gamma}$ couple the evolving wavepackets, allowing for transitions between the various surfaces. These transitions represent a wavepacket in an initial channel γ changing to a final channel γ' as a result of scattering. The term channel refers to a specific arrangement of $B + H_2$ together with a choice of quantum numbers. The process for calculating the probability of making these transitions is the subject of subsequent sections on scattering and the channel packet method.

Nonadiabatic behavior is most frequently associated with coupling between electronic and nuclear degrees of freedom. Representing the Hamiltonian in the angular momentum basis $\left| \begin{matrix} J \\ M \end{matrix} \; P, \begin{matrix} j \\ k \end{matrix}, l, s, \begin{matrix} j_a \\ \omega \end{matrix}, r, R \right\rangle$ has resulted in an effective potential energy matrix V_{eff}^{D} which contains off-diagonal terms. This nonadiabaticity is the result of coupling between rotational and vibrational degrees of freedom as well as coupling between electronic and nuclear degrees of freedom.

The Split-Operator Propagator

The time-dependent Schrödinger eq. (2) gives the solution to the initial-value problem [19]

$$\psi\left(x,t\right) = e^{-\frac{it\hat{H}}{\hbar}} \psi\left(x,0\right) = \hat{U}\psi\left(x,0\right) \qquad (46)$$

In many cases this general form of the evolution operator $\hat{U}$ must be approximated. The split-operator method is one technique for calculating $\hat{U}$, thereby giving the time evolution of an initial state based on knowledge of the system's Hamiltonian.

The Split-Operator Approximation

The split-operator method uses the approximation [20]

$$\hat{U}\left(\Delta t\right) = e^{-\frac{i\hat{H}\Delta t}{\hbar}} = e^{-\frac{i\left(\hat{V}+\hat{T}\right)\Delta t}{\hbar}} = e^{-\frac{i}{2\hbar}\hat{V}\Delta t} e^{-\frac{i}{\hbar}\hat{T}\Delta t} e^{-\frac{i}{2\hbar}\hat{V}\Delta t} + O\left(\Delta t^{3}\right);\; e^{-\frac{i}{2\hbar}\hat{V}\Delta t} e^{-\frac{i}{\hbar}\hat{T}\Delta t} e^{-\frac{i}{2\hbar}\hat{V}\Delta t} \qquad (47)$$

where $O\left(\Delta t^3\right)$ represents terms that are third-order or higher in Δt.

The equivalence of this approximation up to third-order or higher terms may be shown by considering Taylor series expansions:

$$\begin{aligned}
e^{-\frac{i}{2\hbar}\hat{V}\Delta t}e^{-\frac{i}{\hbar}T\Delta t}e^{-\frac{i}{2\hbar}\hat{V}\Delta t} &= \left(1-\frac{i}{2\hbar}\hat{V}\Delta t-\frac{1}{8\hbar^2}\hat{V}^2\Delta t^2+O_1\left(\Delta t^3\right)\right)\left(1-\frac{i}{\hbar}\hat{T}\Delta t-\frac{1}{2\hbar^2}\hat{T}^2\Delta t^2+O_2\left(\Delta t^3\right)\right)\cdot \\
&\quad \left(1-\frac{i}{2\hbar}\hat{V}\Delta t-\frac{1}{8\hbar^2}\hat{V}^2\Delta t^2+O_3\left(\Delta t^3\right)\right) \\
&= \left(1-\frac{i}{\hbar}\hat{T}\Delta t-\frac{1}{2\hbar^2}\hat{T}^2\Delta t^2-\frac{i}{2\hbar}\hat{V}\Delta t-\frac{1}{2\hbar^2}\hat{V}\hat{T}\Delta t^2-\frac{1}{8\hbar^2}\hat{V}^2\Delta t^2+O_4\left(\Delta t^3\right)\right)\cdot \\
&\quad \left(1-\frac{i}{2\hbar}\hat{V}\Delta t-\frac{1}{8\hbar^2}\hat{V}^2\Delta t^2+O_3\left(\Delta t^3\right)\right) \\
&= \left(1-\frac{i}{\hbar}\left(\hat{T}+\frac{1}{2}\hat{V}\right)\Delta t-\frac{1}{2\hbar^2}\left(\hat{T}^2+\hat{V}\hat{T}+\frac{1}{4}\hat{V}^2\right)\Delta t^2+O_4\left(\Delta t^3\right)\right)\cdot \\
&\quad \left(1-\frac{i}{2\hbar}\hat{V}\Delta t-\frac{1}{8\hbar^2}\hat{V}^2\Delta t^2+O_3\left(\Delta t^3\right)\right) \\
&= 1-\frac{i}{2\hbar}\hat{V}\Delta t-\frac{1}{8\hbar^2}\hat{V}^2\Delta t^2-\frac{i}{\hbar}\left(\hat{T}+\frac{1}{2}\hat{V}\right)\Delta t-\frac{1}{2\hbar^2}\left(\hat{T}+\frac{1}{2}\hat{V}\right)\hat{V}\Delta t^2 \\
&\quad -\frac{1}{2\hbar^2}\left(\hat{T}^2+\hat{V}\hat{T}+\frac{1}{4}\hat{V}^2\right)\Delta t^2+O_5\left(\Delta t^3\right) \\
&= 1-\frac{i}{\hbar}\left(\hat{V}+\hat{T}\right)\Delta t-\frac{1}{2\hbar^2}\left(\hat{V}^2+\hat{T}\hat{V}+\hat{V}\hat{T}+\hat{T}^2\right)\Delta t^2+O_5\left(\Delta t^3\right) \\
&= 1-\frac{i}{\hbar}\left(\hat{V}+\hat{T}\right)\Delta t-\frac{1}{2\hbar^2}\left(\hat{V}+\hat{T}\right)^2\Delta t^2+O_5\left(\Delta t^3\right) \\
&= e^{-\frac{i\left(\hat{V}+\hat{T}\right)\Delta t}{\hbar}}
\end{aligned}$$

As shown in eq. (47), the split-operator approximation ignores all terms that are third-order or higher in Δt. Therefore the term $O\left(\Delta t^3\right)$ is the error associated with this approximation, which can be made arbitrarily low by selecting a sufficiently small time step Δt.

Diagonal Representations

The motivation for this approximation is the relative simplicity gained by representing each operator in a basis in which it is diagonal [20].

When the effective potential V is not diagonal, as is seen for the effective diabatic PESs of $B+H_2$, the matrix representation of V can be diagonalized using a unitary transformation [21] into the adiabatic representation. This transformation will depend on the coordinates being propagated over – in the case of the diabatic effective PESs of $B+H_2$, the transformation may be represented by $U_{AD}\left(r,R\right)$, and the potential is diagonalized at each point on the grid by

$$V_{eff}^{A} = U_{AD}{}^{\dagger} V_{eff}^{D} U_{AD} \tag{48}$$

The wavepacket is also transformed from the diabatic to adiabatic representation by

$$\phi^{A} = U_{AD}{}^{\dagger} \phi^{D} \tag{49}$$

If the matrix representation of $\hat{V}$ and $\hat{T}$ are diagonal in the appropriate representation, so will the matrix representation of the exponential of those operators, $e^{-\frac{i}{2\hbar}\hat{V}\Delta t}$ and $e^{-\frac{i}{\hbar}\hat{T}\Delta t}$. Recall that an exponential with a matrix in the argument is defined by its Taylor series expansion. Successive powers of a diagonal matrix will be diagonal, and the series may be reduced to a diagonal matrix whose elements are the exponent of the original matrix. For example, if V is the matrix representation of $\hat{V}$ in a basis where it is diagonal,

$$V = \begin{pmatrix} V_{11} & 0 & 0 \\ 0 & V_{22} & 0 \\ 0 & 0 & V_{33} \end{pmatrix}$$

then

$$e^{-\frac{i}{2\hbar}V\Delta t}=\begin{pmatrix} e^{-\frac{i}{2\hbar}V_{11}\Delta t} & 0 & 0 \\ 0 & e^{-\frac{i}{2\hbar}V_{22}\Delta t} & 0 \\ 0 & 0 & e^{-\frac{i}{2\hbar}V_{33}\Delta t} \end{pmatrix} \qquad (50)$$

Changing Representations: The Fourier Transform

Assuming the potential energy operator $\hat{V}$ and the kinetic energy operator $\hat{T}$ are functions only of the spacial coordinates and momentum respectively, $\hat{V}$ is diagonal in the coordinate adiabatic representation, while $\hat{T}$ is diagonal in the momentum diabatic representation.

To show this, consider the matrix element of a potential which depends only on the coordinate *x*, $\langle x'|\hat{V}|x\rangle$. Since $\hat{V}$ is only a function of *x*, we may expand it as a series in terms of $\hat{x}$.

$$\begin{aligned}\langle x'|\hat{V}|x\rangle &= \langle x'|C_0+C_1\hat{x}+C_2\hat{x}^2+\ldots|x\rangle \\ &= \langle x'|C_0|x\rangle+\langle x'|C_1\hat{x}|x\rangle+\langle x'|C_2\hat{x}^2|x\rangle+\ldots\end{aligned}$$

Since the $|x\rangle$ are eigenstates of the $\hat{x}$ operator, this is

$$\langle x'|\hat{V}|x\rangle = C_0\langle x'|x\rangle + C_1x_j\langle x'|x\rangle + C_2x_j^2\langle x'|x\rangle+\ldots$$

$$\langle x'|\hat{V}|x\rangle = \left(C_0+C_1x+C_2x^2+\ldots\right)\delta\left(x-x'\right) \qquad (51)$$

Since the eigenstates of the position operator are orthogonal, the matrix element is nonzero only if it is on the diagonal. The same may be shown for $\langle k'|\hat{T}|k\rangle$.

Similar to how the unitary transformation U_{AD} is used to change between the diabatic and adiabatic representations, there is a transformation to move between the coordinate and momentum representations – the Fourier transform. To understand how this is done, consider the coordinate representation of our time-evolution operator on an initial state:

$$\langle x | e^{-i\hat{V}\Delta t/2\hbar} e^{-i\hat{T}\Delta t/\hbar} e^{-i\hat{V}\Delta t/2\hbar} | \psi \rangle$$

Using the completeness relation $\int |x\rangle\langle x|\, dx = \int |k\rangle\langle k|\, dk = \hat{I}$, where $\hat{I}$ is the identity operator, we may rewrite this as

$$\begin{aligned}
&\langle x | e^{-i\hat{V}\Delta t/2\hbar} e^{-i\hat{T}\Delta t/\hbar} e^{-i\hat{V}\Delta t/2\hbar} | \psi \rangle \\
&= \langle x | e^{-i\hat{V}\Delta t/2\hbar} \hat{I}\hat{I} e^{-i\hat{T}\Delta t/\hbar} \hat{I}\hat{I} e^{-i\hat{V}\Delta t/2\hbar} \hat{I} | \psi \rangle \\
&= \langle x | e^{-i\hat{V}\Delta t/2\hbar} \int | x''' \rangle \langle x''' | \int | k' \rangle \langle k' | e^{-i\hat{T}\Delta t/\hbar} \int | k \rangle \langle k | \int | x'' \rangle \langle x'' | e^{-i\hat{V}\Delta t/2\hbar} \int | x' \rangle \langle x' | \psi \rangle \, dx'''\ dk'\ dk\ dx''\ dx'
\end{aligned}$$

This may be rearranged by moving terms that are not functions of the respective integration variables.

$$\begin{aligned}
&\langle x | e^{-i\hat{V}\Delta t/2\hbar} e^{-i\hat{T}\Delta t/\hbar} e^{-i\hat{V}\Delta t/2\hbar} | \psi \rangle \\
&= \int \langle x | e^{-i\hat{V}\Delta t/2\hbar} | x''' \rangle \int \langle x''' | k' \rangle \int \langle k' | e^{-i\hat{T}\Delta t/\hbar} | k \rangle \int \langle k | x'' \rangle \int \langle x'' | e^{-i\hat{V}\Delta t/2\hbar} | x' \rangle \langle x' | \psi \rangle \, dx''' dk' dk dx'' dx'
\end{aligned}$$

Eqs. (51) and (50) have shown that the terms $\langle x' | e^{-i\hat{V}\Delta t/2\hbar} | x \rangle$ and $\langle k' | e^{-i\hat{T}\Delta t/\hbar} | k \rangle$ are diagonal, that is, they contain the delta functions $\delta(x - x'), \delta(k - k')$ respectively. This eliminates three of the integrals giving

$$\begin{aligned}
&\langle x | e^{-i\hat{V}\Delta t/2\hbar} e^{-i\hat{T}\Delta t/\hbar} e^{-i\hat{V}\Delta t/2\hbar} | \psi \rangle \\
&= \langle x | e^{-i\hat{V}\Delta t/2\hbar} | x \rangle \int \langle x | k' \rangle \langle k | e^{-i\hat{T}\Delta t/\hbar} | k \rangle \int \langle k | x' \rangle \langle x' | e^{-i\hat{V}\Delta t/2\hbar} | x' \rangle \langle x' | \psi \rangle \, dk dx'
\end{aligned}$$

Recalling $\langle x_i | x_j \rangle = \langle k_i | k_j \rangle = \delta_{ij}$, this is

$$\begin{aligned}&\langle x | e^{-i\hat{V}\Delta t/2\hbar} e^{-i\hat{T}\Delta t/\hbar} e^{-i\hat{V}\Delta t/2\hbar} | \psi \rangle = \\ &\langle x | e^{-i\hat{V}\Delta t/2\hbar} | x \rangle \int \langle x | k' \rangle \, dx' \langle k | e^{-i\hat{T}\Delta t/\hbar} | k \rangle \int \langle k | x' \rangle \, dk \langle x' | e^{-i\hat{V}\Delta t/2\hbar} | x' \rangle \langle x' | \psi \rangle\end{aligned} \tag{52}$$

Here we can pause and identify these terms. $\langle x | e^{-i\hat{V}\Delta t/2\hbar} | x \rangle$ is the coordinate representation of the first part of the time-evolution operator. $\langle k | e^{-i\hat{T}\Delta t/\hbar} | k \rangle$ is the momentum representation of the second part. The remaining terms, $\int \langle x | k' \rangle \, dk'$ and $\int \langle k | x' \rangle \, dx'$, represent the transformation between the two representations. In fact, recognizing $\langle x | k' \rangle$ as the coordinate representation of the momentum eigenstate, which are plane waves, we can rewrite this as $\frac{1}{\sqrt{2}} \int e^{ikx} dk$, meaning we can cast this as an Inverse Fourier Transform, and $\int \langle k | x' \rangle \, dx'$, its Hermitian conjugate, as the Fourier Transform.

This is an important result in terms of ease of computation. In practice, transformation between the two representations is typically accomplished using a Fast Fourier Transform (FFT) algorithm. On a grid of size *N*, the FFT requires $O(N \log_2 N)$ operations [22], making this propagation scheme viable for relatively large grids.

The Split-Operator Calculation

Putting the transformations described in eqs. (48) and (52) together, if given a wavepacket in the diabatic coordinate representation at time $t = 0$, $\phi^D(r, R, 0)$, first transform this to the adiabatic representation

$$U_{AD}^{\dagger}(r, R)\, \phi^D(r, R, 0)$$

Next apply the first of the potential operators $e^{-iV^A\Delta t/2\hbar}$

$$e^{-iV^A\Delta t/2\hbar}U_{AD}{}^{\dagger}\left(r,R\right)\phi^D\left(r,R,0\right)$$

where V^A is the diagonal adiabatic coordinate representation of the potential. This is transformed back into the diabatic representation and then moved into the momentum representation via the Fourier transform, given by the operator F

$$FU_{AD}e^{-iV^A\Delta t/2\hbar}U_{AD}{}^{\dagger}\left(r,R\right)\phi^D\left(r,R,0\right)$$

This is multiplied by the exponential kinetic energy operator $e^{-iT^D\Delta t/\hbar}$ where T^D is diagonal in the diabatic momentum representation, then moved back to the coordinate representation via the inverse Fourier transform F^{-1}

$$F^{-1}e^{-iT^D\Delta t/\hbar}FU_{AD}e^{-iV^A\Delta t/2\hbar}U_{AD}{}^{\dagger}\left(r,R\right)\phi^D\left(r,R,0\right)$$

The wavepacket is again transformed to the adiabatic representation and multiplied by the adiabatic representation of the second of the exponential potential operators

$$e^{-iV^A\Delta t/2\hbar}U_{AD}{}^{\dagger}F^{-1}e^{-iT\Delta t/\hbar}FU_{AD}e^{-iV^A\Delta t/2\hbar}U_{AD}{}^{\dagger}\left(r,R\right)\phi^D\left(r,R,0\right)$$

Finally this is transformed to the diabatic representation to yield the wavepacket at $t=\Delta t$

$$\phi^D\left(r,R,\Delta t\right)=U_{AD}e^{-iV^A\Delta t/2\hbar}U_{AD}{}^{\dagger}F^{-1}e^{-iT\Delta t/\hbar}FU_{AD}e^{-iV^A\Delta t/2\hbar}U_{AD}{}^{\dagger}\left(r,R\right)\phi^D\left(r,R,0\right) \qquad (53)$$

The choice to begin and end with the wavepacket in the diabatic representation is arbitrary. Propagating in the adiabatic representation eliminates the first and last transformations from/to the diabatic representation.

$$\phi^A\left(r,R,\Delta t\right)=e^{-iV^A\Delta t/2\hbar}U_{AD}{}^{\dagger}F^{-1}e^{-iT\Delta t/\hbar}FU_{AD}e^{-iV^A\Delta t/2\hbar}\left(r,R\right)\phi^A\left(r,R,0\right) \qquad (54)$$

Scattering Theory

The split-operator propagator allows us to take a wavepacket in an initial known state and propagate it in time. This tool may be applied to examine the behavior of a wavepacket used to describe molecular dynamics as governed by a suitable potential. Tracking possible changes of state in the wavepacket as a result of these dynamics is the domain of scattering theory.

Asymptotic Reactants and Products

Experimentally, the actual quantum scattering event takes place on a scale that is unobservable. As a result, instead of discussing the interaction event scattering theory relates widely separated reactants located in the asymptotic limit before a collision to products located in the asymptotic limit after the collision. A reactant wavepacket in the asymptotic limit before coming into contact with the potential will be called $\left|\psi_{in}\right\rangle$, while an asymptotic product wavepacket is called $\left|\psi_{out}\right\rangle$.

The Møller Operators

There are several definitions which aid in this process of relating initial states to asymptotic wavepackets. The full Hamiltonian of the system can be broken into two parts, $H = H_0 + V$, where V contains all terms describing the interaction between reactants or products [2]. The term H_0 is the asymptotic Hamiltonian describing the system in the asymptotic limit when $V \to 0$, that is, where there is no interaction between reactants and products. The full and asymptotic Hamiltonians are used to define a set of isometric operators, known as Møller operators [23]:

$$\hat{\Omega}_{+} = \lim_{t \to -\infty} e^{i\hat{H}t/\hbar} e^{-i\hat{H}_0 t/\hbar} \tag{55}$$

$$\hat{\Omega}_- = \lim_{t\to\infty} e^{i\hat{H}t/\hbar} e^{-i\hat{H}_0 t/\hbar} \tag{56}$$

These operators are made up of two time-evolution operators. The result of $\hat{\Omega}_+$ acting on a state $|\psi\rangle$ is to first propagate it backwards in time to $t=-\infty$ under the asymptotic Hamiltonian $\hat{H}_0$, then to propagate it forwards in time to $t=0$ using the full Hamiltonian $\hat{H}$. Similarly the effect of $\hat{\Omega}_-$ on the state $|\phi\rangle$ is to propagate it forwards in time to $t=\infty$ under $\hat{H}_0$, then to propagate it backwards in time to $t=0$ using $\hat{H}$.

The Intertwining Relation

These two Hamiltonians and the Møller operators satisfy the intertwining relation [23]:

$$\hat{H}\hat{\Omega}_\pm = \hat{\Omega}_\pm \hat{H}_0 \tag{57}$$

To see this, consider

$$\begin{aligned}
e^{i\hat{H}\tau/\hbar}\hat{\Omega}_\pm &= e^{i\hat{H}\tau/\hbar}\left[\lim_{t\to\mp\infty} e^{i\hat{H}t/\hbar} e^{-i\hat{H}_0 t/\hbar}\right] \\
&= \lim_{t\to\mp\infty}\left[e^{i\hat{H}(\tau+t)/\hbar} e^{-i\hat{H}_0 t/\hbar}\right] \\
&= \lim_{t\to\mp\infty} e^{i\hat{H}(\tau+t)/\hbar} e^{-i\hat{H}_0(\tau+t)/\hbar} e^{i\hat{H}_0\tau/\hbar} \\
&= \hat{\Omega}_\pm e^{i\hat{H}_0\tau/\hbar}
\end{aligned}$$

Differentiating with respect to τ and then setting $\tau = 0$ yields eq. (57).

The Møller States

The new states obtained by applying the Møller operators to a state at $t=0$ are called the Møller states:

$$
\begin{aligned}
\left|\psi_{+}\right\rangle &= \hat{\Omega}_{+}\left|\psi\right\rangle \\
\left|\psi_{-}\right\rangle &= \hat{\Omega}_{-}\left|\phi\right\rangle
\end{aligned}
\tag{58}
$$

The Møller operators give the actual states at $t = 0$ that would evolve from (or to) the asymptote represented by the state they operate on [23]. Each state $\left|\psi\right\rangle$ at $t = 0$ is related to an in or out asymptote $\left|\psi_{in/out}\right\rangle$ by the Møller operators:

$$\left|\psi\right\rangle = \hat{\Omega}_{+}\left|\psi_{in}\right\rangle = \hat{\Omega}_{-}\left|\psi_{out}\right\rangle \tag{59}$$

The Scattering Matrix

The Møller operators are isometric, so eq. (59) may be inverted.

$$\left|\psi_{out}\right\rangle = \hat{\Omega}_{-}^{\dagger}\left|\psi\right\rangle = \hat{\Omega}_{-}^{\dagger}\hat{\Omega}_{+}\left|\psi_{in}\right\rangle \tag{60}$$

The scattering operator is defined as

$$\hat{S} = \hat{\Omega}_{-}^{\dagger}\hat{\Omega}_{+} \tag{61}$$

The scattering operator relates asymptotic reactant states to asymptotic product states.

$$\left|\psi_{out}\right\rangle = \hat{S}\left|\psi_{in}\right\rangle \tag{62}$$

If the Møller states are obtained from arbitrary product and reactant states at $t = 0$ as given by eq. (58), the overlap of the Møller states represents the probability amplitude that the reactant state $\left|\psi\right\rangle$ will scatter into the product state $\left|\phi\right\rangle$ [23]. This overlap is given by

$$\left\langle\psi_{-}\middle|\psi_{+}\right\rangle \tag{63}$$

Recalling the definition of the Møller states, this may be written as

$$
\begin{aligned}
\left\langle\psi_{-}\middle|\psi_{+}\right\rangle &= \left\langle\phi\right|\hat{\Omega}_{-}^{\dagger}\hat{\Omega}_{+}\left|\psi\right\rangle \\
&= \left\langle\phi\right|\hat{S}\left|\psi\right\rangle
\end{aligned}
\tag{64}
$$

So the matrix element $\langle\phi|\hat{S}|\psi\rangle$ gives the probability amplitude that $|\psi\rangle$ will scatter to $|\phi\rangle$.

Representing the States

A common choice for representing the states $|\psi\rangle$ and $|\phi\rangle$ is the basis of eigenstates of the asymptotic Hamiltonian $\hat{H}_0$, which we will label as $|k_\gamma,\gamma\rangle$ where γ identifies the quantum numbers associated with all internal degrees of freedom. These eigenstates have eigenvalues given by

$$\hat{H}_0|k_\gamma,\gamma\rangle = E|k_\gamma,\gamma\rangle = \left(\frac{\hbar^2 k_\gamma{}^2}{2m} + E_\gamma\right)|k_\gamma,\gamma\rangle \tag{65}$$

where $\frac{\hbar^2 k_\gamma{}^2}{2m}$ is the relative kinetic energy and E_γ is the energy associated with internal degrees of freedom, and E is the total energy.

Another set of states that will later prove useful is obtained by operating on this original basis with the Møller operators:

$$|k_\gamma,\gamma\pm\rangle = \hat{\Omega}_\pm|k_\gamma,\gamma\rangle \tag{66}$$

These new states are eigenstates of the full Hamiltonian $\hat{H}$. From the definition in (66)

$$\begin{aligned}\hat{\Omega}_\pm\hat{H}_0|k_\gamma,\gamma\rangle &= \hat{\Omega}_\pm\left(\frac{\hbar^2 k_\gamma{}^2}{2m} + E_\gamma\right)|k_\gamma,\gamma\rangle \\ &= \left(\frac{\hbar^2 k_\gamma{}^2}{2m} + E_\gamma\right)\hat{\Omega}_\pm|k_\gamma,\gamma\rangle\end{aligned}$$

$$\hat{\Omega}_\pm\hat{H}_0|k_\gamma,\gamma\rangle = \left(\frac{\hbar^2 k_\gamma{}^2}{2m} + E_\gamma\right)|k_\gamma,\gamma\pm\rangle \tag{67}$$

Also using the intertwining relation

$$\hat{\Omega}_{\pm}\hat{H}_0\left|k_\gamma,\gamma\right\rangle = \hat{H}\hat{\Omega}_{\pm}\left|k_\gamma,\gamma\right\rangle$$

$$\hat{\Omega}_{\pm}\hat{H}_0\left|k_\gamma,\gamma\right\rangle = \hat{H}\left|k_\gamma,\gamma\pm\right\rangle \tag{68}$$

Taken together, (67) and (68) show

$$\hat{H}\left|k_\gamma\pm,\gamma\right\rangle = \left(\frac{\hbar^2 k_\gamma{}^2}{2m} + E_\gamma\right)\left|k_\gamma,\gamma\pm\right\rangle \tag{69}$$

which shows $\left|k\pm,\gamma\right\rangle$ are eigenstates of the full Hamiltonian.

The product and reactant states are represented in the $\left|k_\gamma,\gamma\right\rangle$ basis as

$$\left|\psi\right\rangle = \int_{-\infty}^{\infty}\eta^{+}(k_\gamma)\left|k_\gamma,\gamma\right\rangle dk_\gamma \tag{70}$$

$$\left|\phi\right\rangle = \int_{-\infty}^{\infty}\eta^{-}(k_\gamma)\left|k_\gamma,\gamma\right\rangle dk_\gamma \tag{71}$$

Using this we can write the Møller states as

$$\begin{aligned}\left|\psi_{\pm}\right\rangle &= \hat{\Omega}_{\pm}\left|\psi\right\rangle \\ &= \hat{\Omega}_{\pm}\int_{-\infty}^{\infty}\eta^{\pm}(k_\gamma)\left|k_\gamma,\gamma\right\rangle dk_\gamma \\ &= \int_{-\infty}^{\infty}\eta^{\pm}(k_\gamma)\hat{\Omega}_{\pm}\left|k_\gamma,\gamma\right\rangle dk_\gamma\end{aligned}$$

$$\left|\psi_{\pm}\right\rangle = \int_{-\infty}^{\infty}\eta^{\pm}(k_\gamma)\left|k_\gamma,\gamma\pm\right\rangle dk_\gamma \tag{72}$$

Note the η's are the same in equation (72) as in (70) and (71) – that is, the expansion coefficients for the Møller states in the basis of eigenstates of the full Hamiltonian are the same as those of the asymptotic product and reactant states in the basis of eigenstates of the asymptotic Hamiltonian.

These basis states satisfy the orthogonality relation [2]

$$\left\langle k_{\gamma'},\gamma'-\middle|k_\gamma,\gamma+\right\rangle=\frac{\hbar^2\left(\left|k_{\gamma'}\right|\left|k_\gamma\right|\right)^{1/2}}{m}\delta\left(E'-E\right)S^{\gamma,\gamma'}_{k_{\gamma'},k_\gamma} \tag{73}$$

where $S^{\gamma,\gamma'}_{k',k}$ is the on-shell S-matrix element. This element gives the probability amplitude to scatter from an initial state with momentum k_γ and internal state γ to a state with momentum $k_{\gamma'}$ and internal state γ'. Rewrite this using $E=\frac{\hbar^2 k_\gamma{}^2}{2m}+E_\gamma$ giving

$$\left\langle k_{\gamma'},\gamma'-\middle|k_\gamma,\gamma+\right\rangle=\frac{\hbar^2\left(\left|k_{\gamma'}\right|\left|k_\gamma\right|\right)^{1/2}}{m}\delta\left(\tfrac{\hbar^2}{2m}\left(k_\gamma{}^2-k_{\gamma'}{}^2\right)\right)S^{\gamma,\gamma'}_{k_{\gamma'},k_\gamma} \tag{74}$$

This may be recast using two properties of the Dirac delta function:

$$\delta\left(ax\right)=a^{-1}\delta\left(x\right) \tag{75}$$

$$\delta\left(x^2-a^2\right)=\frac{1}{2\left|a\right|}\left(\delta\left(x-a\right)+\delta\left(x+a\right)\right) \tag{76}$$

Rewriting (74) with (75) and (76) gives

$$\left\langle k_{\gamma'},\gamma'-\middle|k_\gamma,\gamma+\right\rangle=\frac{\hbar^2\left(\left|k_{\gamma'}\right|\left|k_\gamma\right|\right)^{1/2}}{m}\frac{2m}{\hbar^2}\frac{1}{2\left|k_{\gamma'}\right|}S^{\gamma,\gamma'}_{k_{\gamma'},k_\gamma}\left(\delta\left(k_\gamma-k_{\gamma'}\right)+\delta\left(k_\gamma+k_{\gamma'}\right)\right)$$

$$\left\langle k_{\gamma'}, \gamma' - \middle| k_{\gamma}, \gamma + \right\rangle = \frac{\left|k_{\gamma}\right|^{1/2}}{\left|k_{\gamma'}\right|^{1/2}} S^{\gamma,\gamma'}_{k_{\gamma'},k_{\gamma}} \left(\delta\left(k_{\gamma} - k_{\gamma'}\right) + \delta\left(k_{\gamma} + k_{\gamma'}\right)\right) \tag{77}$$

These relations are instrumental in developing a technique for calculating scattering matrix elements based on the correlation function between evolving reactant and product Møller states. This is known as the channel packet method.

The Channel Packet Method

The final piece, calculating the S-matrix elements, has been foreshadowed by the orthogonality relationship expressed in (77). This technique, known as the Channel Packet Method (CPM), is laid out by Weeks and Tannor [2].

Begin by considering the Fourier transform of the Møller state $\left|\psi_{+}\right\rangle$, written in time-dependent form:

$$\left|A_{+}\left(E\right)\right\rangle \equiv \int_{-\infty}^{\infty} e^{iEt/\hbar} \left|\psi_{+}(t)\right\rangle dt = \int_{-\infty}^{\infty} e^{iEt/\hbar} e^{-i\hat{H}t/\hbar} \left|\psi_{+}\right\rangle dt \tag{78}$$

Using the expansion given by (72),

$$\begin{aligned} \left|A_{+}\left(E\right)\right\rangle &= \int_{-\infty}^{\infty} e^{iEt/\hbar} e^{-i\hat{H}t/\hbar} \int_{-\infty}^{\infty} \eta^{+}(k_{\gamma}) \left|k_{\gamma}, \gamma +\right\rangle dk_{\gamma} dt \\ &= \int_{-\infty}^{\infty} \eta^{+}(k_{\gamma'}) \int_{-\infty}^{\infty} e^{iEt/\hbar} e^{-i\hat{H}t/\hbar} \ \left|k_{\gamma}, \gamma +\right\rangle dt \ dk_{\gamma'} \end{aligned}$$

$$\begin{aligned} \left|A_{+}\left(E\right)\right\rangle &= \int_{-\infty}^{\infty} \eta^{+}(k_{\gamma'}) \left|k_{\gamma}, \gamma +\right\rangle \int_{-\infty}^{\infty} e^{i\left(\frac{\hbar^{2}k_{\gamma}{}^{2}}{2m} + E_{\gamma}\right)t/\hbar} e^{-i\left(\frac{\hbar^{2}k_{\gamma'}{}^{2}}{2m} + E_{\gamma}\right)t/\hbar} \ dt \ dk_{\gamma'} \\ &= \int_{-\infty}^{\infty} \eta^{+}(k_{\gamma'}) \left|k_{\gamma}, \gamma +\right\rangle \int_{-\infty}^{\infty} e^{i\frac{\hbar}{2m}\left(k_{\gamma}{}^{2} - k_{\gamma'}{}^{2}\right)t} \ dt \ dk_{\gamma'} \end{aligned} \tag{79}$$

The second part of (79) represents a delta function

$$\int_{-\infty}^{\infty} e^{i\frac{\hbar}{2m}\left(k_{\gamma}{}^{2}-k_{\gamma'}{}^{2}\right)t}\,dt = 2\pi\delta\left(\tfrac{\hbar}{2m}\left(k_{\gamma'}{}^{2}-k_{\gamma}{}^{2}\right)\right) \tag{80}$$

Using (80), along with (75) and (76) rewrite (79) as

$$\left|A_{+}\left(E\right)\right\rangle = \int_{-\infty}^{\infty} \eta^{+}(k_{\gamma'})\left|k_{\gamma},\gamma+\right\rangle\left(\tfrac{2\pi m}{\hbar\left|k_{\gamma}\right|}\left(\delta\left(k_{\gamma'}-k_{\gamma}\right)+\delta\left(k_{\gamma'}+k_{\gamma}\right)\right)\right)\,dk_{\gamma'}$$

$$\left|A_{+}\left(E\right)\right\rangle = \tfrac{2\pi m}{\hbar\left|k_{\gamma}\right|}\left(\eta^{+}(+k_{\gamma})\left|+k_{\gamma},\gamma+\right\rangle+\eta^{+}(-k_{\gamma})\left|-k_{\gamma},\gamma+\right\rangle\right) \tag{81}$$

Next evaluate the scalar product $\left\langle\psi_{-}\middle|A_{+}\left(E\right)\right\rangle$. Using (72) to expand the Møller state this is

$$\left\langle\psi_{-}\middle|A_{+}\left(E\right)\right\rangle = \int_{-\infty}^{\infty} \eta^{-*}\left(k_{\gamma'}\right)\left\langle k_{\gamma'},\gamma'-\right|\tfrac{2\pi m}{\hbar\left|k_{\gamma}\right|}\left(\eta^{+}(+k_{\gamma})\left|+k_{\gamma},\gamma+\right\rangle+\eta^{+}(-k_{\gamma})\left|-k_{\gamma},\gamma+\right\rangle\right)dk_{\gamma'}$$

$$= \tfrac{2\pi m}{\hbar\left|k_{\gamma}\right|}\int_{-\infty}^{\infty}\left(\eta^{-*}\left(k_{\gamma'}\right)\eta^{+}(+k_{\gamma})\left\langle k_{\gamma'},\gamma'-\middle|+k_{\gamma},\gamma+\right\rangle+\eta^{-*}\left(k_{\gamma'}\right)\eta^{+}(-k_{\gamma})\left\langle k_{\gamma'},\gamma'-\middle|-k_{\gamma},\gamma+\right\rangle\right)dk_{\gamma'} \tag{82}$$

Using the orthogonality relation from (77) this is

$$\begin{aligned}\left\langle\psi_{-}\middle|A_{+}\left(E\right)\right\rangle = \frac{2\pi m}{\hbar\left(\left|k_{\gamma'}\right|\left|k_{\gamma}\right|\right)^{1/2}}\int_{-\infty}^{\infty}&\eta^{-*}\left(k_{\gamma}\right)\eta^{+}(+k_{\gamma})S_{k_{\gamma'},k_{\gamma}}^{\gamma,\gamma'}\left(\delta\left(k_{\gamma}-k_{\gamma'}\right)+\delta\left(k_{\gamma}+k_{\gamma'}\right)\right)\\ &+\eta^{-*}\left(k_{\gamma'}\right)\eta^{+}(-k_{\gamma})S_{k_{\gamma'},k_{\gamma}}^{\gamma,\gamma'}\left(\delta\left(k_{\gamma}-k_{\gamma'}\right)+\delta\left(k_{\gamma}+k_{\gamma'}\right)\right)dk_{\gamma'}\end{aligned}$$

$$\begin{aligned}\left\langle \psi_- \middle| A_+ \left(E\right)\right\rangle = \tfrac{2\pi m}{h\left(\left|k_{\gamma'}\right|\left|k_\gamma\right|\right)^{1/2}} \Big[& \eta^{-*}\left(-k_\gamma\right)\eta^{+}(+k_\gamma)S^{\gamma,\gamma'}_{-k_{\gamma'},+k_\gamma} \\ & +\eta^{-*}\left(+k_\gamma\right)\eta^{+}(+k_\gamma)S^{\gamma,\gamma'}_{+k_{\gamma'},+k_\gamma} \\ & +\eta^{-*}\left(-k_\gamma\right)\eta^{+}(-k_\gamma)S^{\gamma,\gamma'}_{-k_{\gamma'},-k_\gamma} \\ & +\eta^{-*}\left(+k_\gamma\right)\eta^{+}(-k_\gamma)\,S^{\gamma,\gamma'}_{+k_{\gamma'},-k_\gamma} \Big]\end{aligned} \tag{83}$$

Recall that the expansion coefficients $\eta^{\pm}\left(k_\gamma\right)$ simply describe the momentum representation of the initial wavepacket we wish to propagate. Hence we are free to impose certain restrictions which will simplify eq (83). For example, we can choose to select an asymptotic product state which only has positive momentum – that is, we impose the restriction

$$\eta^{-}\left(-k_\gamma\right) = 0 \tag{84}$$

It is worth noting that apart from being mathematically expedient, choosing an incoming wavepacket with entirely positive momentum is practical [2], as instead of spreading out in all directions all of the wavepacket will propagate towards the interaction region we wish to examine. Similarly, reactant wavepackets are chosen to have only negative momentum:

$$\eta^{+}\left(+k_\gamma\right) = 0 \tag{85}$$

Imposing the restriction from (84) onto (83) results in all but the second term on the right side being zero:

$$\eta^{\pm}\left(-k_\gamma\right) = 0 \rightarrow \left\langle \psi_- \middle| A_+ \left(E\right)\right\rangle = \tfrac{2\pi m}{h\left(\left|k_{\gamma'}\right|\left|k_\gamma\right|\right)^{1/2}}\eta^{-*}\left(+k_\gamma\right)\eta^{+}(+k_\gamma)S^{\gamma,\gamma'}_{+k',+k} \tag{86}$$

Alternately, by choosing appropriate combinations of the asymptotic product and/or reactant states containing all positive or all negative momentum, all but the first, third, or fourth terms may be set to zero. Each of these cases gives a simplified form of (83), which can be summarized as

$$\left\langle \psi_- \middle| A_+(E) \right\rangle = \frac{2\pi m}{\hbar\left(\left|k_{\gamma'}\right|\left|k_\gamma\right|\right)^{1/2}}\left[\eta^{\pm *}(\pm k')\,\eta^{+}(\pm k)\,S^{\gamma,\gamma'}_{\pm k',\pm k}\right] \tag{87}$$

This expression can now be inverted to solve for the on-shell S-matrix element

$$S^{\gamma'\gamma}_{\pm k',\pm k} = \frac{\hbar\left(\left|k_{\gamma'}\right|\left|k_\gamma\right|\right)^{1/2}\left\langle \psi_- \middle| A_+(E) \right\rangle}{2\pi m \eta^{-*}(\pm k')\,\eta^{+}(\pm k)} \tag{88}$$

For its final form, use eq. (78) to write this as

$$S^{\gamma'\gamma}_{\pm k',\pm k} = \frac{\hbar\left(\left|k_{\gamma'}\right|\left|k_\gamma\right|\right)^{1/2}\int_{-\infty}^{\infty} e^{iEt/\hbar} C(t)\,dt}{2\pi m \eta^{-*}(\pm k')\,\eta^{+}(\pm k)} \tag{89}$$

where the correlation function

$$C(t) = \left\langle \psi_- \middle| \psi_+(t) \right\rangle \tag{90}$$

is defined between the stationary product Møller state $\left|\psi_-\right\rangle$ and the evolving reactant Møller state $\left|\psi_+(t)\right\rangle$. The Fourier transform of the correlation $\int_{-\infty}^{\infty} e^{iEt/\hbar} C(t)\,dt$ is explicitly a function of energy. The remaining terms are implicating functions of energy by the relation

$$k = \sqrt{2\mu_{B_{H_2}}\left(E - E_\gamma\right)}\,/\,\hbar \tag{91}$$

The internal energy E_γ is associated with any energy offset of the surface as well as any internal degrees of freedom.

Scattering on the B+H_2 Potential Energy Surfaces

The effective PES for $B + H_2$ on which the wavepackets will be propagated are two-dimensional depending on *r* and *R*. As was used in the derivation of the channel packet method (see for example eqs. (70) and (71)), the product and reactant wavepackets are chosen to be the direct product of eigenstates of the asymptotic Hamiltonian. In the *r* dimension this is an eigenstate of the numerical potential, which must be calculated. As expected from knowledge of the H_2 molecule, this eigenstate will resemble the eigenstate of the Morse oscillator. In the *R* dimension, the eigenstates are those of the free particle. As these are not proper wavefunctions, a linear combination is chosen, which for mathematical convenience will be in the form of a Gaussian.

Initially this wavepacket is chosen to be isolated to only one PES. However eq. (43) shows that successive applications of the full Hamiltonian will mix the states, giving nonzero amplitudes on all PESs. As the wavepacket is propagated forward in time, its correlation function with product states located on each PES may be calculated simultaneously, allowing for the calculation of scattering matrix elements from the reactant state to each of the product states with only one propagation run.

Propagation is facilitated by several practical considerations, which are addressed next.

Absorbing Boundary Conditions

Although the split-operator method of propagation takes advantage of the relatively efficient FFT algorithm, it is nonetheless desirable to limit computation time. This is accomplished by using the smallest practical grid.

As laid out in eq. (89), calculating S-matrix elements using the CPM involves calculating the time-dependent correlation function between reactant and product Møller states. This is typically done by choosing one Møller state to evolve in time, while leaving the other alone. Since the correlation function is defined over all time, from $-\infty$ to ∞, strictly speaking the evolving Møller state needs to be propagated over all time. However, the product Møller states may be selected to be localized [24], so propagation need only be done over the time when the correlation function is nonzero – that is, until the evolving Møller state has propagated sufficiently far out of the interaction region such that there is no significant overlap.

In many cases this still requires propagating for a relatively long time. While waiting for the last residues of the evolving Møller state to leave the interaction region, the rest of the Møller state may have diffused over a large area. Since the split-operator propagator uses the FFT, which operates on a finite set of points under the assumption that the complete data set is periodic [22], should any portion of the evolving Møller state reach the edge of the grid it will erroneously reappear on the other side. It will then continue to propagate, potentially reentering the interaction region and introducing error into the correlation function.

Simply increasing the grid size to accommodate the evolving Møller state over the entire time interval necessary to calculate the correlation function will greatly increase the computational effort required. A more efficient solution is to introduce absorbing boundary conditions (ABCs) [24]. ABCs are nonphysical potentials that are added near the edge of the grid so that when evolving states approach them they are attenuated. ABCs are placed outside the interaction region in a location where the product Møller state has zero amplitude. They must also be located so that they do no attenuate portions of the wavepacket which will eventually enter the region of the product Møller state. These rules ensure the correlation function between the product Møller state and evolving reactant Møller states is not affected, causing the ABC to not alter the calculation of the S-matrix elements.

Absorbing boundary conditions are imaginary-valued, such that the new potential takes the form

$$\hat{V} = \hat{V}_0 \pm i\hat{V}_{abc} \tag{92}$$

where $\hat{V}_0$ is the original potential. Adding the ABC causes the time-evolution operator to become

$$\begin{aligned} \hat{U}\left(\Delta t\right) &= e^{-i\hat{H}\Delta t/\hbar} \\ &= e^{-i\hat{T}\Delta t/\hbar - i\left(\hat{V}_0 \pm i\hat{V}_{abc}\right)\Delta t/\hbar} \end{aligned} \tag{93}$$

The sign is chosen depending on whether the propagation will go forward or backward in time. If Δt is positive, the time-evolution operator will attenuate the wavepacket if $\hat{V}_{abc}$ is chosen to be negative. If Δt is negative, $\hat{V}_{abc}$ is chosen to be positive.

The ABC must be chosen so that it completely attenuates the wavepacket. Its amplitude must be sufficient to ensure it does not transmit any of the wavepacket, and its shape should be such that it does not reflect the wavepacket. A common choice is that of the Gaussian – in one dimension it would take the form

$$V_{abc}\left(x\right) = Ae^{-\left(x-x_0\right)^2/B} \tag{94}$$

Where A and B are chosen to meet the criteria described above. If the Gaussian is too narrow, some of the incoming wavepacket will be reflected. If it is too broad, the ABC may intrude into the interaction region, introducing error.

Other Practical Grid Considerations

The use of absorbing boundary conditions removes the necessity of using a huge grid by attenuating any part of the wavepacket that propagates well away from the interaction region. However there are still several practical considerations when selecting a grid for propagation.

Møller States and the Asymptotic Limit

Calculating S-matrix elements using the CPM involves obtaining the time-dependent correlation function between the reactant and product Møller states. Logically the first step in this process is to calculate the Møller states. Judicious selection of the initial states can greatly simplify this step, and will play a small role in grid selection.

The Møller states are defined (see eq. (58) along with the definition of the Møller operators in eqs. (55) and (56)) by propagating the reactant (product) state backwards (forwards) in time to $t = \mp\infty$ under the asymptotic Hamiltonian $\hat{H}_0$, then forwards (backwards) to $t = 0$ under the full Hamiltonian $\hat{H}$. It is straightforward to perform these propagations using the split-operator propagator. However the required computation time (and the small but theoretically nonzero error associated with the propagator) may be avoided entirely by defining the initial states to already be in the asymptotic limit. This choice means that during the propagation $\hat{H} = \hat{H}_0$ and the Møller operators are the identity operator, and the Møller states are simply the initial product and reactant states.

As previously stated, it is desirable to limit the size of the coordinate grid in order to reduce the computation time required. Of course it is necessary to make the grid big enough to 'fit the problem on'. Practically speaking this means it must extend far enough from the interaction region to allow the product and reactant states to be defined in the asymptotic limit. The grid is further extended beyond this point in order to add absorbing boundary conditions, which must be located where the non-evolving Møller state has zero amplitude in order to not interfere with the calculation of the correlation function.

Fourier Transform Pairs: The Coordinate and Momentum Grids

For each dimension the coordinate (and momentum) grid are completely specified by any two of the following parameters (for each dimension of the propagation space): the range $\left(x_{\max} - x_{\min}\right)$, the interval between adjacent points $\left(\Delta x\right)$, and the total number of gridpoints $\left(N_x\right)$. Given any two, the third parameter is simply calculated by some form of the equation

$$\Delta x = \frac{x_{\max} - x_{\min}}{N_x - 1} \tag{95}$$

The choice of which parameters to specify is arbitrary, although for practical considerations directly specifying the range is often advantageous. Although it may seem more natural to specify the interval Δx and let this determine the number of points, frequent use of the FFT algorithm means it will be advantageous to have N_x be a power of 2 [22]. Thus N_x is often the second parameter specified.

As seen by eq. (52), the coordinate and momentum grids are related by the Fourier transform. Therefore when selecting the coordinate grid, the momentum grid is defined as well. The relation between the two is given by [22]

$$\Delta k = \frac{2\pi}{x_{\max} - x_{\min}} \tag{96}$$

The number of points in the momentum grid is of course the same as the number of points in the coordinate grid.

$$N_k = N_x \tag{97}$$

These two parameters completely specify the momentum grid. The range of momentum is calculated from Δk and N_k along with knowledge that the momentum grid will be centered around zero:

$$k_{\max/\min} = \pm \frac{N_k \Delta k}{2} \tag{98}$$

This gives another piece to consider when selecting the grid. Since the range of momentum is never directly chosen and is instead determined by the fineness of the coordinate grid, care should be taken to ensure that during the propagation the wavepacket never reaches momentum values greater than that given by eq. (98). As previously discussed, the FFT assumes periodicity, and similar to the case of the wavepacket going off the grid in the coordinate representation which motivated use of absorbing boundary conditions, the wavepacket can go off the grid in the momentum representation introducing error into the propagation. In the case of the coordinate grid, the localized nature of the product states meant portions of the wavepacket reaching the edge of the grid were no longer relevant to the calculation of the correlation function between the Møller states, and thus could be attenuated by employing absorbing boundary conditions. No equivalent argument exists to allow us attenuation in the momentum representation and the momentum grid simply must be large enough to contain the evolving wavepacket.

Fourier Transform Pairs: The Energy and Time Grids

Besides transforming between the coordinate and momentum representations of the wavepacket for use in the split-operator propagator, another use of the Fourier transform is encountered when calculating S-matrix elements using the channel packet method. That is the Fourier transform of the time-dependent correlation function (eq. (90)), which maps the correlation function, as a function of time, to the S-matrix elements, which are functions of energy. Thus time and energy are Fourier transform pairs, and share the same relationship as the coordinate/momentum pairs:

$$\Delta E = \frac{2\pi}{t_{\max} - t_{\min}} \tag{99}$$

As previously discussed, the correlation function is defined over all time but is only nonzero when the Møller states overlap significantly. The time when the correlation function is nonzero determines the propagation time range $\left(t_{\max} - t_{\min}\right)$. If the initial reactant and product states are chosen to be located in the asymptotic limit, by definition the correlation function is zero at that time and all of the overlap between the fixed and evolving Møller state lies in the future. In that case $t_{\min} = 0$ and $t_{\max}$ must be sufficiently large to capture all overlap between the evolving states. That is, propagation continues until the correlation function goes to zero.

Care should be taken to not truncate the correlation function prematurely. It is not uncommon to encounter long, low-amplitude correlations as residuals of the evolving wavepacket oscillate in the interaction region. Although small in magnitude they recur over a long period of time, so they contribute significantly to the integral over all time.

The time range is therefore determined by the requirement to capture the correlation function all times when it is nonzero. The other piece needing to be specified is either the time step Δt or, equivalently, the number of points N_t. Since the accuracy of the split-operator depends on the smallness of Δt (see eq. (47)), the time step is often the parameter selected. The time range and time step completely specify the energy grid as given by eq. (99) along with

$$N_E = N_t \tag{100}$$

and knowledge that the energy grid will be centered around zero.

If the time range $\left(t_{\max} - t_{\min}\right)$ is fixed by the requirement to capture all of the overlap between the fixed and evolving Møller state and Δt is made successively smaller in the interest of greater accuracy of propagation, the energy grid is made successively larger. It may be the case that the requirement of the split-operator propagator for a small Δt will result in the energy grid being much larger than necessary. In that case, the correlation function may be downsampled before undergoing the Fourier transform when calculating S-matrix elements. Equivalently, the correlation function need not be calculated at every propagation time step.

III. Results and Discussion

The B+H₂ Effective Potential Energy Surfaces

Obtaining the Surfaces

The diabatic effective potential energy surfaces $V_{eff}^{D}\left(r,R\right)_{\gamma,\gamma'}$ as given by eq. (42) are calculated by Fortran code developed by Garvin [1]. The first part of this work was to create a shell script to interact with that existing software to facilitate specifying a coordinate grid and basis size *n* and to save the resulting surfaces in a usable format. First diabatic surfaces as a function of *r* and *R* are calculated for every element in the $n \times n$ diabatic effective potential energy matrix. At every point on the coordinate grid this matrix is diagonalized. The resulting diagonal elements form the *n* adiabatic potential energy surfaces $V_{eff}^{A}\left(r,R\right)_{\gamma}$ which are saved along with the diabatic-to-adiabatic transformation $U_{AD}\left(r,R\right)$ which diagonalized the potential matrix at that point.

The Diabatic Surfaces

A representative selection of diabatic effective PESs $\left\langle \begin{matrix} j' & j_a' \\ k' , & \omega' \end{matrix} \middle| V_{eff}^{D}\left(r,R\right) \middle| \begin{matrix} j & j_a \\ k , & \omega \end{matrix} \right\rangle$ are shown here for several values of j,k,j_a,ω. Both diagonal surfaces and nondiagonal coupling surfaces are considered.

The ground state surface $\left\langle \begin{matrix} 0 & \frac{1}{2} \\ 0 , & \frac{1}{2} \end{matrix} \middle| V_{eff}^{D}\left(r,R\right) \middle| \begin{matrix} 0 & \frac{1}{2} \\ 0 , & \frac{1}{2} \end{matrix} \right\rangle$ quickly resolves to the asymptotic H_2 potential as *R* increases.

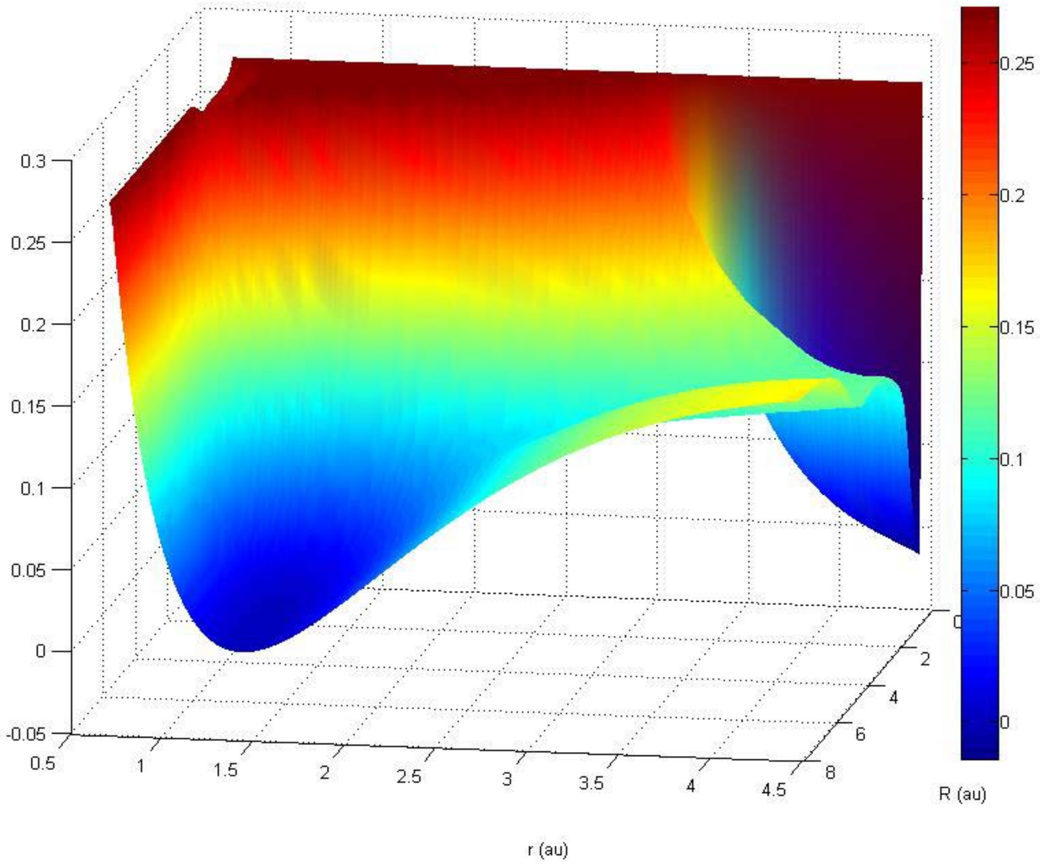

Figure 5. Diabatic Effective Potential Energy Surface $\left\langle \begin{matrix} 0 & \frac{1}{2} \\ 0, & \frac{1}{2} \end{matrix} \right| V_{eff}^{D}\left(r,R\right) \left| \begin{matrix} 0 & \frac{1}{2} \\ 0, & \frac{1}{2} \end{matrix} \right\rangle$

Contours are shown for values from 0 to 0.27 au, with lines every 0.01 au. The process of expanding the numerical surfaces in a truncated basis results in nonphysical features at energies greater than 0.27 au. Since this energy is much higher than those accessible in the collision considered the surfaces have been truncated at 0.27 au. As a result in certain regions, for example the region $r < 3$ au, $R < 2$ au in this plot, contour hatching is visible where the surface has a constant value.

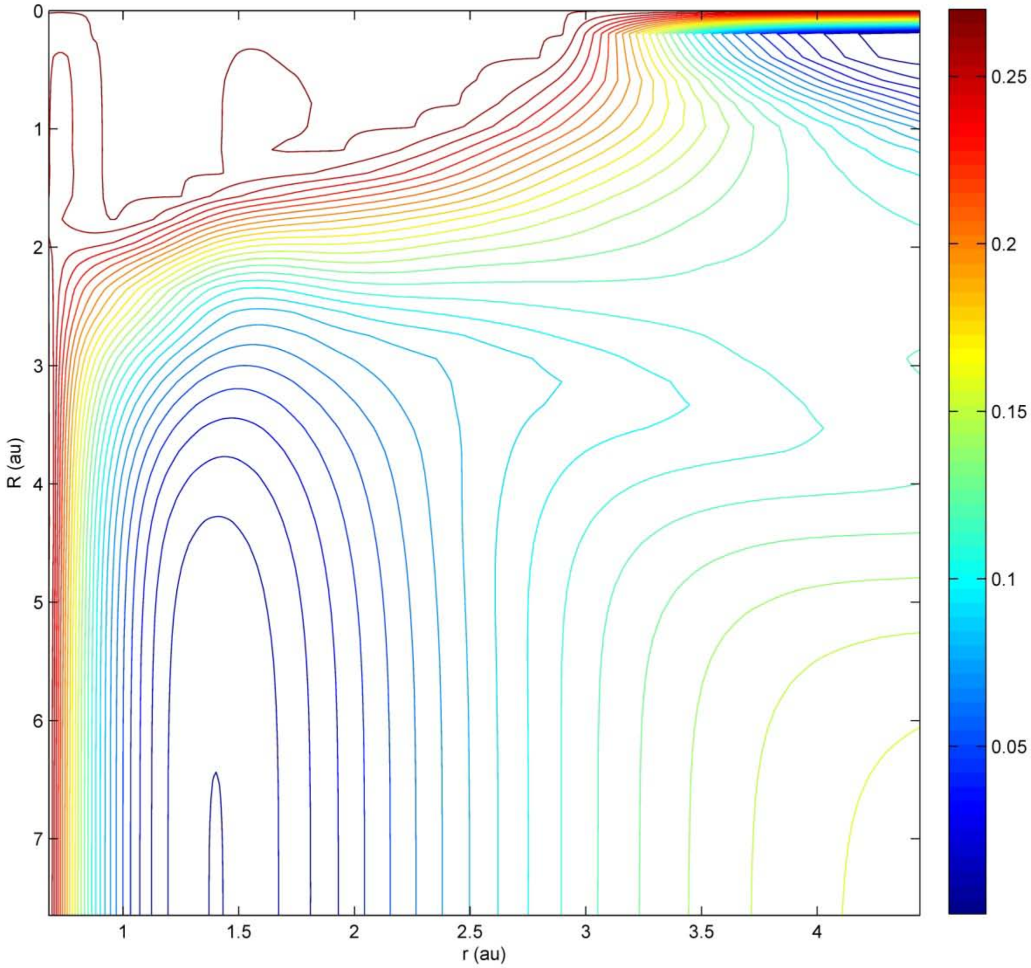

Figure 6. Diabatic Effective Potential Energy Surface $\left\langle \begin{matrix} 0 & \frac{1}{2} \\ 0, & \frac{1}{2} \end{matrix} \middle| V_{eff}^{D}\left(r, R\right) \middle| \begin{matrix} 0 & \frac{1}{2} \\ 0, & \frac{1}{2} \end{matrix} \right\rangle$ **Contour Plot**

The excited surface $\left\langle \begin{matrix} 2 & \frac{3}{2} \\ 0, & \frac{1}{2} \end{matrix} \middle| V_{eff}^{D}(r,R) \middle| \begin{matrix} 2 & \frac{3}{2} \\ 0, & \frac{1}{2} \end{matrix} \right\rangle$ is qualitatively similar to the ground state. It primarily differs in the region of larger *r*, and the asymptotic H_2 potential has been raised in energy and slightly broadened due to the $\frac{\hbar^2 j(j+1)}{2\mu_{H_2} r^2}$ term in the Hamiltonian.

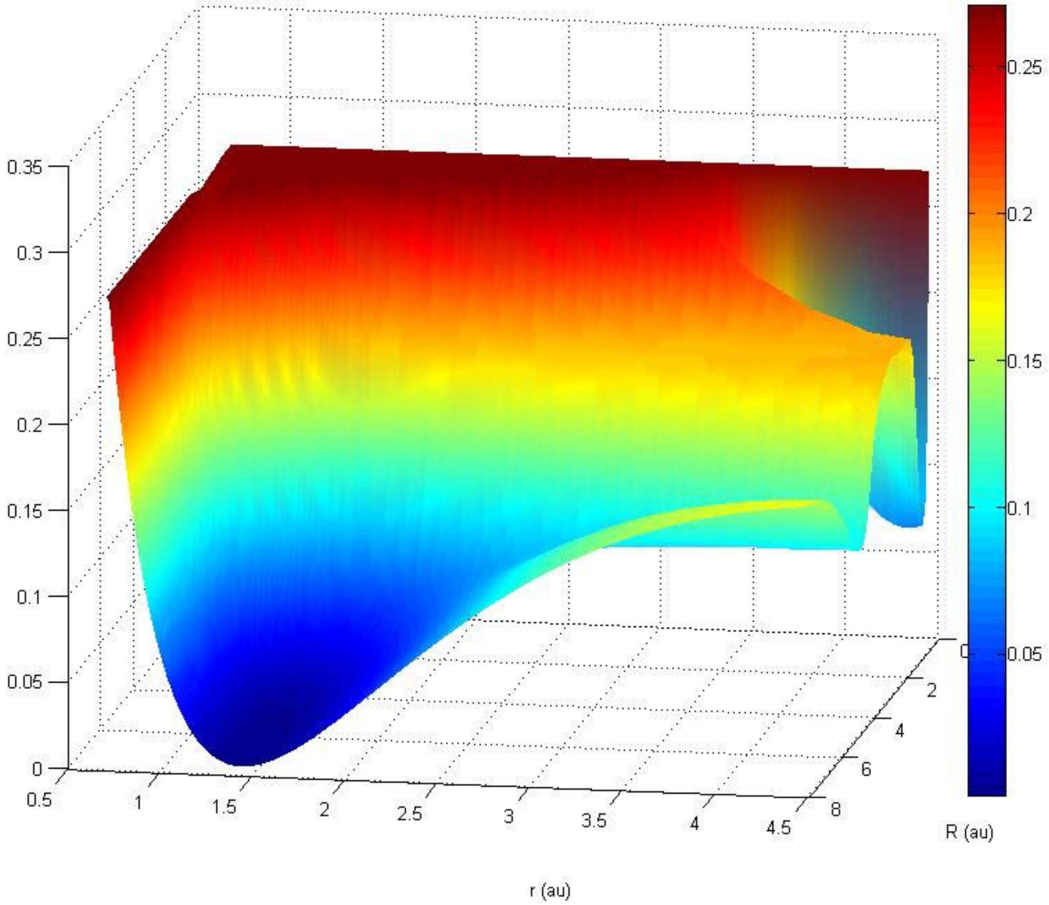

Figure 7. Diabatic Effective Potential Energy Surface $\left\langle \begin{matrix} 2 & \frac{3}{2} \\ 0, & \frac{1}{2} \end{matrix} \middle| V_{eff}^{D}(r,R) \middle| \begin{matrix} 2 & \frac{3}{2} \\ 0, & \frac{1}{2} \end{matrix} \right\rangle$

Contours are shown for values from 0 to 0.27 au, with lines every 0.01 au.

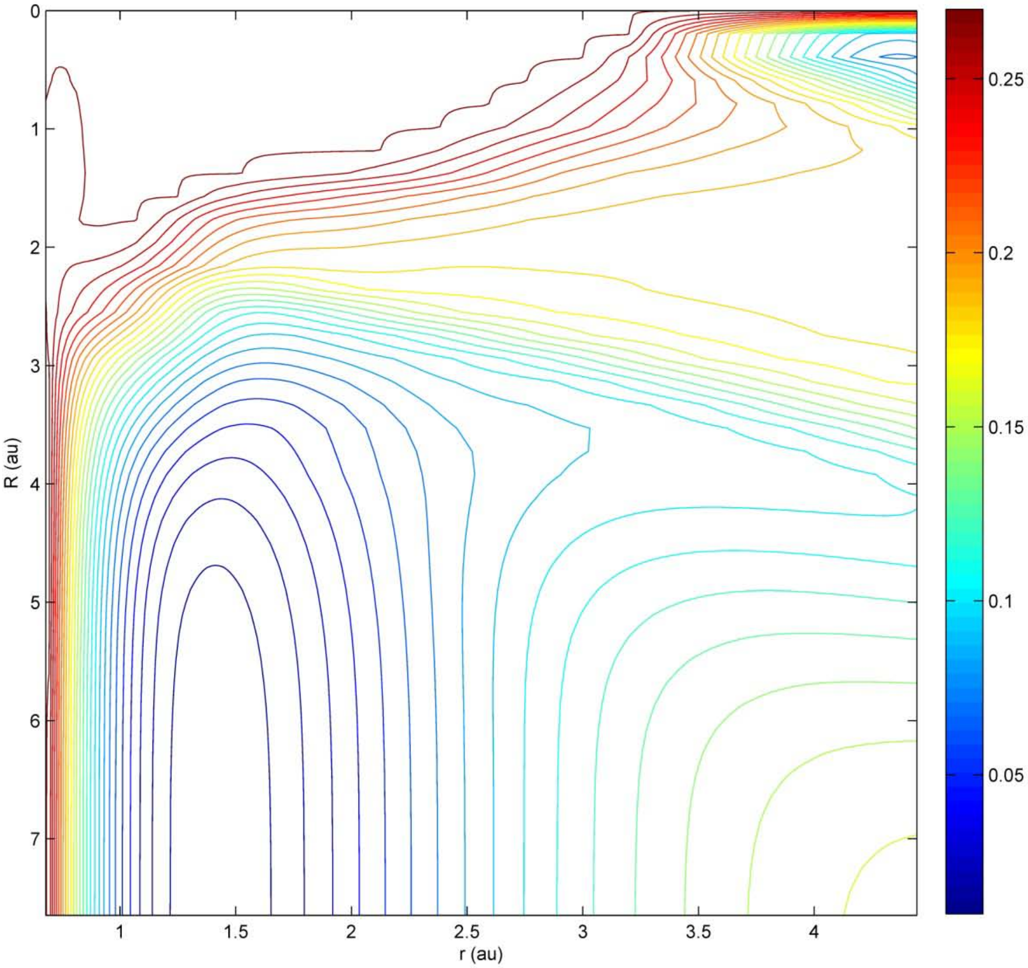

Figure 8. Diabatic Effective Potential Energy Surface $\left\langle {2 \atop 0}, {\frac{3}{2} \atop \frac{1}{2}} \middle| V_{eff}^{D}(r,R) \middle| {2 \atop 0}, {\frac{3}{2} \atop \frac{1}{2}} \right\rangle$ **Contour Plot**

Off-diagonal terms in the diabatic effective potential energy matrix represent coupling surfaces. A selection of them are shown here.

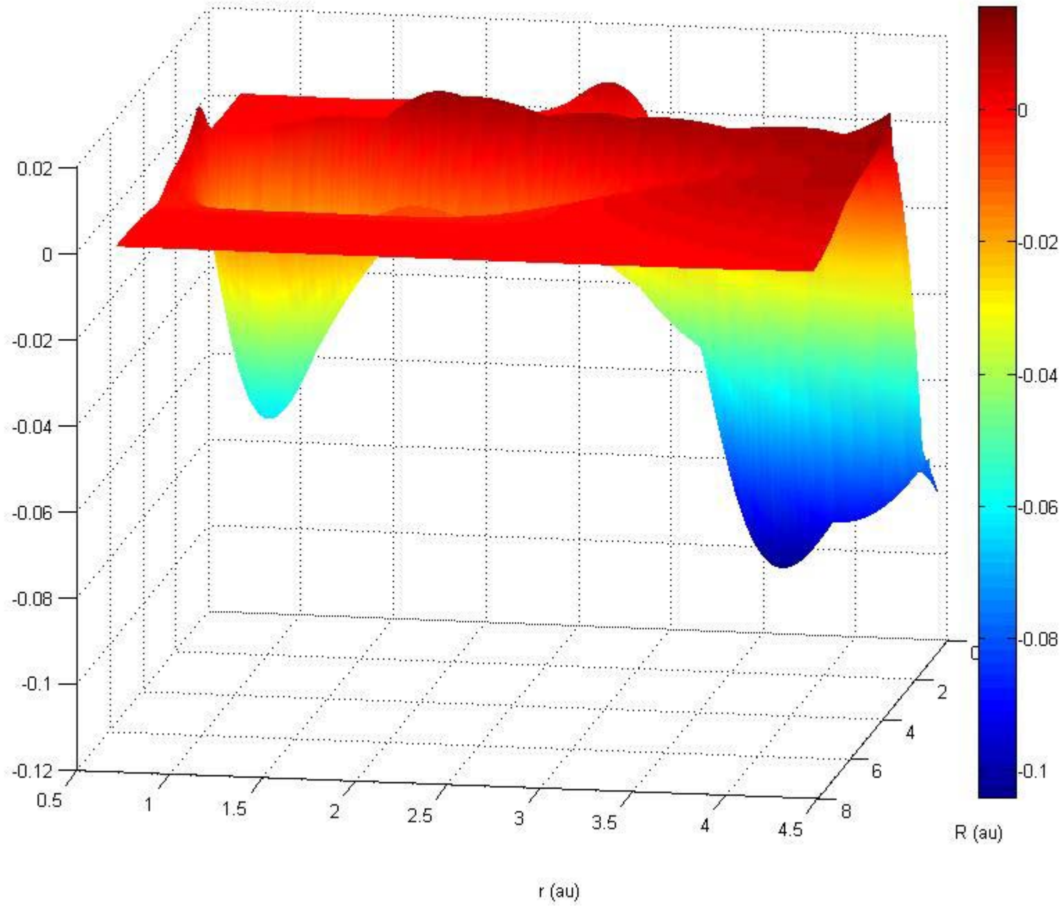

Figure 9. The Coupling Surface $\left\langle \begin{matrix}0 & \frac{1}{2}\\ 0, & \frac{1}{2}\end{matrix} \right| V_{eff}^{D}\left(r,R\right) \left| \begin{matrix}0 & \frac{3}{2}\\ 0, & \frac{1}{2}\end{matrix}\right\rangle$

The coupling surface is near zero for the region $R > 6$ au . This indicates that a wavepacket initially located on the ground state $\left| \begin{matrix}0 & \frac{1}{2}\\ 0, & \frac{1}{2}\end{matrix}\right\rangle$ will couple only very weakly to the state $\left| \begin{matrix}0 & \frac{3}{2}\\ 0, & \frac{1}{2}\end{matrix}\right\rangle$ in this region.

Contours are shown from -0.12 au to .02 au with lines every 0.005 au. Contour line hatching is again visible in regions where the surface has a constant value.

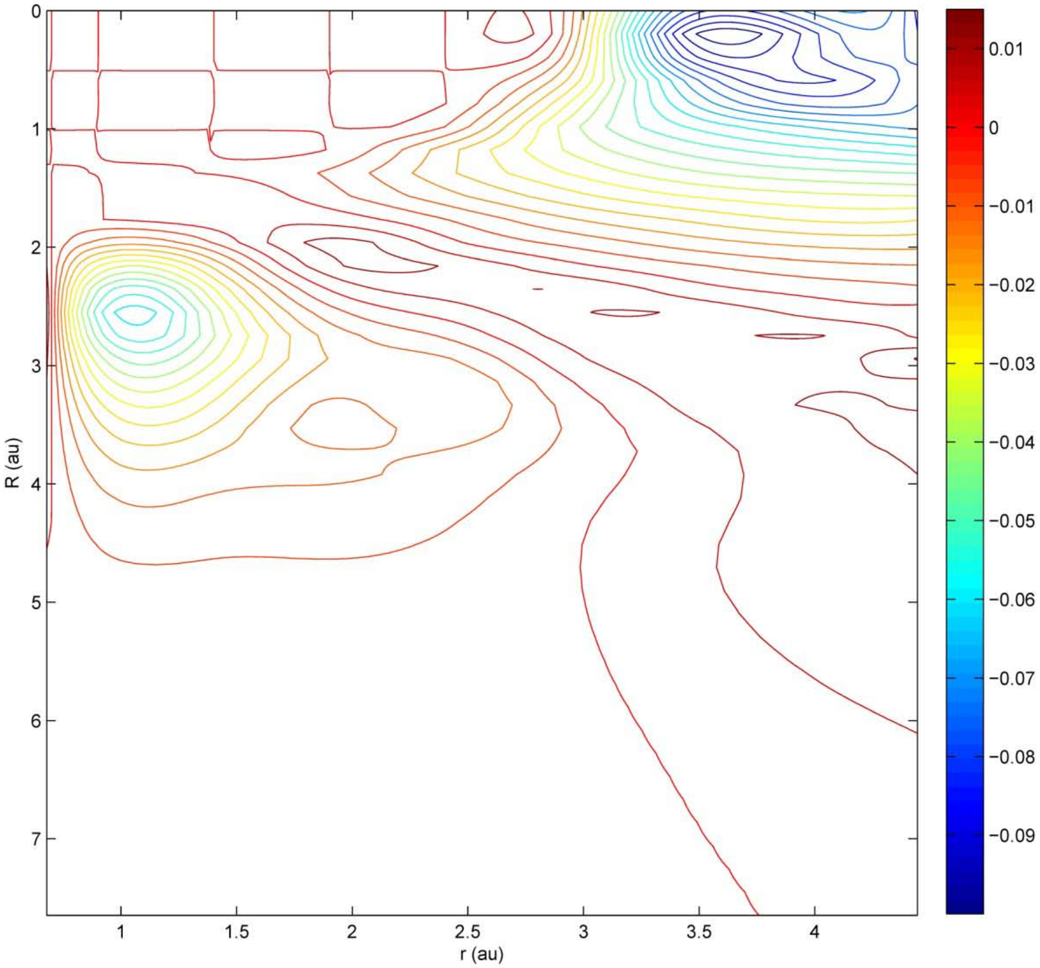

Figure 10. The Coupling Surface $\left\langle \begin{matrix} 0 & \frac{1}{2} \\ 0, & \frac{1}{2} \end{matrix} \middle| V_{eff}^{D}(r,R) \middle| \begin{matrix} 0 & \frac{3}{2} \\ 0, & \frac{1}{2} \end{matrix} \right\rangle$ **Contour Plot**

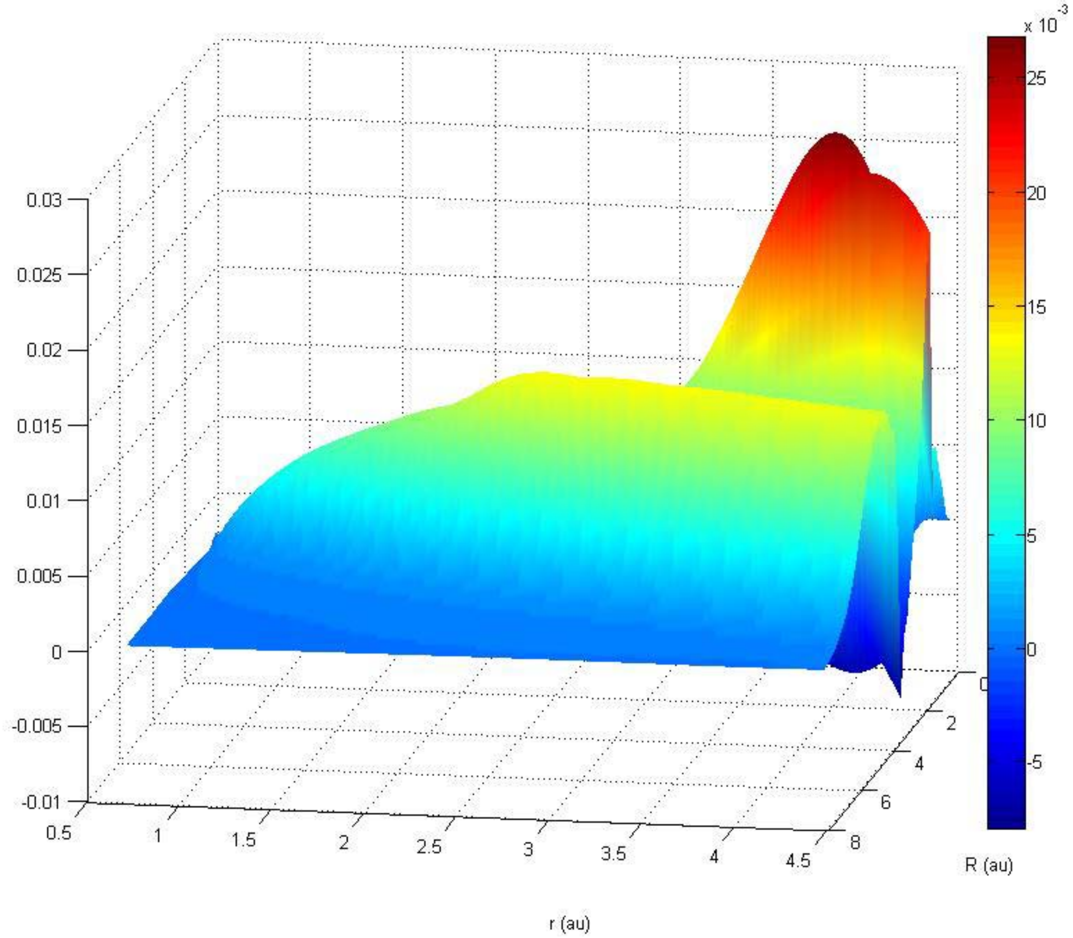

Figure 11. The Coupling Surface $\left\langle {0 \atop 0},{\tfrac{3}{2} \atop \tfrac{1}{2}} \right| V_{eff}^{D}\left(r,R\right) \left| {1 \atop 1},{\tfrac{1}{2} \atop -\tfrac{1}{2}} \right\rangle$

Contours are shown from -0.01 au to 0.025 au with lines every 0.001 au.

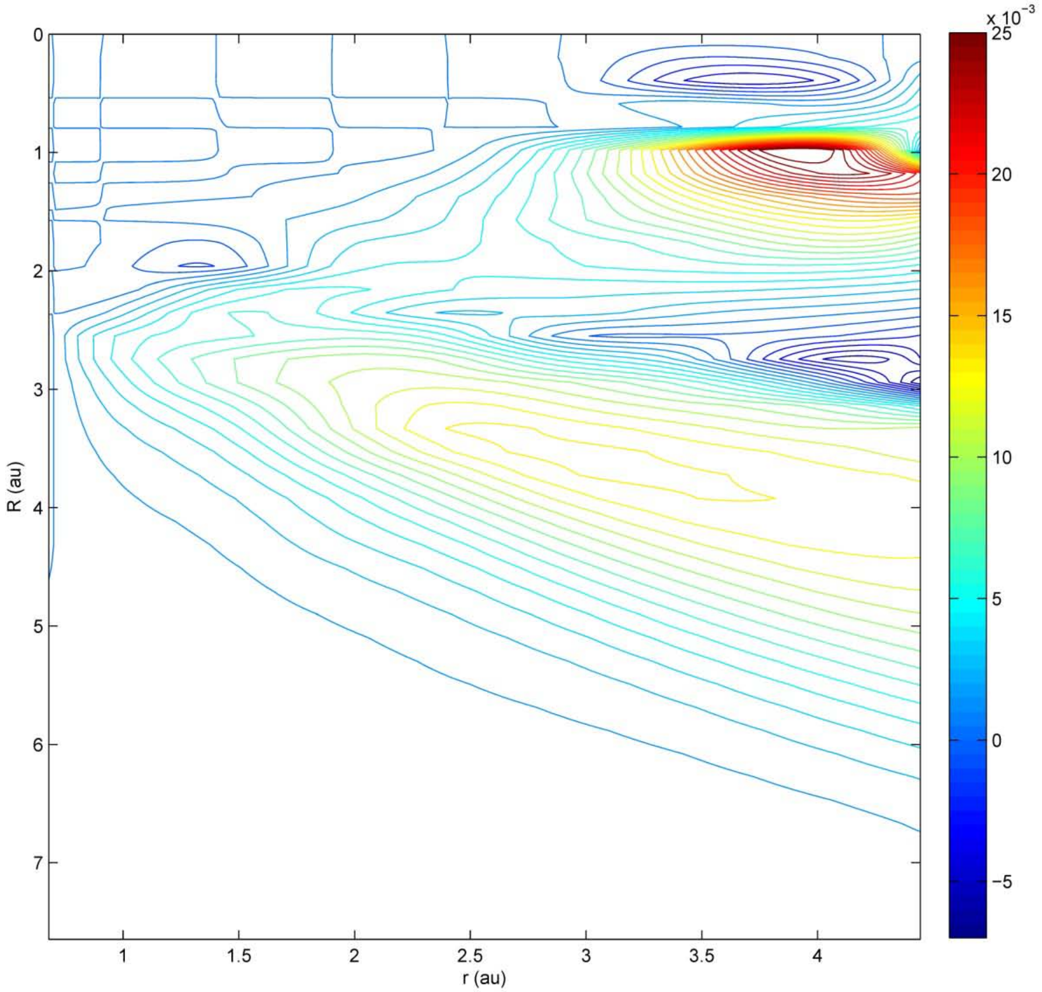

Figure 12. The Coupling Surface $\left\langle \begin{matrix} 0 & \frac{3}{2} \\ 0, & \frac{1}{2} \end{matrix} \right| V_{eff}^{D}\left(r,R\right) \left| \begin{matrix} 1, & \frac{1}{2} \\ 1, & -\frac{1}{2} \end{matrix} \right\rangle$ **Contour Plot**

The Adiabatic Surfaces

While the diabatic surfaces are calculated directly from eq. (42), the adiabatic surfaces are obtained by diagonalizing the diabatic effective potential energy matrix at every point on the coordinate grid. This results in several key differences between the diabatic and the adiabatic surfaces. Unlike the diabatic surfaces the adiabatic surfaces change as a function of the basis size *n* – while increasing *n* simply results in more diabatic surfaces, the adiabatic surfaces change as the transformation mixes in the additional diabatic surfaces. Additionally there is no clear labeling scheme as each adiabatic surface is a mixture of diabatic states with varying $\gamma = \left| \begin{matrix} j & j_a \\ k & \omega \end{matrix} \right\rangle$ basis states. Often they are ordered by increasing energy as this is a common scheme for sorting eigenvalues used by diagonalization algorithms. In fact this ordering is arbitrary, and it is sufficient that the adiabatic potential energy matrix be diagonal at each point on the coordinate grid and that the unitary transformation that diagonalized the matrix at that particular point is known.

The following series of figures shows how the first (lowest) adiabatic surface changes as the basis size is increased. Contours are shown from 0 to 0.27 au with lines every 0.01 au.

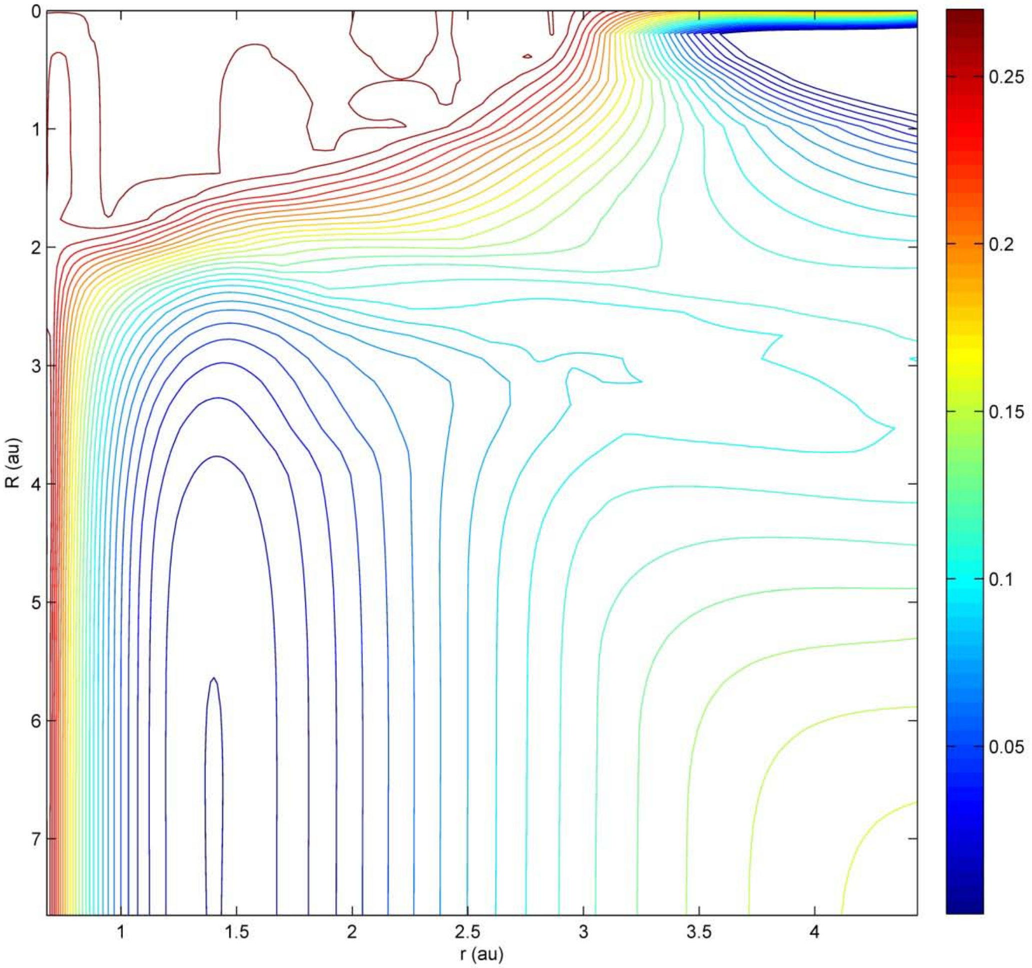

Figure 13. First Adiabatic Surface with Basis Size $n = 2$ Contour Plot

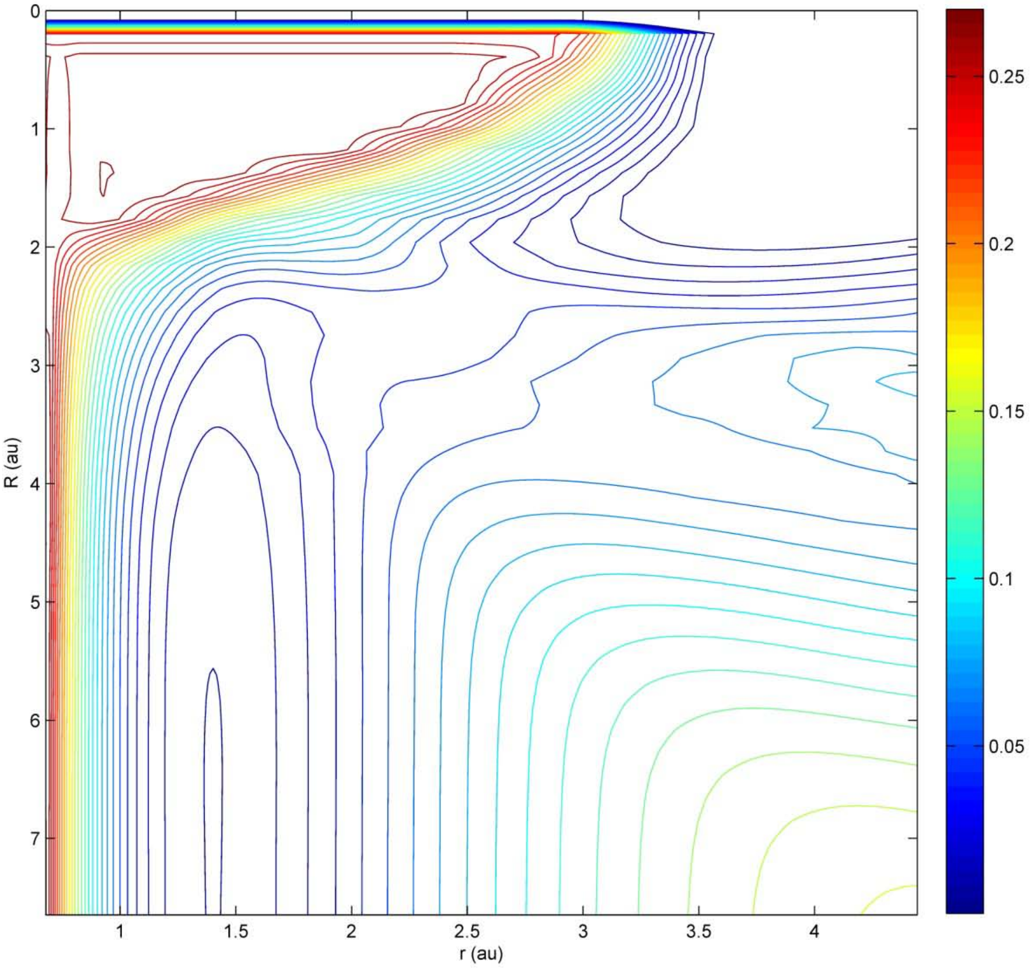

Figure 14. First Adiabatic Surface with Basis Size $n = 8$ Contour Plot

The most interesting change here is the height of the surface in the region around $R = 3$ au, $r = 2.5$ au. This indicates the potential energy that must be overcome in order to access the region of low energy in the upper right corner. This area represents the reaction $B + H_2 \rightarrow BH + H$. As the basis size increase this barrier to reaction decreases.

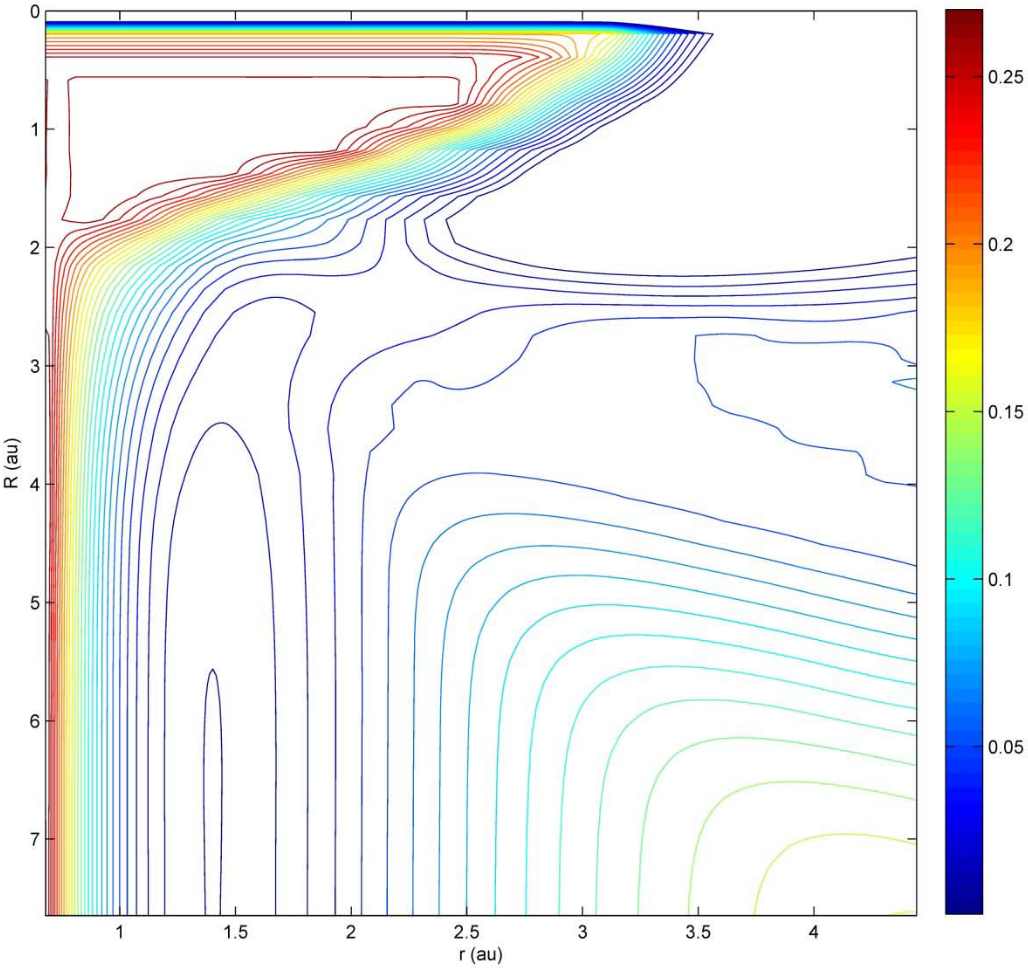

Figure 15. First Adiabatic Surface with Basis Size $n = 14$ Contour Plot

Although the surface does change slightly the addition of states higher than $j = 4$, which corresponds to a basis size $n = 14$, these additions do not appreciably decrease the barrier. Contour plots of this surface with basis sizes $n = 20,\ 26$ appear nearly identical.

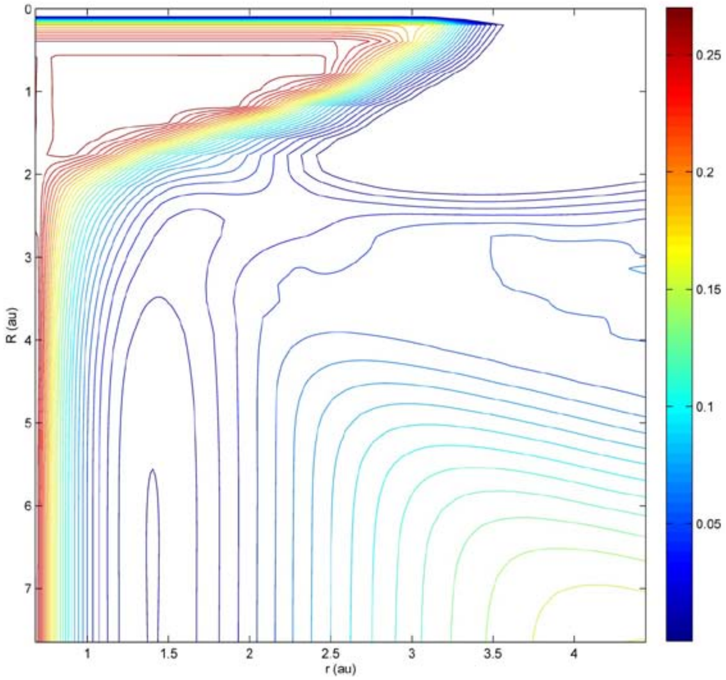

Figure 16. First Adiabatic Surface with Basis Size $n = 20$ Contour Plot

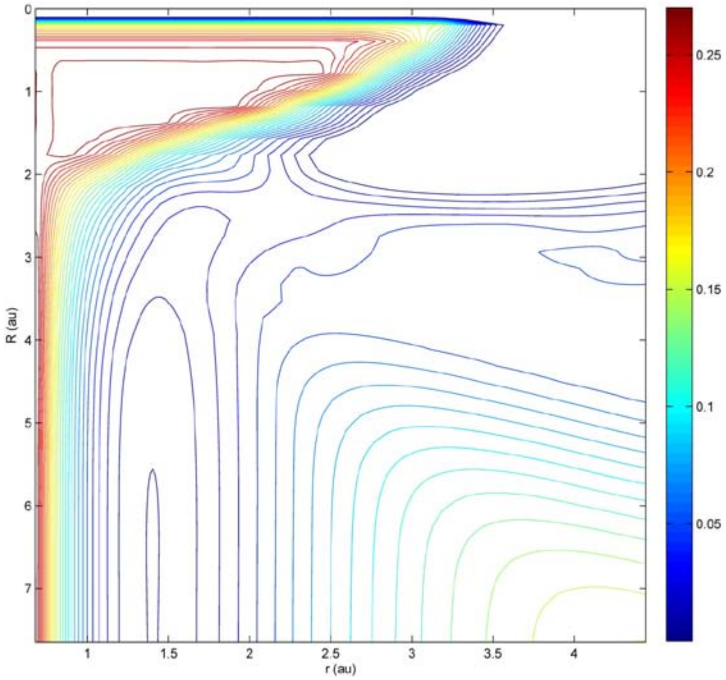

Figure 17. First Adiabatic Surface with Basis Size $n = 26$ Contour Plot

Finally consider the lowest adiabatic potential energy surfaces calculated with a basis size $n = 32$. This is the basis size used in this work.

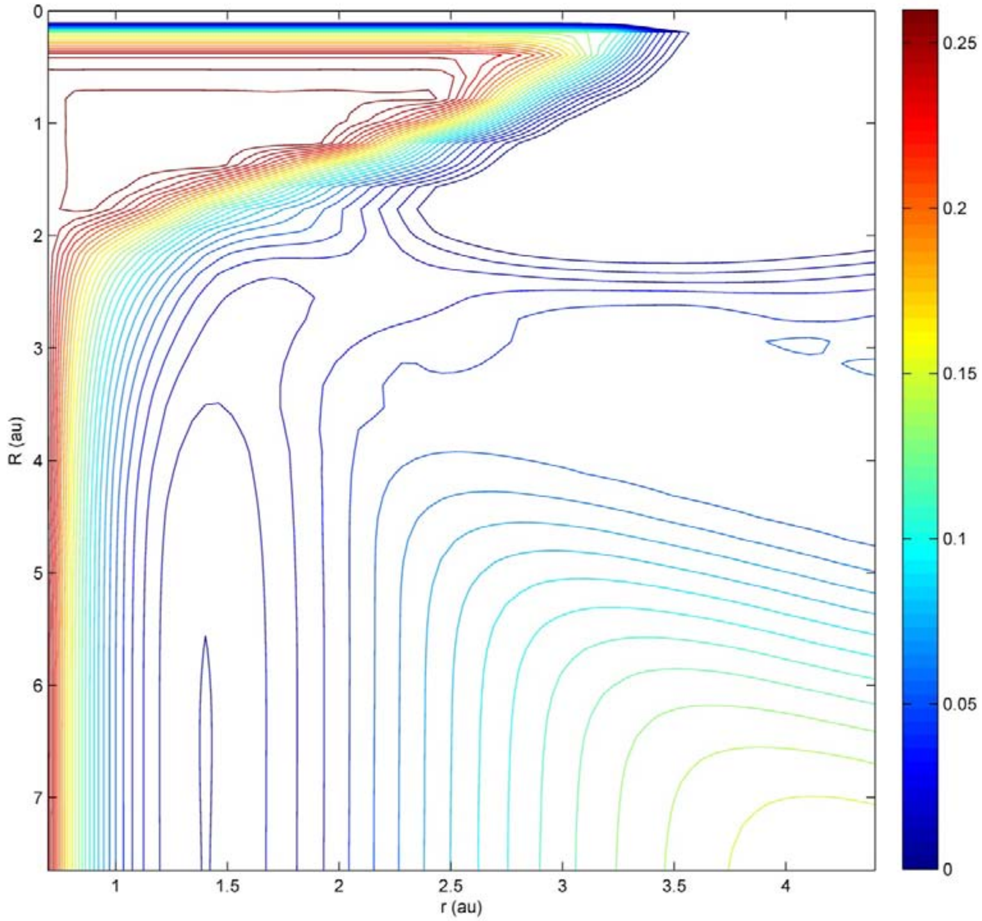

Figure 18. First Adiabatic Surface with Basis Size $n = 32$ Contour Plot

Asymptotic Eigenstates

In preparation for propagating on these surfaces eigenstates of the asymptotic Hamiltonian need to be prepared. In the limit of large *R* the diagonal diabatic potential energy surfaces as given by eq. (42) become

$$\left\langle \begin{matrix} j & j_a \\ k & \omega \end{matrix} \middle| V_{eff}^{D} \middle| \begin{matrix} j & j_a \\ k & \omega \end{matrix} \right\rangle = \frac{j(j+1)}{2\mu_{H_2} r^2} + V_{H_2}(r) + E_{el} + E_{so} + E_{off} \tag{101}$$

The energy offset is chosen to be

$$E_{off} = -E_{el} - V_{H_2}(r_{eq}) \tag{102}$$

placing the zero of the energy between the spin-orbit split $j = 0$ states at the minimum of the $V_{H_2}(r)$ potential.

In the asymptotic limit the R cross-section of the surfaces follow the H_2 rotor spectrum with each level being split by spin-orbit coupling.

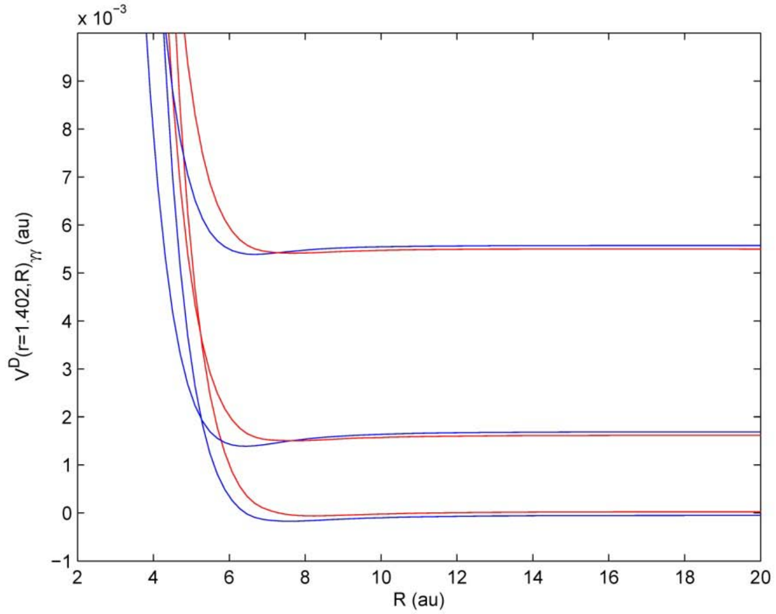

Figure 19. Diabatic Potential Energy Surfaces Cross-section at r_{eq}

The asymptotic potential in the R dimension is that of the free particle. When selecting a wavepacket for propagation any normalizable superposition of plane waves is appropriate. For convenience a Gaussian is chosen.

In the asymptotic limit the cross-section of the $j = 0$ surface should be the $V_{H_2}(r)$ potential. When compared to the $V_{H_2}(r)$ potential of Liu-Siegbahn-Truhlar-Horowitz [25] [26] (LSTH), it was noted that although there was good agreement at the points included in the original *ab initio* calculation, the interpolation between those points differed to some degree. By supplying the interpolation routine with additional points from the LSTH potential, this discrepancy was resolved as shown in the following figure.

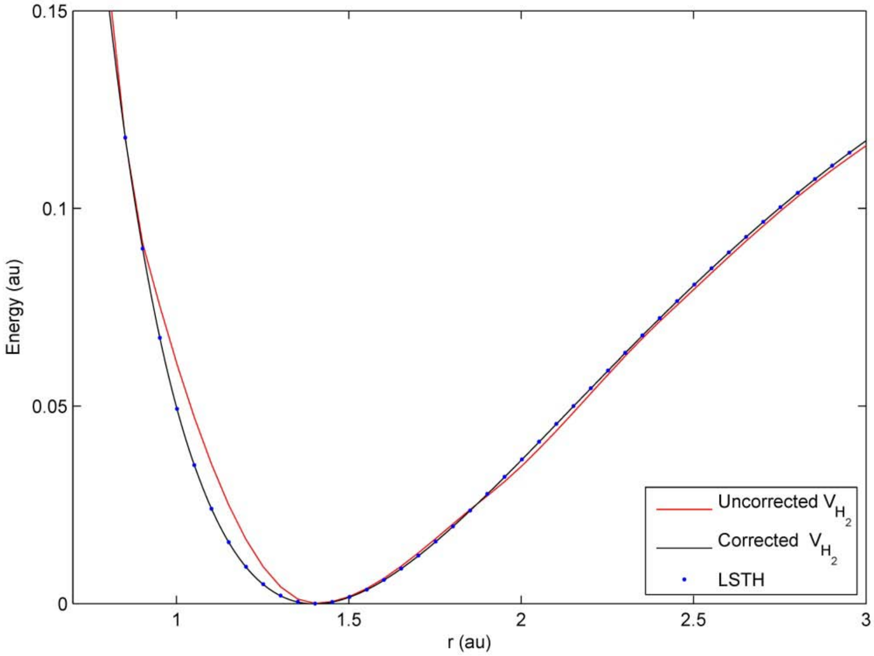

Figure 20. Correction to Asymptotic H_2 Potential

The cross-sections for values of *j* higher than 0 are offset by the appropriate rotor and spin orbit energies, and the shape is slightly changed by the presence of the $\frac{j(j+1)}{2\mu_{H_2} r^2}$ term.

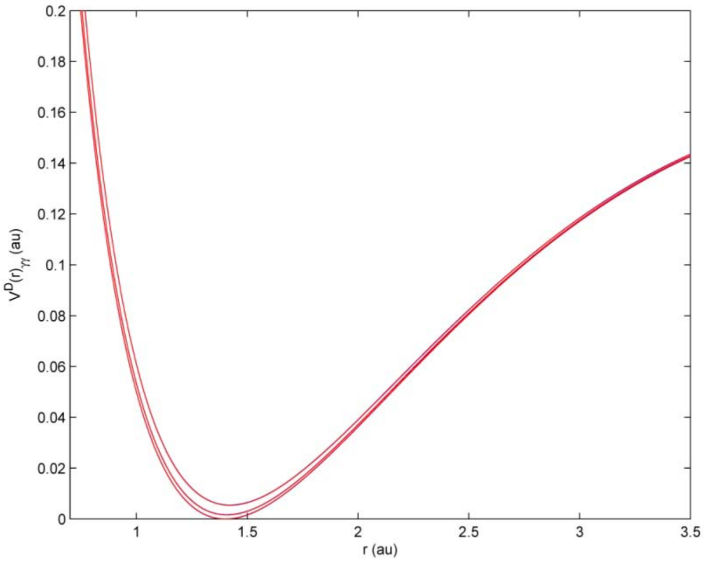

Figure 21. Cross-sections of the Diabatic PESs for $j = 0, 2, 4$ at Limit of Large *R*

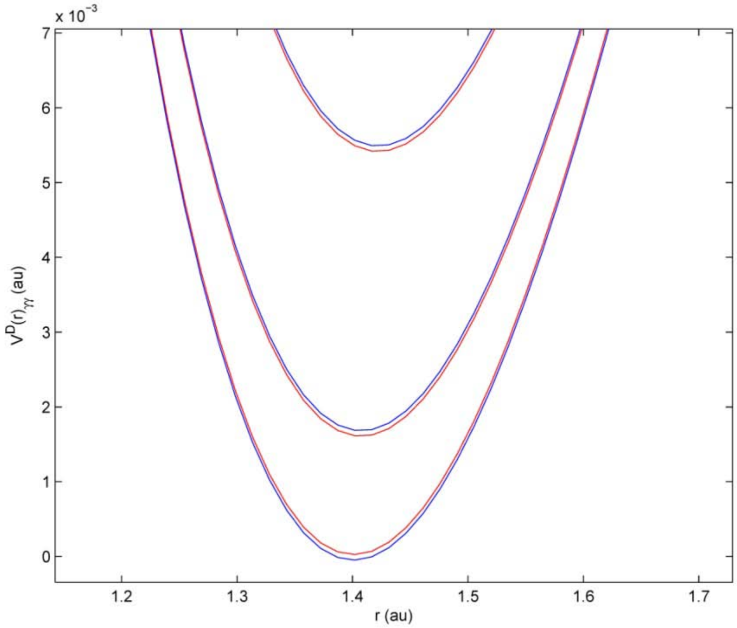

Figure 22. Detail of Diabatic PES Cross-sections for $j = 0, 2, 4$ Around $r = 1.402$ au Showing Spin-Orbit Splitting

Unlike the case in the *R*-direction, the eigenstates in the *r*-direction must be determined numerically. This is done by expanding in a basis of the eigenstates of the simple harmonic oscillator.

In the asymptotic limit and at some fixed *R* the Hamiltonian is given by

$$\hat{H}_a = \hat{T} + \hat{V}_r = \frac{\hat{p}_r^2}{2\mu_{H_2}} + V_r \qquad (103)$$

where V_r is a the numerical cross-section of diabatic potential energy surface

$$\langle \gamma | \hat{V}_{eff}^{D} | \gamma \rangle = \frac{j(j+1)}{2\mu_{H_2} r^2} + V_{H_2}(r) + E_{so}$$

The kinetic energy operator is the same as in the Hamiltonian for the simple harmonic oscillator, so we can write the Hamiltonian as

$$\hat{H}_a = \hat{T} + \hat{V}_r = \hat{H}_{sho} - \left(\hat{V}_{sho} + \hat{V}_r\right)$$

Where $\hat{H}_{sho}$ is the Hamiltonian of the simple harmonic oscillator

$$\hat{H}_{sho} = \frac{\hat{p}_r^2}{2\mu_{H_2}} + \frac{1}{2}k\left(\hat{r} - r_{eq}\right)^2 = \frac{\hat{p}_r^2}{2\mu_{H_2}} + \frac{1}{2}k\hat{x}^2$$

The eigenstates of the simple harmonic oscillator are the number states $|n\rangle$ described by the eigenvalue equation $\hat{H}_{sho}|n\rangle = \square w(n + 1/2)|n\rangle$. These eigenstates have the coordinate representation

$$\langle x | n \rangle = \psi_n(x) = \left(2^n n! \sqrt{\pi}\right)^{-1/2} \mathcal{H}_n(\beta x) e^{-(\beta x)^2 / 2}$$

where $\beta = \sqrt{\frac{\mu_{H_2}\omega}{\square}}$, $\omega = \sqrt{\frac{k}{\mu_{H_2}}}$ and $\mathcal{H}_n$ are the Hermite polynomials.

The treatment of the harmonic oscillator eigenstates is facilitated by defining the raising and lowering operators $\hat{a}$ and $\hat{a}^{\dagger}$

$$\hat{a} = \frac{\beta}{\sqrt{2}}\left(\hat{x} + i\frac{\hat{p}}{m\omega}\right) \qquad \hat{a}^{\dagger} = \frac{\beta}{\sqrt{2}}\left(\hat{x} - i\frac{\hat{p}}{m\omega}\right)$$

which operate on the eigenstates to give

$$\hat{a}\left|n\right\rangle = \sqrt{n}\left|n-1\right\rangle \qquad \hat{a}^{\dagger}\left|n\right\rangle = \sqrt{n+1}\left|n+1\right\rangle$$

The raising and lower operators are related to the coordinate operator by

$$\hat{x} = \frac{\hat{a} + \hat{a}^{\dagger}}{\sqrt{2}\beta}$$

The eigenstates of the simple harmonic oscillator are complete. Representing $\hat{H}_a$ in this basis gives

$$\begin{aligned}
\left\langle n'\right|\hat{H}_a\left|n\right\rangle &= \left\langle n'\right|\hat{H}_{sho} + \left(\hat{V}_r - \hat{V}_{sho}\right)\left|n\right\rangle \\
&= \left\langle n'\right|\hat{H}_{sho}\left|n\right\rangle - \frac{1}{2}k\left\langle n'\right|\hat{x}^2\left|n\right\rangle + \left\langle n'\right|\hat{V}_r\left|n\right\rangle \\
&= \hbar\omega\left(n + \frac{1}{2}\right)\delta_{n'n} - \frac{1}{2}\frac{k}{\sqrt{2}\beta}\left\langle n'\right|\left(\hat{a}^{\dagger} + \hat{a}\right)^2\left|n\right\rangle + \left\langle n'\right|\hat{V}_r\left|n\right\rangle
\end{aligned}$$

The raising and lowering operators satisfy the relation $\hat{a}\hat{a}^{\dagger} - \hat{a}^{\dagger}\hat{a} = \hat{I}$ where $\hat{I}$ is the identity operator.

$$\begin{aligned}
\left\langle n'\right|\hat{H}_a\left|n\right\rangle = \hbar\omega&\left(n + \frac{1}{2}\right)\delta_{n'n} \\
&- \frac{1}{2}\frac{k}{\sqrt{2}\beta}\left[\left\langle n'\right|\hat{a}^{\dagger}\hat{a}^{\dagger}\left|n\right\rangle + 2\left\langle n'\right|\hat{a}^{\dagger}\hat{a}\left|n\right\rangle + \left\langle n'\middle|n\right\rangle + \left\langle n'\right|\hat{a}\hat{a}\left|n\right\rangle\right] \\
&+ \left\langle n'\right|\hat{V}_r\left|n\right\rangle
\end{aligned}$$

Moving into the coordinate representation gives

$$\begin{aligned}\langle n'|\hat{H}_a|n\rangle = &\left[\square\omega\left(n+\frac{1}{2}\right)-\frac{1}{2}\frac{k}{\sqrt{2}\beta}(1+2n)\right]\delta_{n'n} \\ &-\frac{1}{2}\frac{k}{\sqrt{2}\beta}\left[(n+1)^{1/2}(n+2)^{1/2}\delta_{n'n+2}+n^{1/2}(n-1)^{1/2}\delta_{n'n-2}\right] \\ &+\int\psi_{n'}^{*}(x)V_r\psi_n(x)\,dx\end{aligned} \tag{104}$$

which gives a method for numerically determining each matrix element $\langle n'|\hat{H}_a|n\rangle$. This result is exact if an infinite number of basis states are used. In practice the basis must be truncated. The result is an *m* x *m* matrix $\langle n'|\hat{H}_a|n\rangle$, where *m* is the number of basis states used. This matrix is then diagonalized and the resulting diagonal elements are the eigenvalues of the system while the columns of the unitary transformation matrix used to diagonalize it give the expansion coefficients of its eigenvectors in the chosen basis. These eigenvectors are labeled $\phi_{\gamma_1}^{V_{H_2}}(r)$, where *i* indexes the surface

This work will consider energies on the order of the ground and first excited vibrational state. The first two eigenvalues and their associated eigenvectors were calculated for the asymptotic limit of large *R* for every potential energy surface corresponding to a diagonal element of the effective potential energy matrix. These eigenstates were observed to converge when more than 10 basis states of the harmonic oscillator are used to represent the Hamiltonian. To guarantee convergence 40 basis states were used for the calculation.

The ground and first excited state are shown for the cross-section of the ground-state potential energy surface $\left\langle \begin{matrix} 0 & \frac{1}{2} \\ 0 & \frac{1}{2} \end{matrix} \right| \hat{V}_{eff}^{D}\left(r, R = 30\text{ au}\right) \left| \begin{matrix} 0 & \frac{1}{2} \\ 0 & \frac{1}{2} \end{matrix} \right\rangle$.

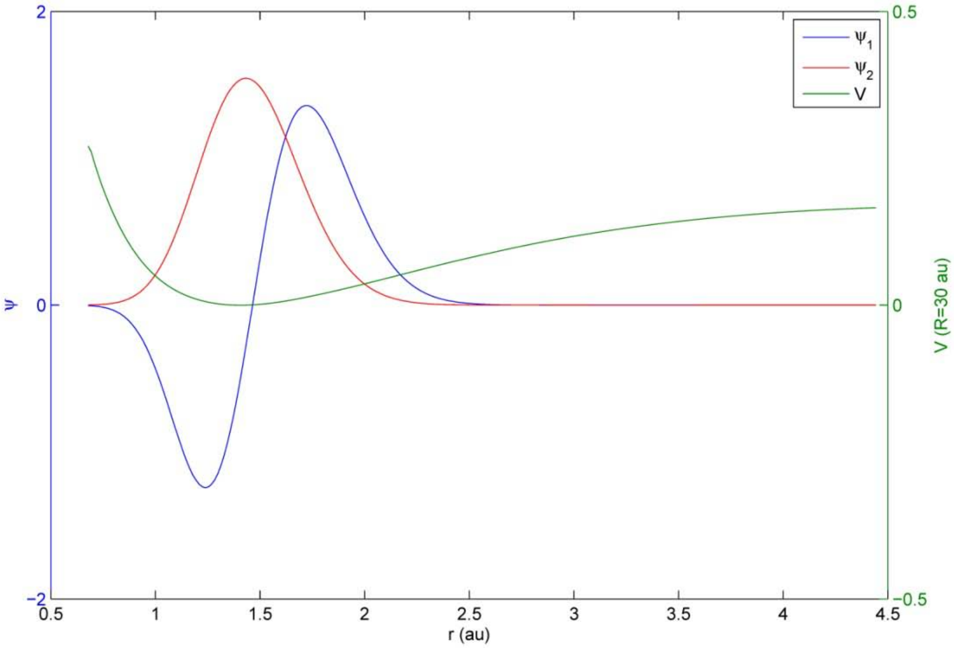

Figure 23. Cross-section of First Diabatic PES with First Two Vibrational Eigenstates

To facilitate propagation on a specific grid the numerically determined eigenstates $\phi_{\gamma_i}^{V_{H_2}}\left(r\right)$ are sampled at the gridpoints used for the propagation.

The numerically determined eigenvalues are precisely the internal energies referenced in equation (91). They incorporate the offset of each surface from zero in the asymptotic limit as well as the energy associated with the internal vibrational degree of freedom. These numerically determined total internal energies are shown in Table 1 for various values of $\gamma = \left\lvert\begin{matrix} j & j_a \\ k & \omega \end{matrix}\right\rangle$ and v.

Table 1. Summary of Internal Energies

γ v	$\left\lvert\begin{matrix}0 & \frac{1}{2}\\ 0 & \frac{1}{2}\end{matrix}\right\rangle$	$\left\lvert\begin{matrix}0 & \frac{3}{2}\\ 0 & \frac{1}{2}\end{matrix}\right\rangle$	$\left\lvert\begin{matrix}2 & \frac{1}{2}\\ 0 & \frac{1}{2}\end{matrix}\right\rangle$	$\left\lvert\begin{matrix}2 & \frac{3}{2}\\ 0 & \frac{1}{2}\end{matrix}\right\rangle$	$\left\lvert\begin{matrix}4 & \frac{1}{2}\\ 0 & \frac{1}{2}\end{matrix}\right\rangle$	$\left\lvert\begin{matrix}4 & \frac{3}{2}\\ 0 & \frac{1}{2}\end{matrix}\right\rangle$
$v = 0$	0.9884	0.9957	1.1499	1.1573	1.5212	1.5287
$v = 1$	2.8848	2.8922	3.0383	3.0457	3.3911	3.3984
E_{int} are in 10^{-2} au.						
γ v	$\left\lvert\begin{matrix}6 & \frac{1}{2}\\ 0 & \frac{1}{2}\end{matrix}\right\rangle$	$\left\lvert\begin{matrix}6 & \frac{3}{2}\\ 0 & \frac{1}{2}\end{matrix}\right\rangle$	$\left\lvert\begin{matrix}8 & \frac{1}{2}\\ 0 & \frac{1}{2}\end{matrix}\right\rangle$	$\left\lvert\begin{matrix}8 & \frac{3}{2}\\ 0 & \frac{1}{2}\end{matrix}\right\rangle$	$\left\lvert\begin{matrix}10 & \frac{1}{2}\\ 0 & \frac{1}{2}\end{matrix}\right\rangle$	$\left\lvert\begin{matrix}10 & \frac{3}{2}\\ 0 & \frac{1}{2}\end{matrix}\right\rangle$
$v = 0$	2.0895	2.0969	2.8360	2.8433	3.7384	3.7458
$v = 1$	3.9305	3.9379	4.6388	4.6461	5.4944	5.5017

Since the internal energies incorporate the total energy offset as well as the energy of the internal degrees of freedom they represent the minimum energy required to access those states. They therefore provide a useful guide for determining $j_{\max}$ in order to truncate the effective potential energy matrix. In this work $j_{\max} = 10$ is used, giving a basis size $n = 32$.

Propagation

The Initial Wavepacket

In preparation for propagation the initial wavepacket is prepared in the diabatic coordinate representation. The selection of $j_{\max} = 10$ means the wavepacket is represented by a 32×1 vector. This work investigates scattering matrix elements from the state $\gamma = \left| \begin{matrix} 0 & \frac{1}{2} \\ 0 & \frac{1}{2} \end{matrix} \right\rangle$, which will subsequently be referred to as the ground state. The initial wavepacket is defined to have amplitude only on this surface.

$$\psi_{in}^{D}\left(r,R\right) = \begin{bmatrix} \psi_{in}^{D}\left(r,R\right)_{\gamma_1} \\ 0 \\ \square \\ 0 \end{bmatrix} \tag{105}$$

On the ground state the initial wavepacket $\psi_{in}^{D}\left(r,R\right)_{\gamma_1}$ is selected to be an eigenstate of the asymptotic Hamiltonian. As previously discussed, this wavepacket is formed from the direct product of a Gaussian in the *R*-direction and the ground state of the asymptotic V_{H_2} potential in the *r*-direction:

$$\psi_{in}^{D}\left(r,R\right)_{\gamma_1} = \phi_{\gamma_1}^{V_{H_2}}\left(r\right) \cdot \left(2\pi\delta^2\right)^{-1/4} e^{-\left(R-R_0\right)^2/4\delta^2 + ik_0^{in}\left(R-R_0\right)} \tag{106}$$

An initial offset $R_0 = 30$ au is selected to place the wavepacket in the asymptotic limit along with a spread parameter $\delta = 0.35$ and momentum offset $k_0^{in} = -6.75$.

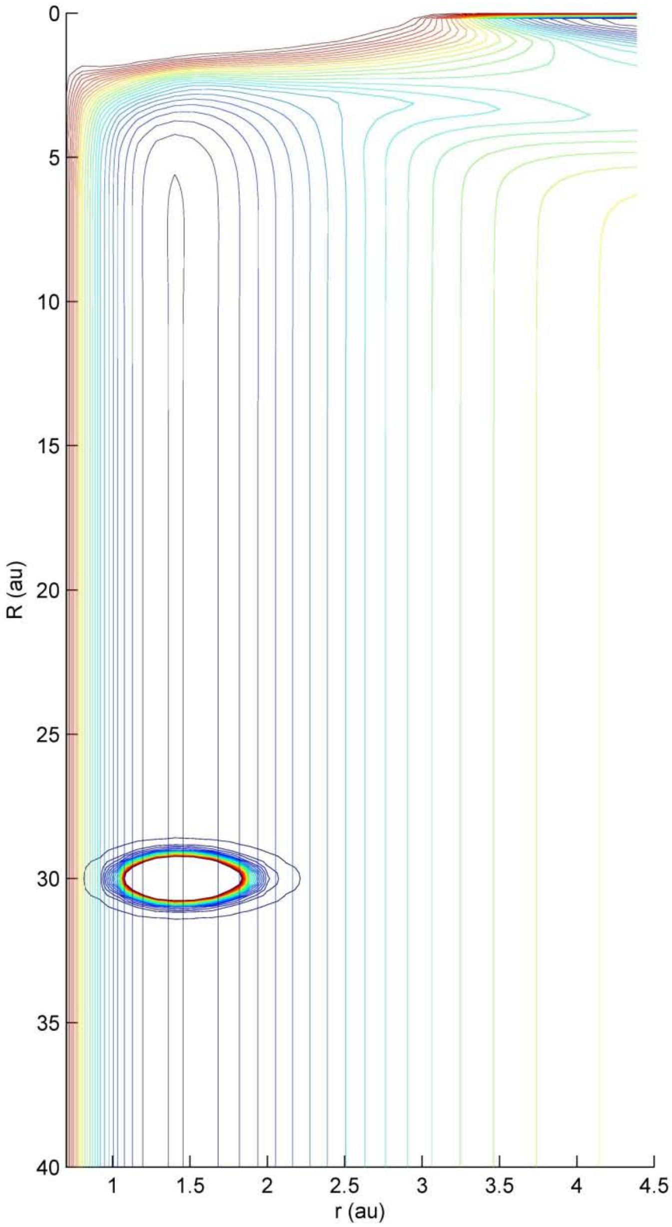

Figure 24. Initial Wavepacket on the Ground State at $t = 0$ au

The Møller states

Since the wavepacket is located in the asymptotic limit, it is also the reactant Møller state.

$$\left|\psi_{-}\right\rangle = \Omega_{-}\left|\psi_{in}^{\gamma_1}\right\rangle = \left|\psi_{in}^{\gamma_1}\right\rangle$$

The product Møller states are selected to have the same form in the *R*-dimension but with a momentum offset $k_0^{out} = -k_0^{in} = +6.75$. As with the reactant Møller states, their location in the asymptotic limit eliminates the need to numerically propagate these states forwards and backwards in time. Two product Møller states are defined for every surface, one with an *r*-dimension cross-section of the vibrational ground state and another with a cross-section of the first excited vibrational state.

The width of the momentum representation of the Møller states will determine the range of energies considered by the propagation. Consider again the equation for calculating scattering matrix elements using the channel packet method:

$$S^{\gamma'\gamma}_{\pm k',\pm k} = \frac{\hbar\left(\left|k_{\gamma'}\right|\left|k_{\gamma}\right|\right)^{1/2} \int_{-\infty}^{\infty} e^{iEt/\hbar} C(t)\,dt}{2\pi m \eta^{-*}(\pm k')\,\eta^{+}(\pm k)} \tag{107}$$

Here all terms are shown explicitly as functions of energy. The denominator contains the expansion coefficients $\eta^{\pm}$ of the momentum representation of the Møller states in the *R*-dimension. Since they were chosen to be a Gaussian in the coordinate representation, these expansion coefficients are known – they are simply given by the inverse Fourier transform of the coordinate Gaussian, which is known analytically:

$$\eta^{\pm}(k) = \left(\frac{2\delta^2}{\pi}\right)^{1/4} e^{-\delta^2\left(k-k_0^{out/in}\right)^2 - iR_0 k} \tag{108}$$

To see the range of energies contained in these states the $\eta^{\pm}$ are expressed as a function of energy using the relation $k = \sqrt{2\mu_{B_{H_2}}\left(E - E_{\text{int}}\right)} / \hbar$.

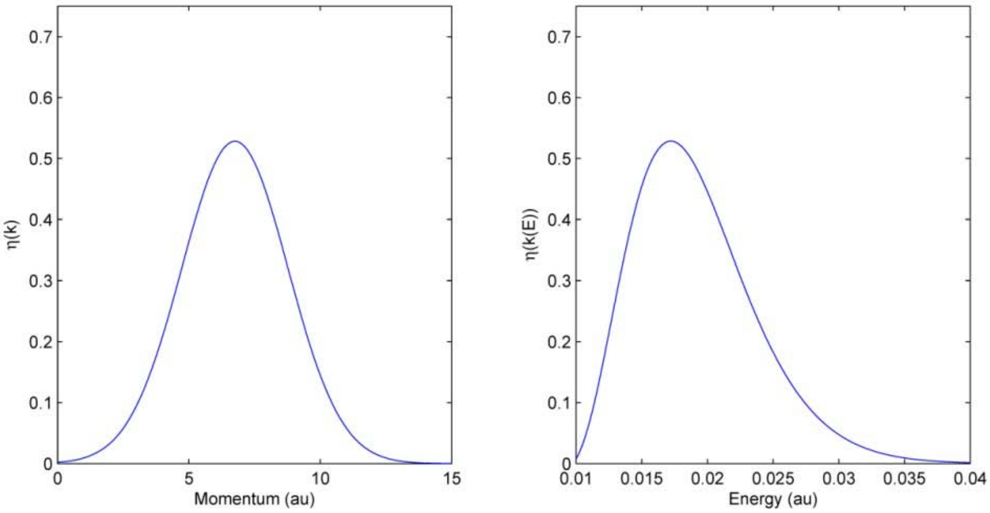

Figure 25. P_R **Cross-section of Initial Wavepacket**

This range of energies is selected to be broad but contained below the cutoff energy associated with the truncation of the potential energy matrix at $j_{\max} = 10$.

Another consideration when selecting these paramaters is the requirement derived from the channel packet method that the wavepacket momentum be either all positive or all negative. This requirement must be balanced against the desire to obtain usable data at low energies. The division by $\eta^{-*}\left(\pm k'(E)\right)\eta^{+}\left(\pm k(E)\right)$ in eq. (107) results in division by near-zero noise at the edge of the Gaussian. It is therefore desirable to locate the Gaussian such that is has a non-negligable amplitude at $k = 0 \rightarrow E = E_{\text{int}}$.

The Reaction Channel

While the selected wavepacket only has energies less than those associated with the $j = 12$ states, it does contain energies higher than the barrier to reaction seen in the lowest adiabatic potential energy surface:

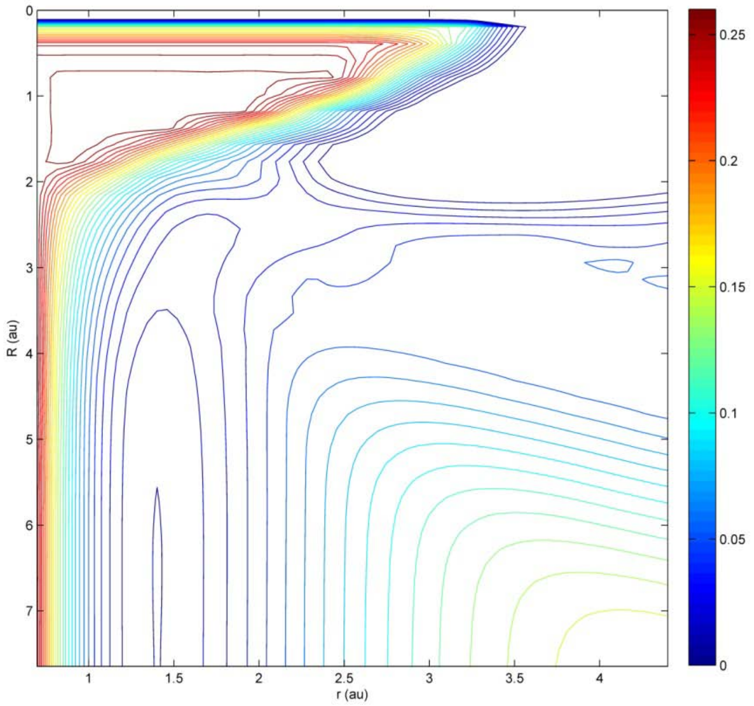

Figure 26. Barrier to Reaction in Lowest Adiabatic Potential Energy Surface

The initial wavepacket is centered at $r = 1.402$ au, $R = 30$ au and is moving entirely in the $-R$ direction. As it enters the interaction region portions of the wavepacket with energies higher than $\square 0.025$ au can move into the region of low potential around $r > 2.5$ au, $R < 2$ au and exit the grid. Crossing into this region represents the reaction $B + H_2 \rightarrow BH + H$. Propagation on the $BH + H$ surfaces is beyond the scope of this work, so the simplifying assumption that any wavepacket exiting in that direction will completely react is required. The investigation of whether portions of the wavepacket can cross onto the $BH + H$ surfaces and subsequently return and exit the grid along the original reaction channel represents an opportunity for further studies. That study would require the formulation of the $BH + H$ effective potential energy surfaces.

Absorbing Boundary Conditions

The assumption that the portions of the wavepacket that cross the barrier will entirely exit is implimented through the use of absorbing boundary conditions. Without the use of absorbing boundary conditions any portion of the wavepacket leaving the grid would erroneously appear on the opposite side due to the FFT's assumption of periodicity, reflect, and return to the interaction region by an unphysical mechanism. To prevent this an ABC is located in the region $r > 3$ au. The shape of the ABC is a Gaussian

$$V_{abc,1}(r,R) = -iA_1 e^{-\frac{(r-r_{\max})^2}{B_1}} \tag{109}$$

with parameters $A_1 = 0.025,\ B_1 = 1/3$.

With this choice of parameters the ABC will only absorb portions of the wavepacket which are reacting. These ABCs are made relatively wide to prevent reflection while completely absorbing anything entering the reaction region.

Another ABC is located at the edge of the grid at large *R*. The majority of the wavepacket will not react and will exit the interaction region along this channel. This ABC prevents portions of the wavepacket exiting in this channel from crossing back to $R = 0$, reflecting off the potential there, and reentering the interaction region. This ABC is a broader, shallower Gaussian compared to $V_{abc,1}$ with the form

$$V_{abc,2}(r,R) = -iA_2 e^{-\frac{(R-R_{\max})^2}{B_2}} \tag{110}$$

with the parameters $A_2 = 0.005,\ B_1 = 20$.

The Time Grid

An investigation of the propagation on these surfaces concluded that error associated with the split-operator approximation converged to zero around a time step of $\Delta t_c = 1.5$ au. For these calculations this time step was chosen to be $\Delta t = 1$ au. The total propagation time of $T_{\max} = 4 \times 10^6$ was chosen to ensure all of the wavepacket exited the interaction region. This long propagation time is necessary to capture the entire period where the correlation function is nonzero.

A summary of the propagation parameters is shown in Table 2.

Table 2. Propagation Parameters

Parameter	**Symbol**	**Value (au)**
Coordinate gridsize	N_R N_r	256 32
Coordinate grid range	$r_{\min}, r_{\max}$ $R_{\min}, R_{\max}$	0.6702, 4.402 0, 50
Time step size	Δt	1
Total propagation time	$T_{\max}$	4×10^6
Initial wavepacket position	r_0, R_0	1.402, 30
Initial wavepacket momentum	$k_0^{in/out}$	☐6.75
Initial wavepacket spread	δ	0.35
Amplitude, spread of ABC 1	A_1, B_1	0.025, 1/3
Amplitude, spread of ABC 2	A_2, B_2	0.005, 20
Masses	μ_{B,H_2}, μ_{H_2}	3109.0,918.6

Propagation

Now all the pieces are in place to propagate on these surfaces. Having defined the initial wavepacket on the ground state

$$\psi_{in}^{D}\left(r,R,t=0\right)=\begin{bmatrix}\psi_{in}^{D}\left(r,R\right)_{\gamma_1}\\0\\\vdots\\0\end{bmatrix}$$

the correlation function between the wavepacket and each of the 64 (32 surfaces with $v=0{,}1$) product Møller states. This gives the correlation functions at time $t=0$.

To begin the propagation algorithm the diabatic-to-adiabatic transformtion $U_{AD}^{\dagger}\left(r,R\right)$ is applied. At every point on the coordiante grid $U_{AD}^{\dagger}$ is a 32 x 32 matrix, which is multiplied by the 32 x 1 diabatic wavepacket giving the adiabatic wavepacket at every point

$$\psi^{A}\left(r,R\right)=\begin{bmatrix}\psi^{A}\left(r,R\right)_{\gamma_1}\\\vdots\\\psi^{A}\left(r,R\right)_{\gamma_n}\end{bmatrix}.$$

This is then multiplied by the first of the potential energy operators, $e^{-iV_{eff}^{A}\Delta t/2\hbar}$ which is diagonal in this representation. This intermediate wavepacket is then transformed back into the diabatic representation. Next it is moved into the momentum representation by taking the two-dimensional Fourier transform of each of its 32 rows $\psi^{A}\left(r,R\right)_{\gamma_i}$. In the diabatic momentum representation the kinetic energy operator is diagonal.

$$e^{-i\hat{T}\Delta t/\hbar}\left(k_r,k_R\right)=\left[\begin{pmatrix}e^{-i\hbar\left(k_r^2/2\mu_{H_2}+k_R^2/2\mu_{B,H_2}\right)\Delta t} & & 0\\ & \ddots & \\ 0 & & e^{-i\hbar\left(k_r^2/2\mu_{H_2}+k_R^2/2\mu_{B,H_2}\right)\Delta t}\end{pmatrix}\right]$$

After transforming back to the adiabatic coordinate representation the second potential energy operator is applied in the same way, giving the evolved wavepacket at the next time step in the adiabatic representation. This is transformed to the diabatic representation giving $\psi^D\left(r,R,t=\Delta t\right)$. The correlation functions between this evolved wavepacket and each of the product Møller states is calculated for $t=\Delta t$. This process is iterated for the desired number of time steps.

Visualizing the Propagation

The wavepacket is defined to be located only on the ground state at $t=0$. The off-diagonal elements of the diabatic effective potential energy matrix have the effect of mixing the wavepacket onto the other surfaces. This process is shown considering the wavepacket's evolution on ground state diabatic surface $\left\langle \begin{matrix} 0 & \frac{1}{2} \\ 0 & \frac{1}{2} \end{matrix} \middle| V_{eff}^D\left(r,R\right) \middle| \begin{matrix} 0 & \frac{1}{2} \\ 0 & \frac{1}{2} \end{matrix} \right\rangle$ and the next higher surface $\left\langle \begin{matrix} 0 & \frac{3}{2} \\ 0 & \frac{1}{2} \end{matrix} \middle| V_{eff}^D\left(r,R\right) \middle| \begin{matrix} 0 & \frac{3}{2} \\ 0 & \frac{1}{2} \end{matrix} \right\rangle$ associated with the boron electronic fine structure transition. At every time point shown the correlation function between the evolving reactant state and the stationary product Møller state (located at $R=30$ au with momentum in the positive R direction) is shown from time $t=0$ au up to the time being considered. The product Møller states are represented by a single black contour.

At $t = 0$ the wavepacket is placed in the asymptotic limit and is located only on the ground state. The initial correlation is zero because the wavepacket has only negative momentum while the product Møller state has only positive momentum.

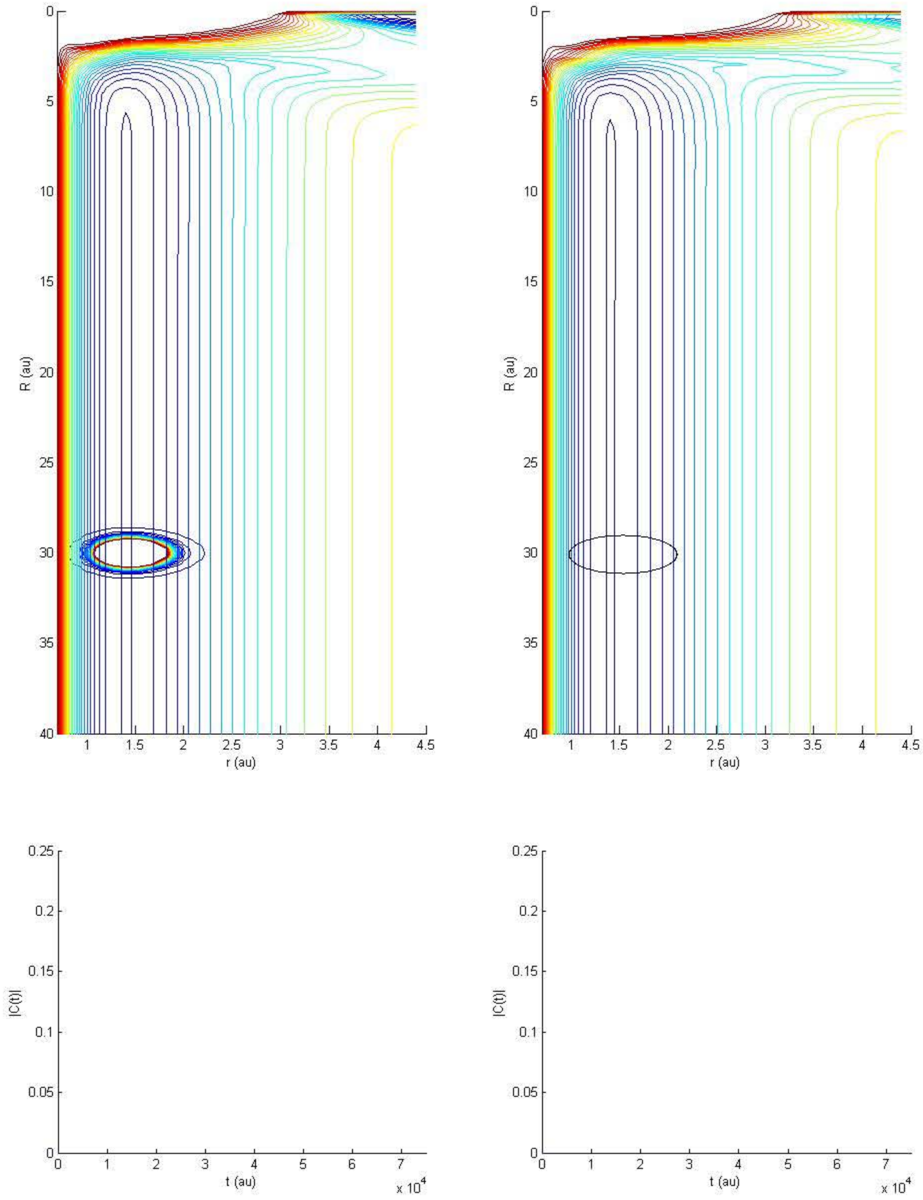

Figure 27. Wavepacket on the First Two Surfaces at $t = 0$ au

At $t = 5000$ au the wavepacket has moved towards the interaction region. No significant coupling to higher surfaces or correlation with the product Møller states is seen.

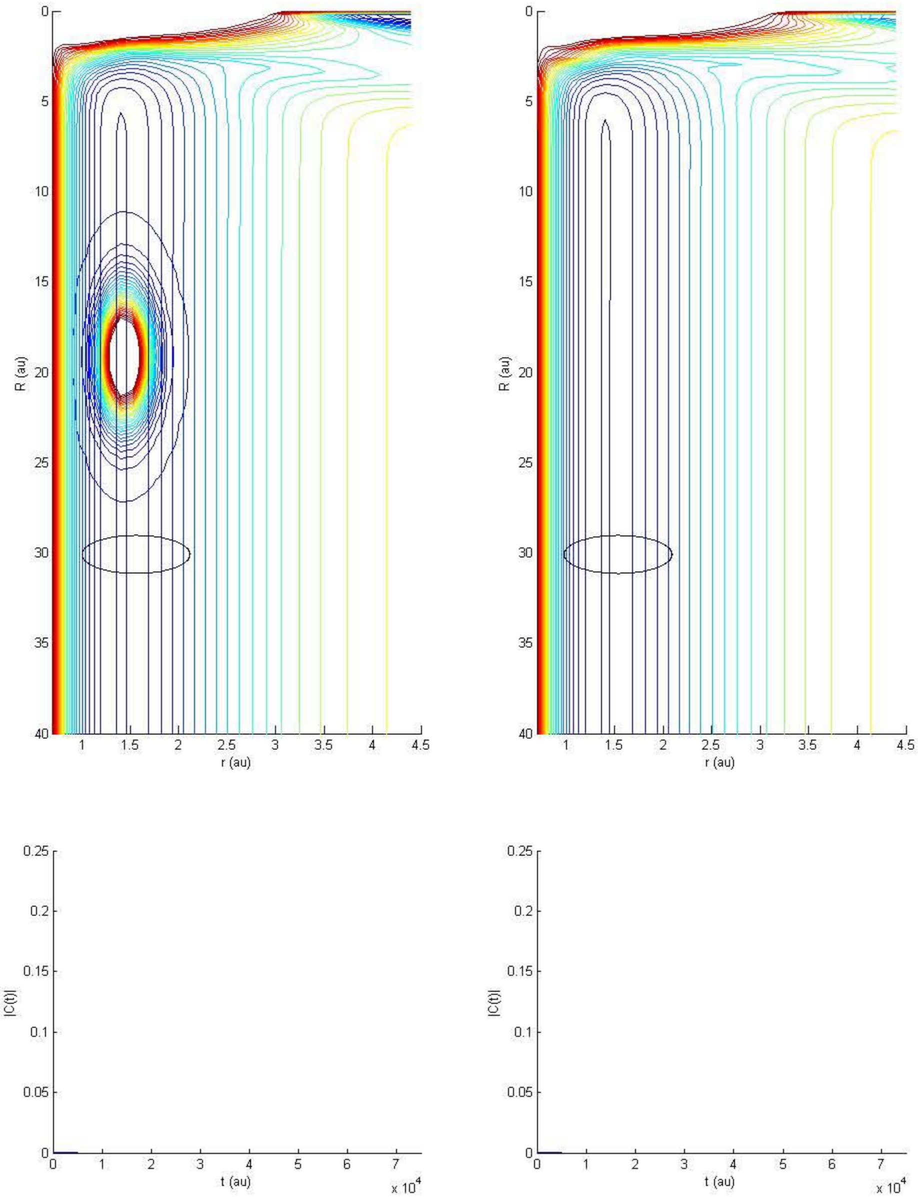

Figure 28. Wavepacket on the First Two Surfaces at $t = 5000$ au

At $t = 12500$ au the wavepacket has entered the interaction region and has coupled to the higher surfaces.

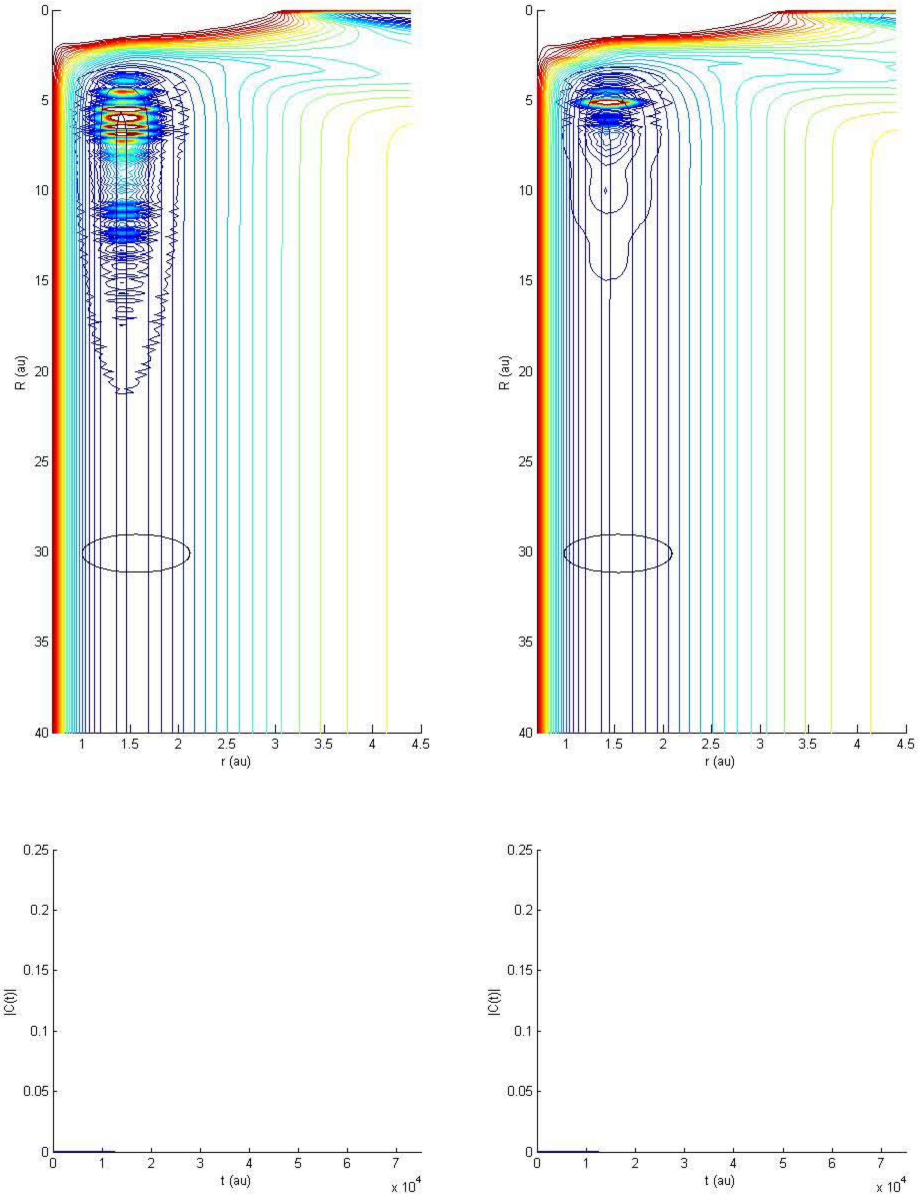

Figure 29. Wavepacket on the First Two Surfaces at $t = 12500$ au

For $t = 20000 - 45000$ au the wavepacket is exiting the interaction region on all of the surfaces. A significant portion is located in the region of the product Møller states resulting in the most significant amplitude in the correlation functions.

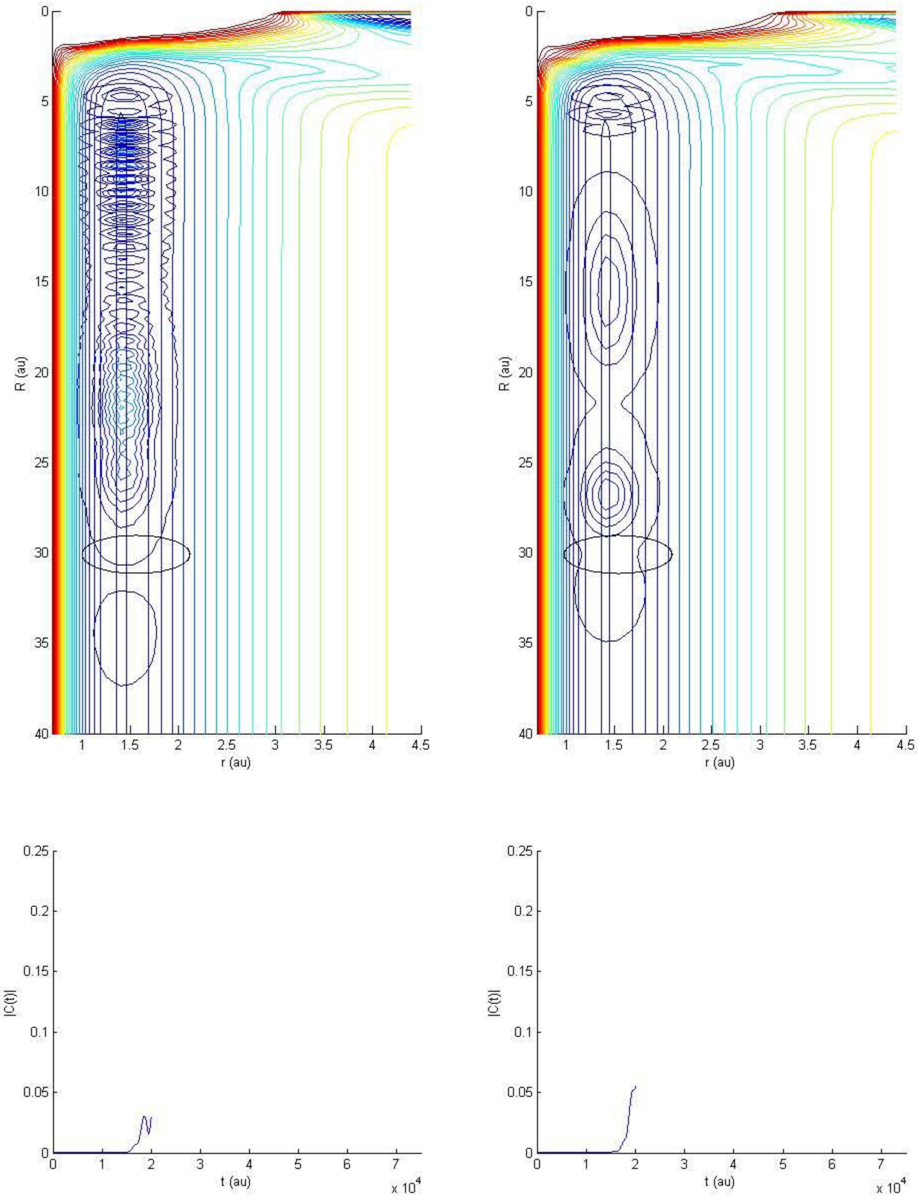

Figure 30. Wavepacket on the First Two Surfaces at $t = 20000$ au

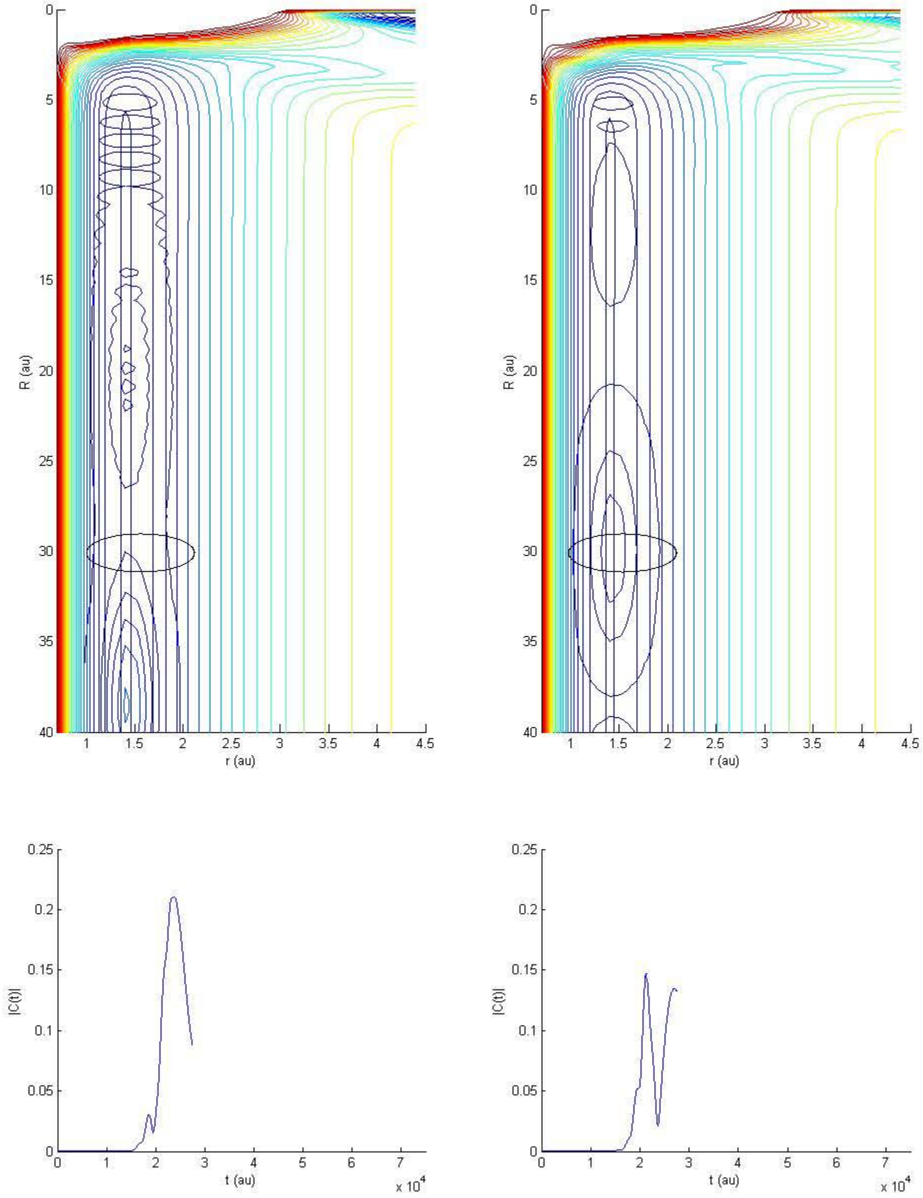

Figure 31. Wavepacket on the First Two Surfaces at $t = 27500$ au

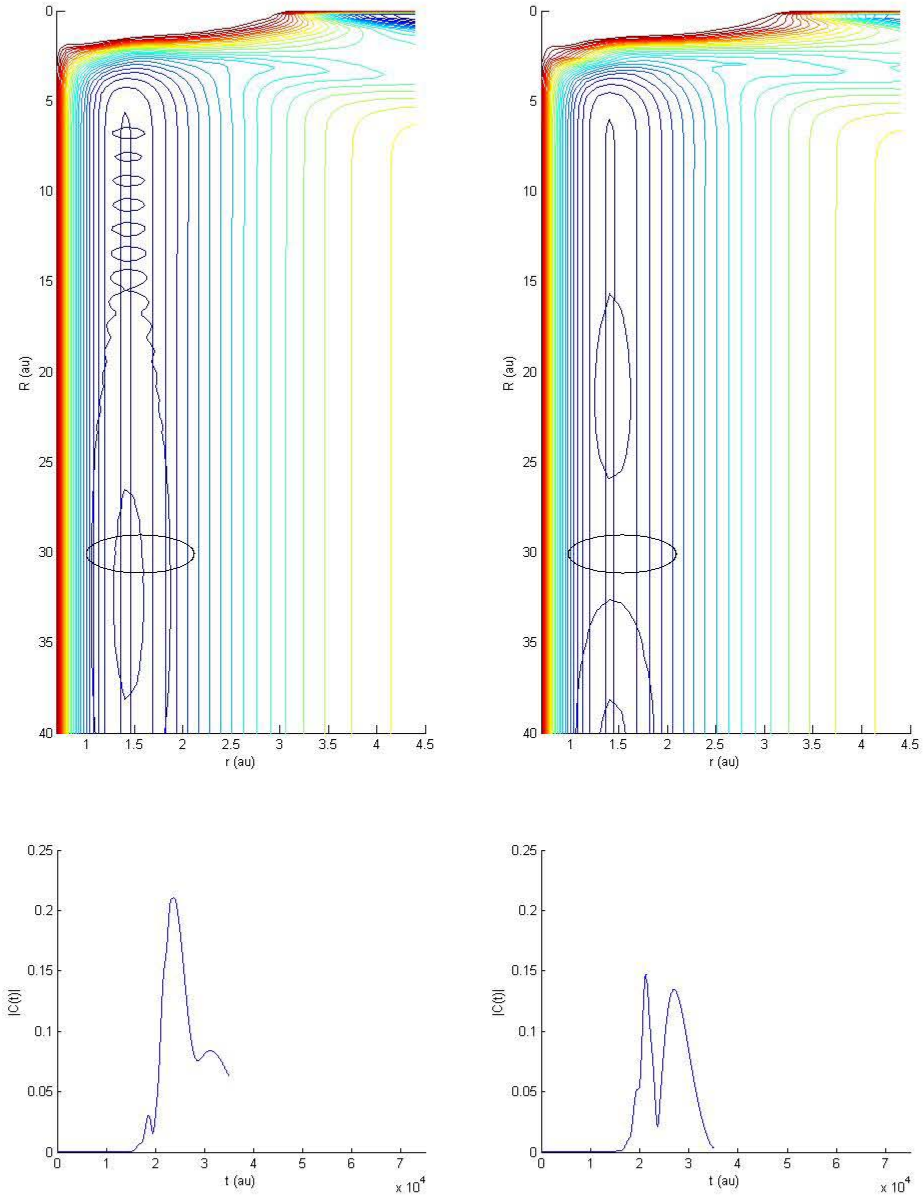

Figure 32. Wavepacket on the First Two Surfaces at $t = 35000$ au

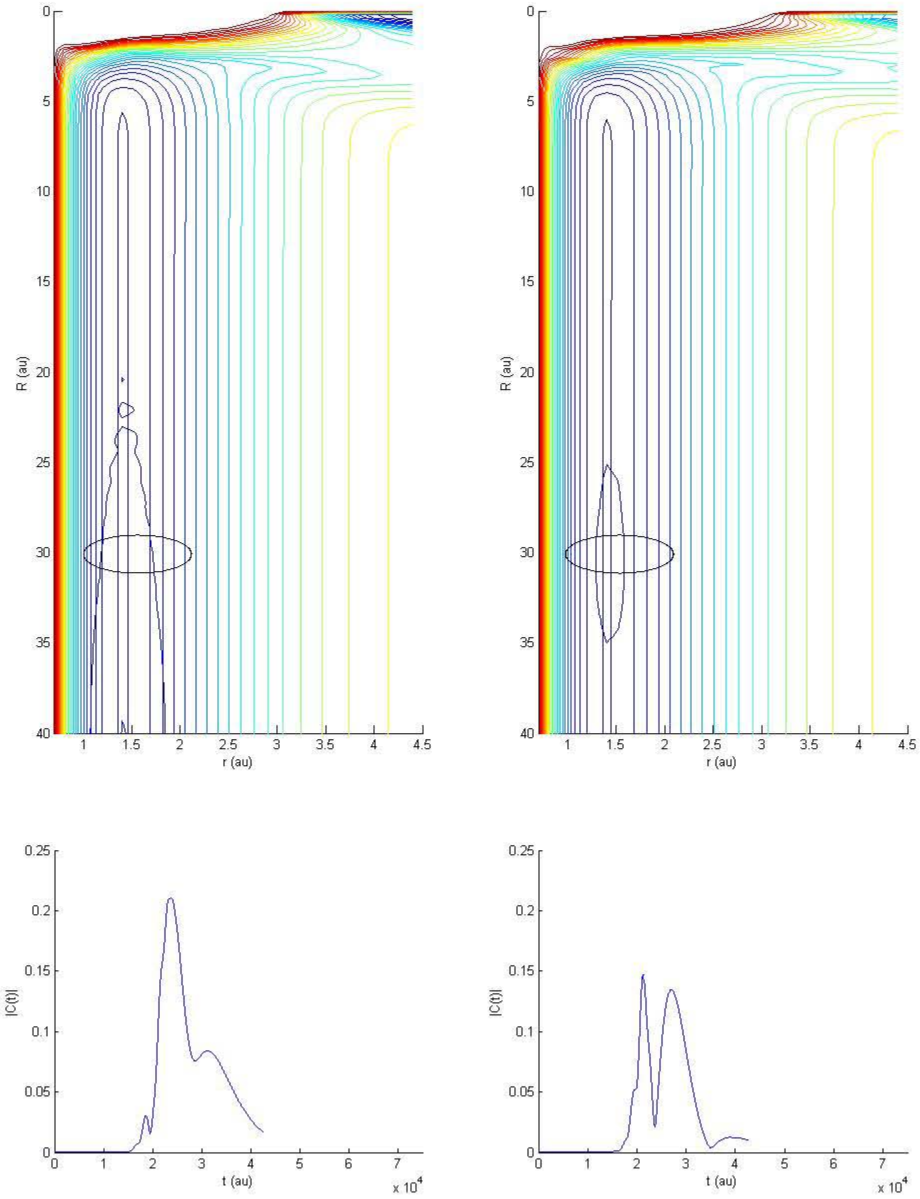

Figure 33. Wavepacket on the First Two Surfaces at $t = 42500$ au

At $t = 50000$ au most of the wavepacket has passed by the product Møller states and the correlation function returns to low amplitude.

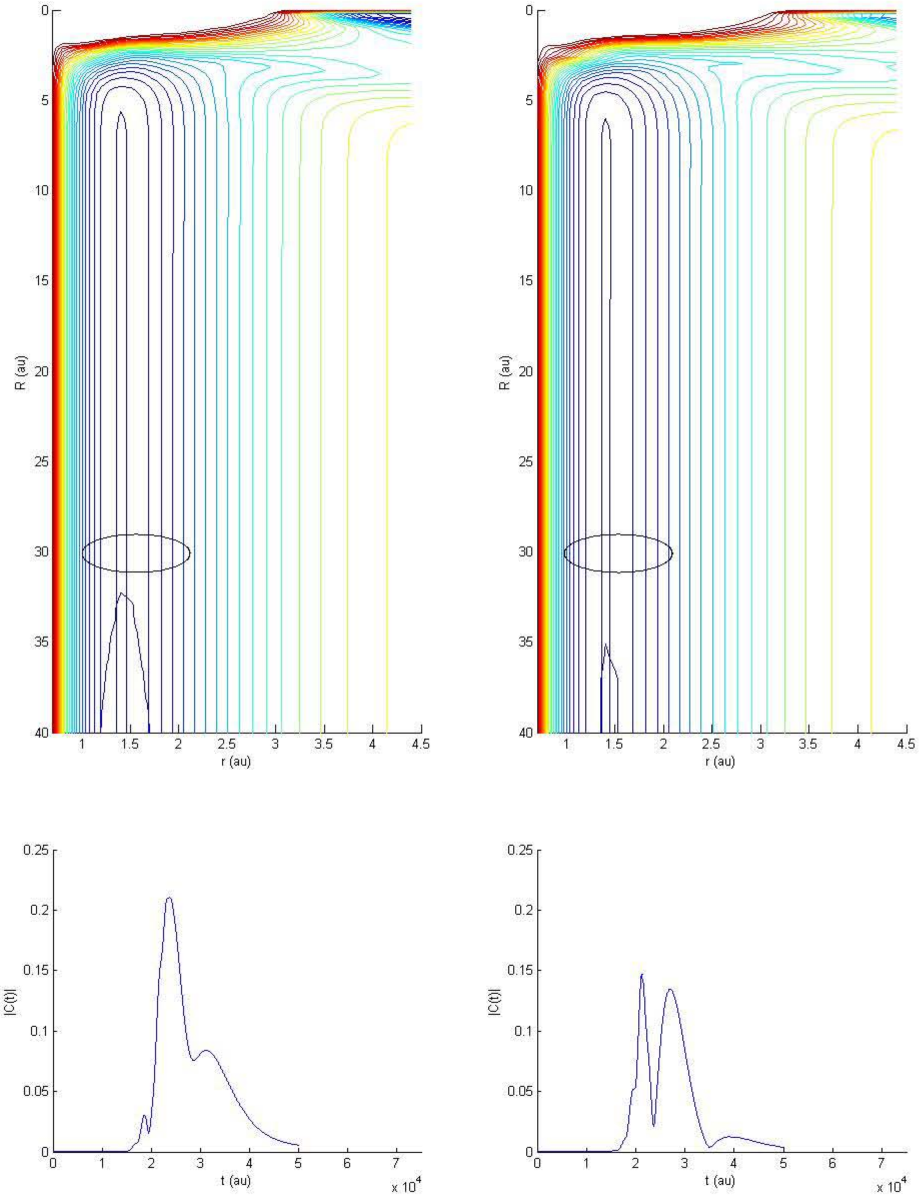

Figure 34. Wavepacket on the First Two Surfaces at $t = 50000$ au

At $t = 65000$ au the wavepacket is no longer visible on this scale. However the remaining low-amplitude long-duration features of correlation function play an important part in forming the scattering matrix elements.

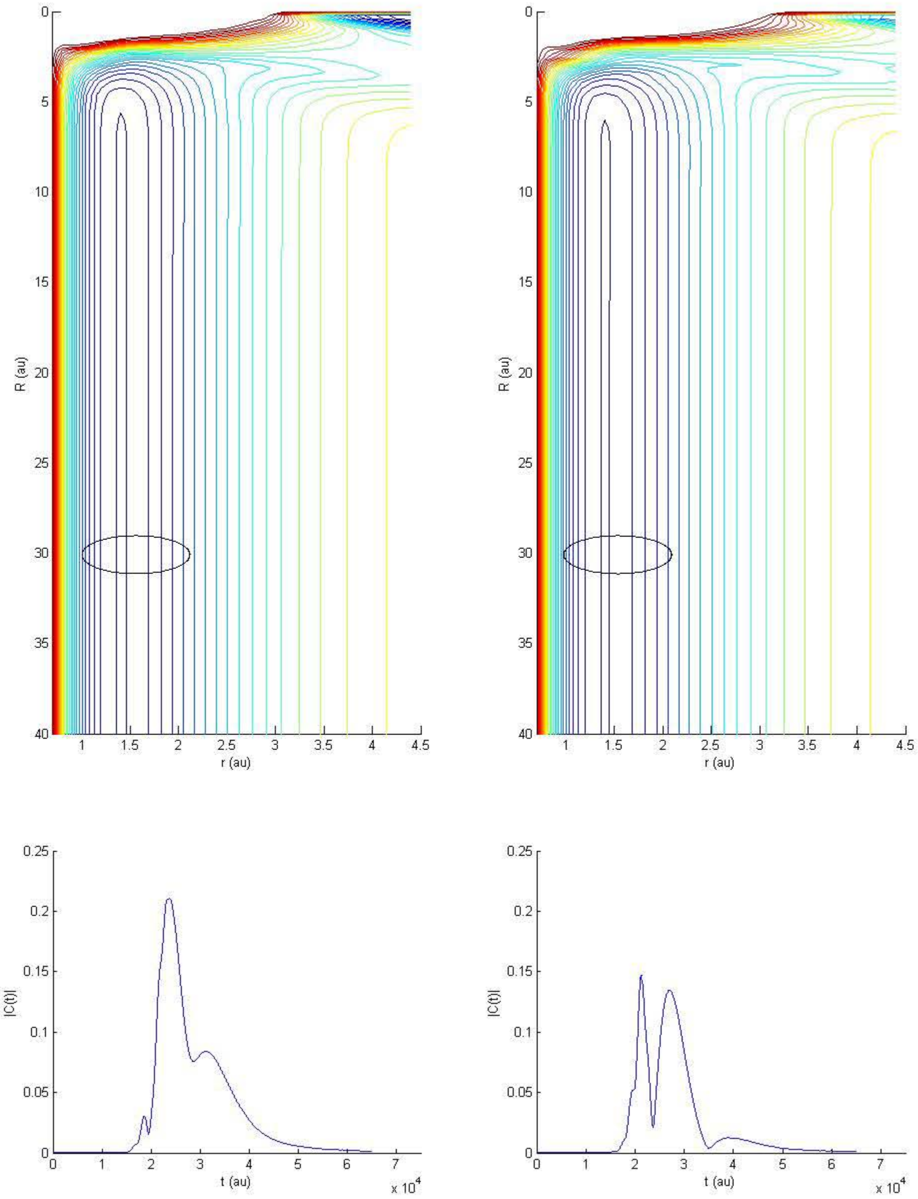

Figure 35. Wavepacket on the First Two Surfaces at $t = 65000$ au

The Scattering Matrix Elements

Calculating the Scattering Matrix Elements

The correlation functions between the product Møller states and the evolving reactant Møller states is used to calculate the scattering matrix elements using the relation

$$S^{\gamma'\gamma}_{\pm k',\pm k}\left(E\right)=\frac{\hbar\left(\left|k_{\gamma'}\right|\left|k_{\gamma}\right|\right)^{1/2}\int\limits_{-\infty}^{\infty}e^{iEt/\hbar}C\left(t\right)dt}{2\pi m\eta^{-*}\left(\pm k'\right)\eta^{+}\left(\pm k\right)}$$

First the Fourier transform of each correlation function is taken. These are multiplied by the appropriate prefactor according to the expansion coefficients of the respective reactant and product Møller states, $\eta^{\pm}\left(k_R\right)=\left(\frac{2\delta^2}{\pi}\right)^{1/4}e^{-\delta^2\left(k_R-k_0^{out/in}\right)^2-iR_0k_R}$. These are implicitly functions of energy using the relation $k=\sqrt{2\mu_{B_{H_2}}\left(E-E_{\text{int}}\right)}/\square$ where the internal energies were calculated numerically and are summarized in Table 1.

The Scattering Matrix Elements for **B+H$_2$**

The scattering matrix elements represent probability amplitudes for scattering to a given state. Here they represent transitions from the ground state $\left|\begin{matrix} j & j_a \\ k & \omega \end{matrix},v\right\rangle=\left|\begin{matrix} 0 & \frac{1}{2} \\ 0 & \frac{1}{2} \end{matrix},0\right\rangle$ to each of the $\left|\begin{matrix} j & j_a \\ k & \omega \end{matrix},v\right\rangle$ states. The probability of these transitions is shown by the amplitude squared of the scattering matrix element and are obtained as a function of energy.

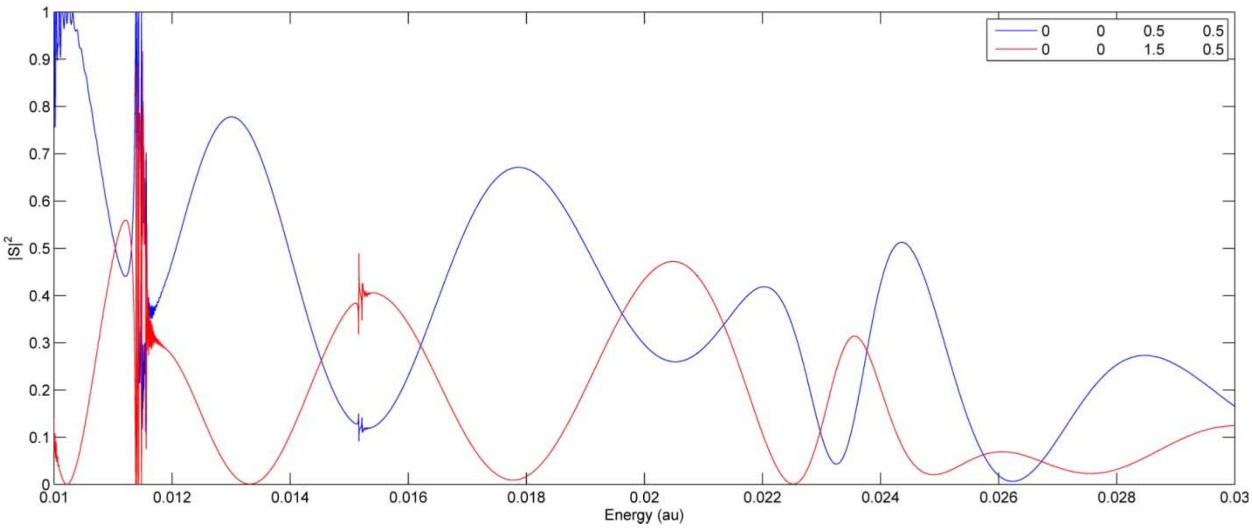

Figure 36. Probability to Transition from $\left|\begin{matrix} 0 & \frac{1}{2},0 \\ 0 & \frac{1}{2} \end{matrix}\right\rangle$ **to** $\left|\begin{matrix} 0 & \frac{1}{2},0 \\ 0 & \frac{1}{2} \end{matrix}\right\rangle$ **and** $\left|\begin{matrix} 0 & \frac{3}{2},0 \\ 0 & \frac{1}{2} \end{matrix}\right\rangle$

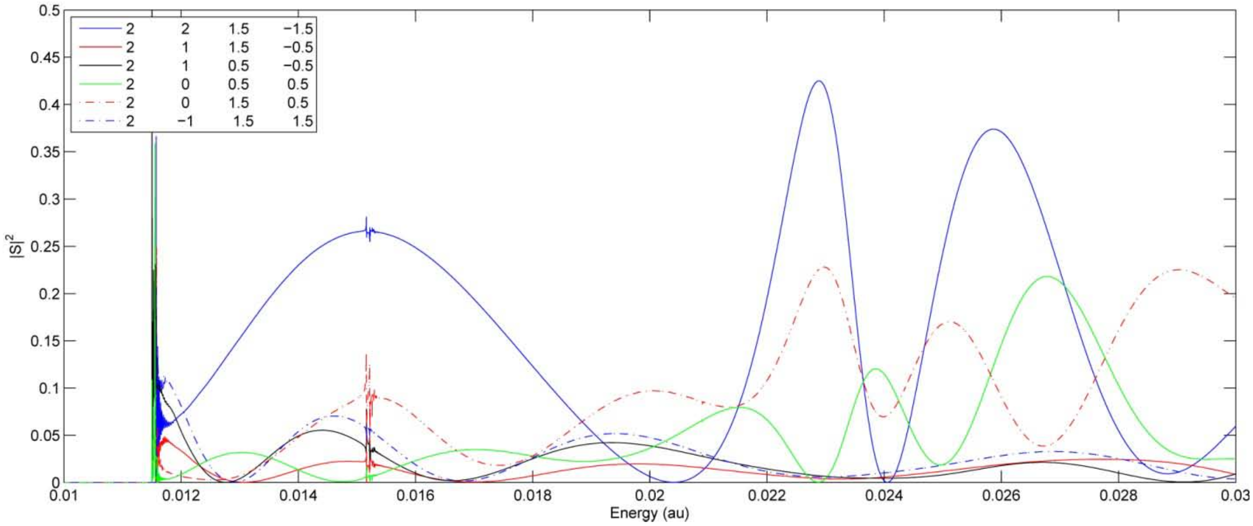

Figure 37. Probability to Transition from $\left|\begin{matrix} 0 & \frac{1}{2},0 \\ 0 & \frac{1}{2} \end{matrix}\right\rangle$ **to the Six Allowed** $\left|\begin{matrix} 2 & j_a,0 \\ j & \omega \end{matrix}\right\rangle$ **States**

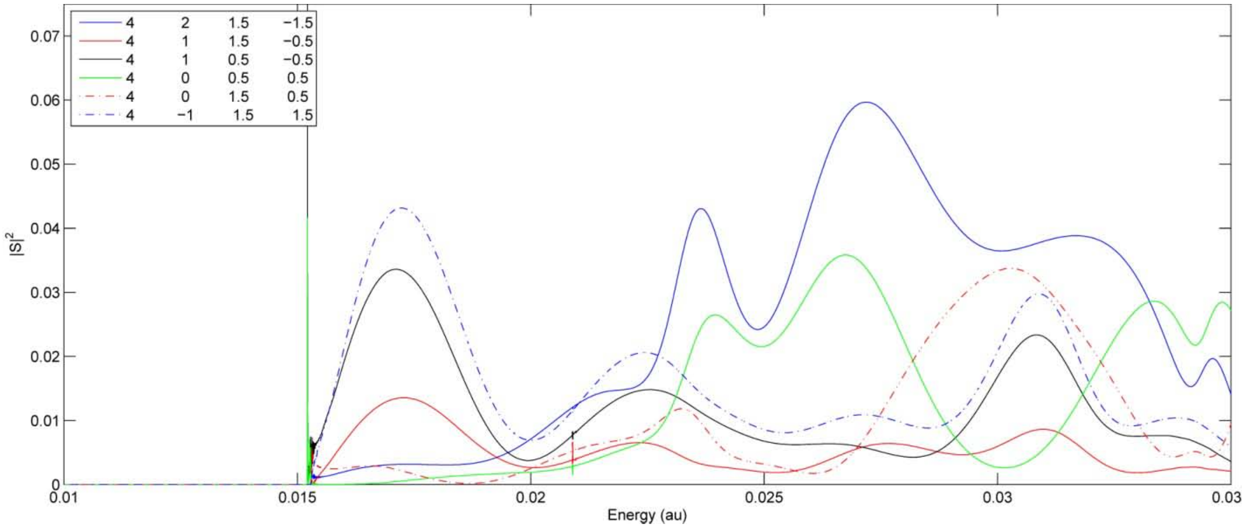

Figure 38. Probability to Transition from $\left|\begin{matrix}0 & \frac{1}{2} \\ 0 & \frac{1}{2}\end{matrix},0\right\rangle$ **to the Six Allowed** $\left|\begin{matrix}4 & j_a \\ j & \omega\end{matrix},0\right\rangle$ **States**

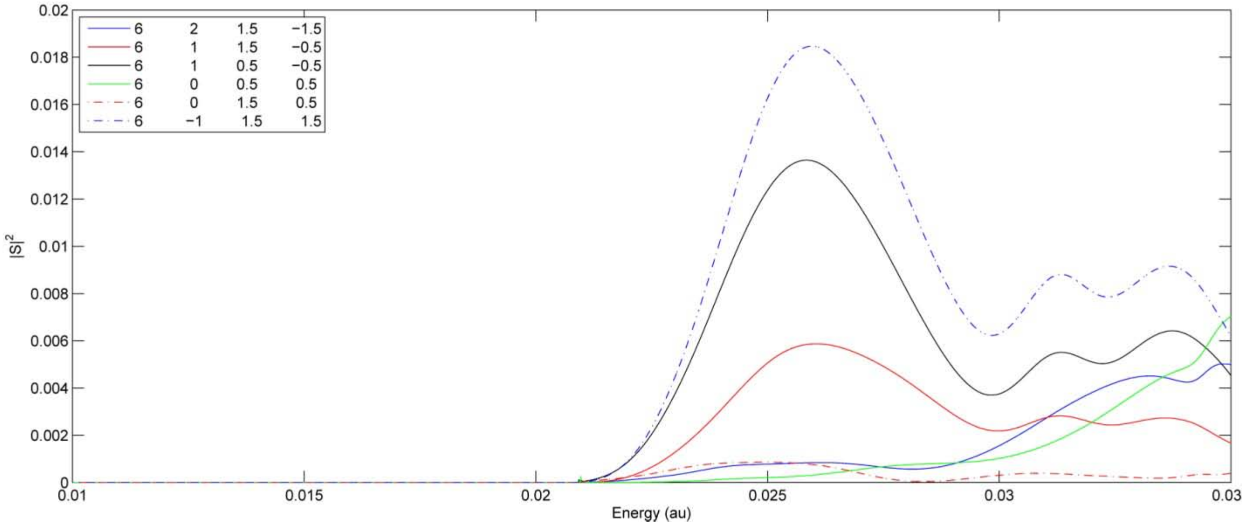

Figure 39. Probability to Transition from $\left|\begin{matrix}0 & \frac{1}{2} \\ 0 & \frac{1}{2}\end{matrix},0\right\rangle$ **to the Six Allowed** $\left|\begin{matrix}6 & j_a \\ j & \omega\end{matrix},0\right\rangle$ **States**

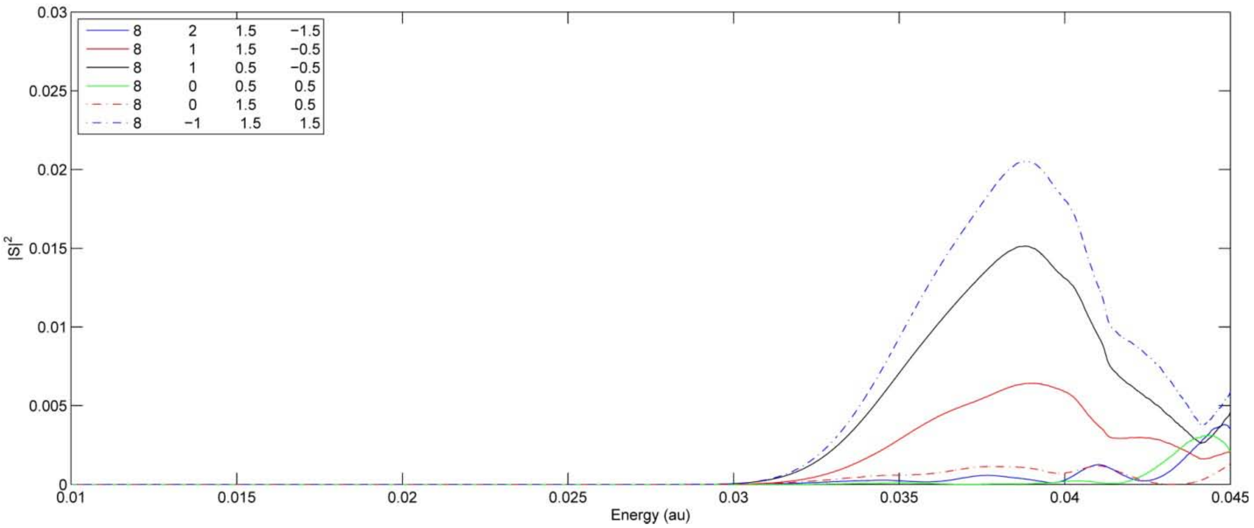

Figure 40. Probability to Transition from $\left|\begin{matrix}0 & \frac{1}{2}\\ 0 & \frac{1}{2}\end{matrix},0\right\rangle$ **to the Six Allowed** $\left|\begin{matrix}8 & j_a\\ j & \omega\end{matrix},0\right\rangle$ **States**

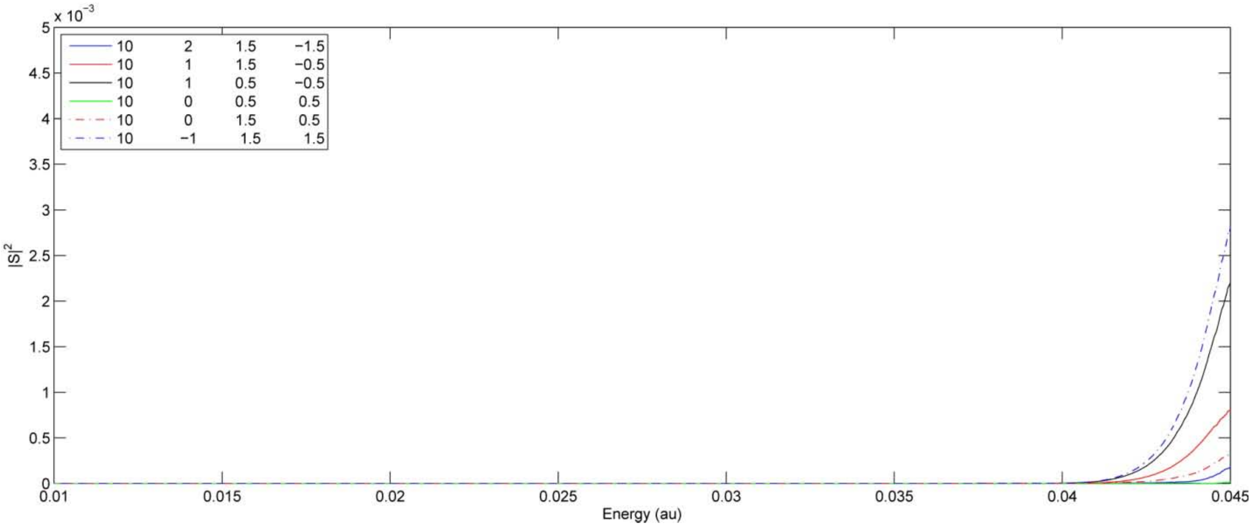

Figure 41. Probability to Transition from $\left|\begin{matrix}0 & \frac{1}{2}\\ 0 & \frac{1}{2}\end{matrix},0\right\rangle$ **to the Six Allowed** $\left|\begin{matrix}10 & j_a\\ j & \omega\end{matrix},0\right\rangle$ **States**

These scattering matrix elements are qualitatively similar to previous calculations using a one dimensional propagator with the restriction $r = r_{eq}$, with broad Stueckelberg-type [27] oscillatory behavior as a function of energy, along with high-frequency

Feshbach resonances [28] corresponding to portions of the wavepacket which couple to higher energy surface and become trapped in quasi-stable states. These Feshbach resonances are the primary driver for the long total propagation time, and are discussed in greater detail in a subsequent section.

Convergence of Basis Size

The effective diabatic potential energy matrix is infinite in dimension. Energetic considerations motivated the truncation of this matrix at some $j_{\max}$. For this work $j_{\max}$ is chosen to be 10, giving a basis size $n = 2 + 3j_{\max} = 32$. Repeating the calculation of the scattering matrix elements for bases of increasing size demonstrates that this truncation is appropriate over specific energy ranges.

Consider the scattering matrix element for a wavepacket entering and leaving on the ground state. This case is often referred to as reflection. The probability for reflection as a function of energy is shown for calculations using $j_{\max} = 0, 2, 4, 6, 8, 10$, which result in basis sizes $n = 2, 8, 14, 20, 26, 32$ respectively.

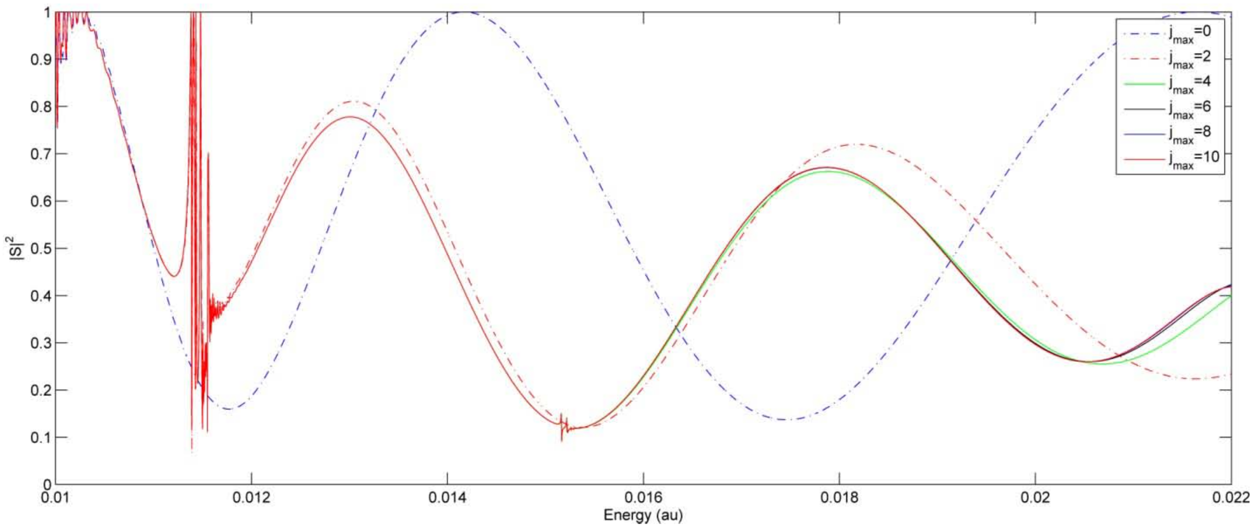

Figure 42. Comparison of Reflection Probability for $j_{\max} = 0, 2, 4, 6, 8, 10$

The energy 0.009883 au represents the internal energy of the ground state, which will serve as a constant offset from zero. The first line to diverge is that of the calculation using $j_{\max} = 0$. As expected this occurs near the energy where the *j* = 2 states become accessible. As energy increases calculations based on lower numbers of basis states diverge indicating the energy range over which they are valid has been exceeded. At no point in this range do the $j_{\max} = 8$ values diverge from the $j_{\max} = 10$ values, indicating that the calculation has converged over this energy range.

Examination of the scattering matrix elements for the fine-structure transition to the $\left|\begin{matrix}0 & \frac{3}{2}\\ 0 & \frac{1}{1}\end{matrix}\right\rangle$ state gives the same conclusion.

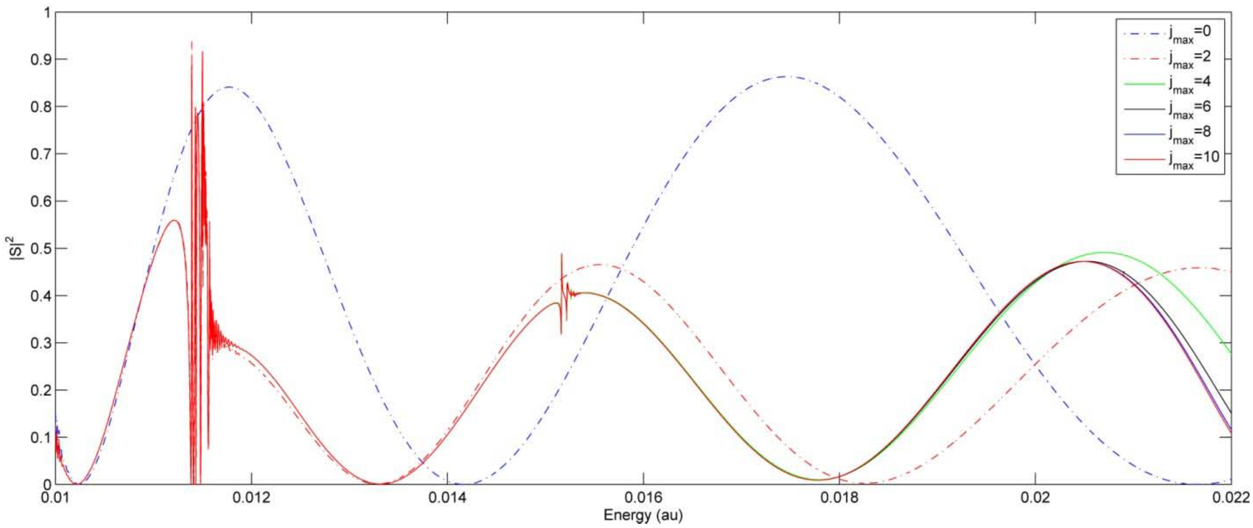

Figure 43. Comparison of Fine Structure Probability for $j_{\max} = 0,2,4,6,8,10$

Sum of Reaction Probabilities

To the extent that all possible reactions have been accounted for the sum of the amplitude squared of all scattering matrix elements should be 1. This is a useful check for consistency and may be used as a diagnostic tool to check for convergence based on time step size and total propagation time. Prematurely stopping the propagation truncates the correlation functions, and their Fourier transform, and subsquently the scattering matrix elements, will exibit ringing. Selection of an inappropriatly large time step introduces an erroneous phase shift in the correlation funtion. This results in a translation occuring to the Fourier transform. While this shift may not be noticible when examing individual scattering matrix elements, the requirement that they sum to unity makes it apparent. The equation for the scattering matrix elements

$$S_{\pm k',\pm k}\left(E\right)=\frac{\square^{2}\left|k\left(E\right)\right|\int_{-\infty}^{\infty}e^{iEt}\left\langle\psi_{-}\middle|\psi_{+}(t)\right\rangle dt}{2\pi\mu_{B_{H_2}}\eta^{-*}\left(\pm k'\left(E\right)\right)\eta^{+}\left(\pm k\left(E\right)\right)}$$

involves dividing the curve associated with the Fourier transform of the correlation function by the product of two Gaussians, so it is sensitive to translation of the numerator with respect to the denominator – instead of summing to one the scattering matrix elements will curve through it.

The sum of the scattering matrix elements for this calculation is shown in Figure 44.

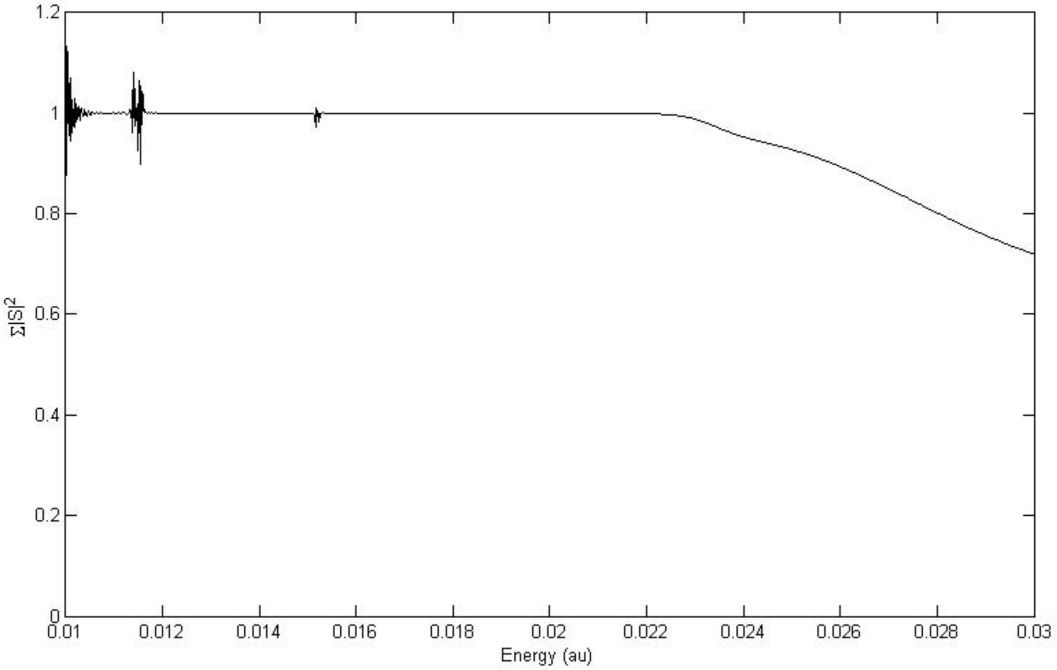

Figure 44. Sum of Scattering Matrix Elements

High frequency oscillations are visible at the internal energy of the ground state $E_{j=0}$ associated with division by near-zero error where the Gaussian in the denominator of eq. XX has reached a very small value. This situation is repeated at energies for the higher states $E_{j=2}$ and $E_{j=4}$. Otherwise the sum is equal to one up to a threshold energy associated with the wavepacket overcoming the barrier to reaction and being attenuated by the absorbing boundary condition. Since this work does not consider the $BH + H$ surfaces, it is not possible to create a product Møller state associated with reaction, which necessitates use of ABCs resulting in loss of probability represented in the final sum. Under the assumption that all of the wavepacket that enters the reaction well will react, the deviation of this sum from one represents the probability for reaction.

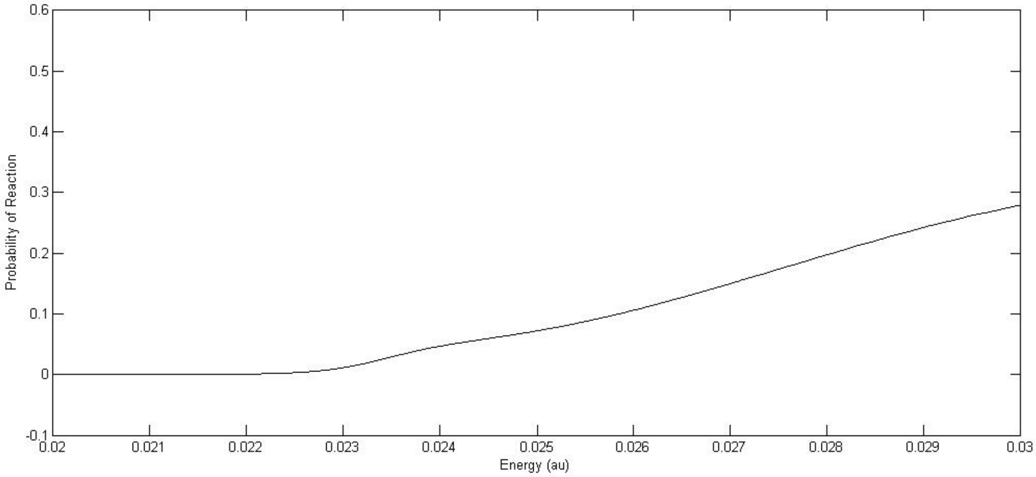

Figure 45. Probability to React to Form *BH+H*

This analysis allows for the prediction that reaction to $BH + H$ will begin to occur with a minimum energy of 0.022 au.

Vibrational Transitions

As expected transitions to higher vibrational eigenstates are not available for energies less than the total internal energies associated with those states. Above $E = 0.03$ au these states become available.

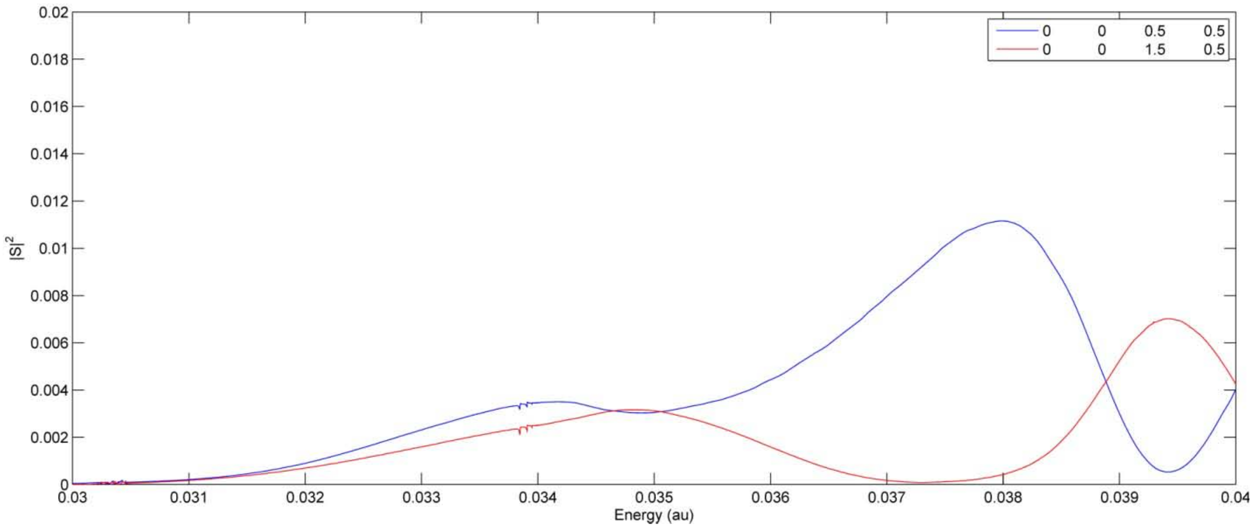

Figure 46. Probability to Transition from $\left|\begin{matrix}0 & \frac{1}{2},0\\ 0 & \frac{1}{2}\end{matrix}\right\rangle$ **to** $\left|\begin{matrix}0 & \frac{1}{2},1\\ 0 & \frac{1}{2}\end{matrix}\right\rangle$ **and** $\left|\begin{matrix}0 & \frac{3}{2},1\\ 0 & \frac{1}{2}\end{matrix}\right\rangle$

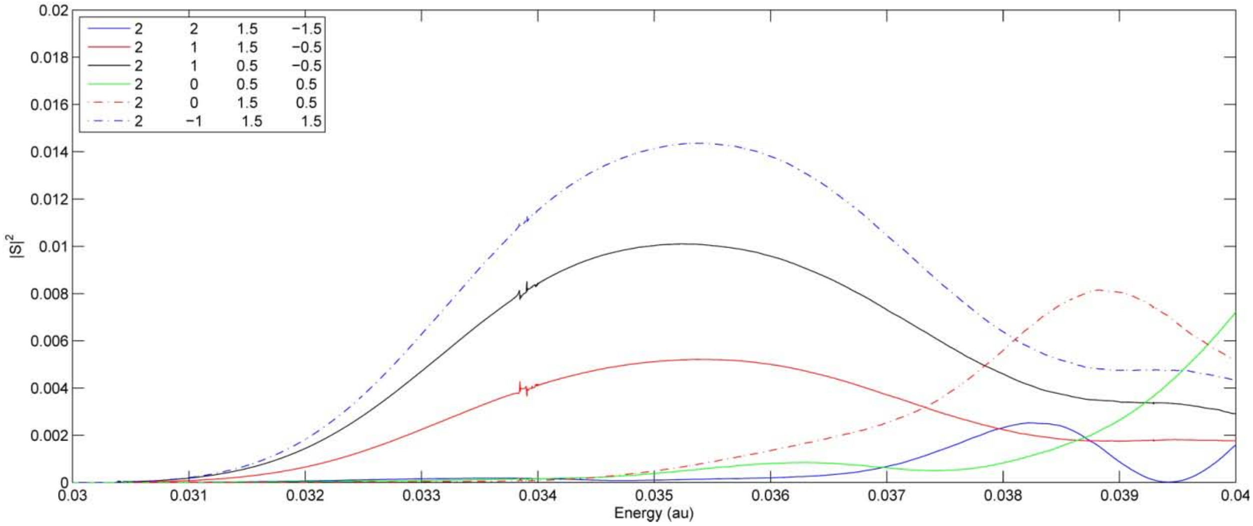

Figure 47. Probability to Transition from $\left|\begin{matrix}0 & \frac{1}{2},0\\ 0 & \frac{1}{2}\end{matrix}\right\rangle$ **to the Six Allowed** $\left|\begin{matrix}2 & j_a,1\\ j & \omega\end{matrix}\right\rangle$ **States**

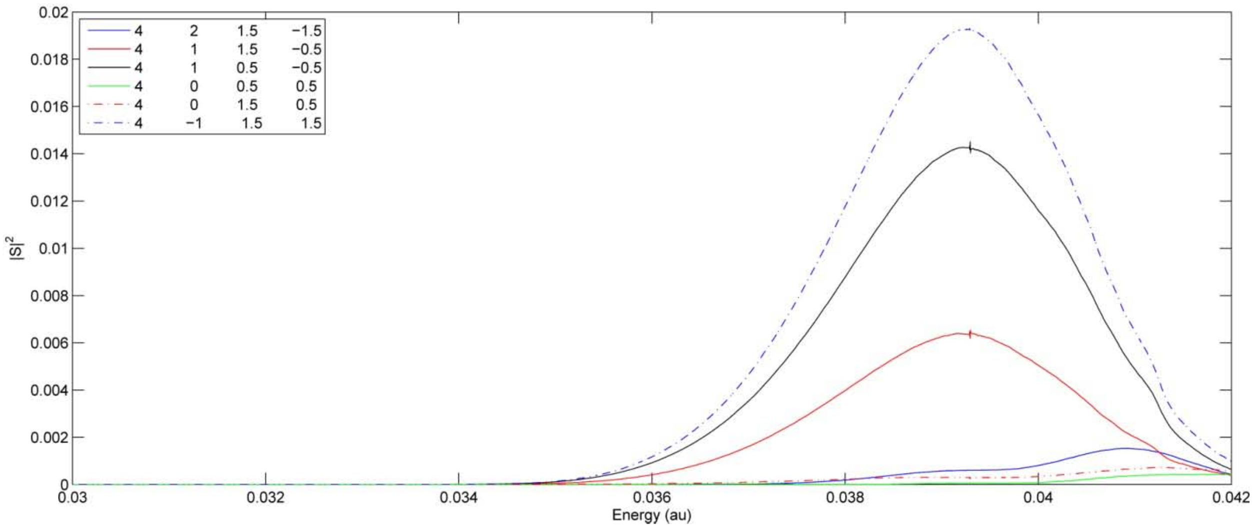

Figure 48. Probability to Transition from $\left|\begin{matrix}0 & \frac{1}{2} \\ 0 & \frac{1}{2}\end{matrix}, 0\right\rangle$ **to the Six Allowed** $\left|\begin{matrix}4 & j_a \\ j & \omega\end{matrix}, 1\right\rangle$ **States**

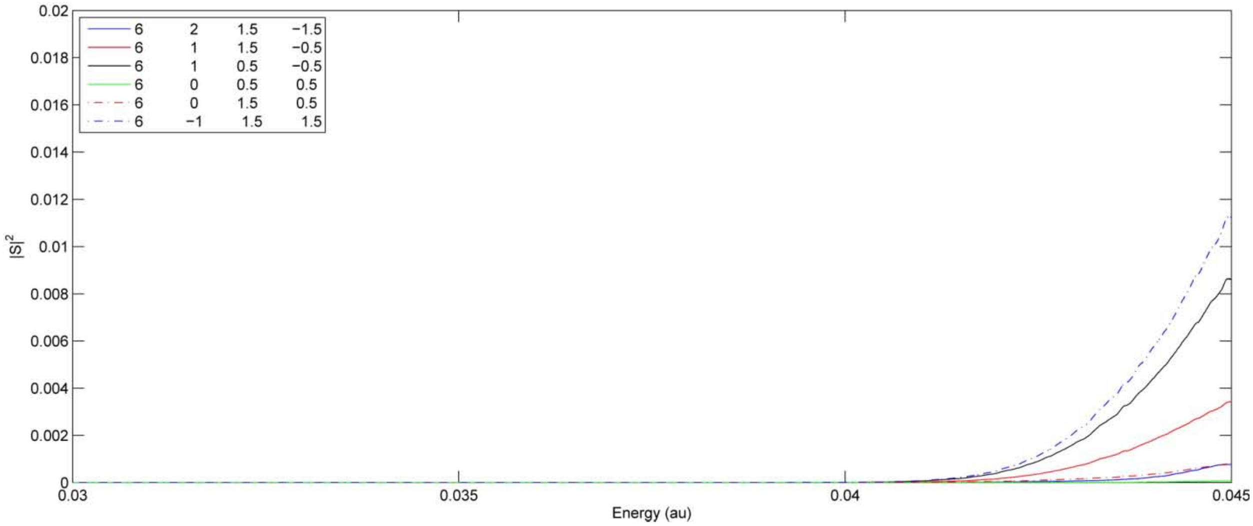

Figure 49. Probability to Transition from $\left|\begin{matrix}0 & \frac{1}{2} \\ 0 & \frac{1}{2}\end{matrix}, 0\right\rangle$ **to the Six Allowed** $\left|\begin{matrix}6 & j_a \\ j & \omega\end{matrix}, 1\right\rangle$ **States**

As expected based on their internal energies, there are no transitions to the $j = 8, v = 1$ or $j = 10, v = 1$ in this energy range. The energies associated with transitions to the higher vibrational eigenstates are at the upper limit of the energies present in the initial wavepacket, so usable data is obtained over a smaller range of energies.

Feshbach Resonances

Portions of the wavepacket that are coupled to higher surfaces have energies near the eigenvalues of the shallow wells on those surfaces. Figure 50 shows the wells for the lowest three adiabatic potential energy surfaces at $r = 1.402$ au .

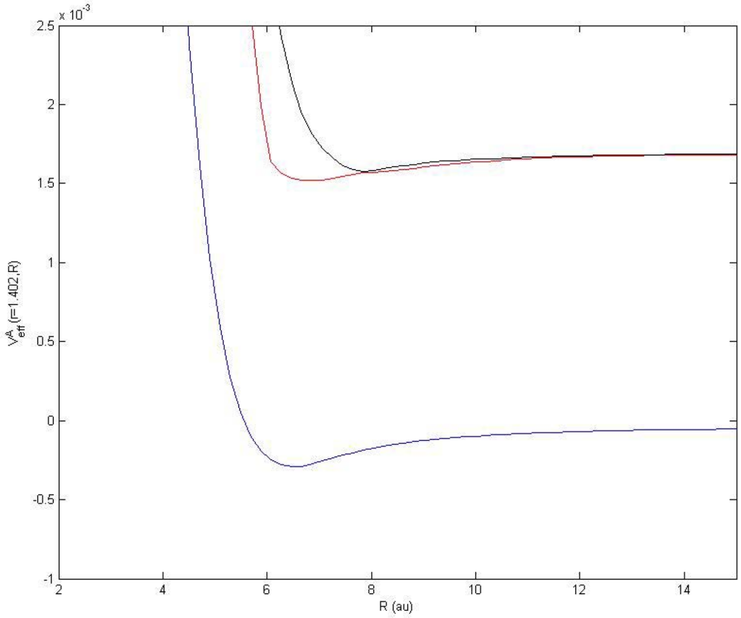

Figure 50. Cross-section of First Three Adiabatic Surfaces at $r = 1.402$ au Showing Shallow Wells

These shallow well potentials cause portions of the wavepacket to be trapped in a quasi-stable state and remain there until they are coupled back down to the lower energy surfaces at which point they will exit the interaction region. This phenomenon results in high amplitude peaks appearing in the scattering matrix elements for those lower surfaces at energies near the eigenstates of the wells of the higher surfaces.

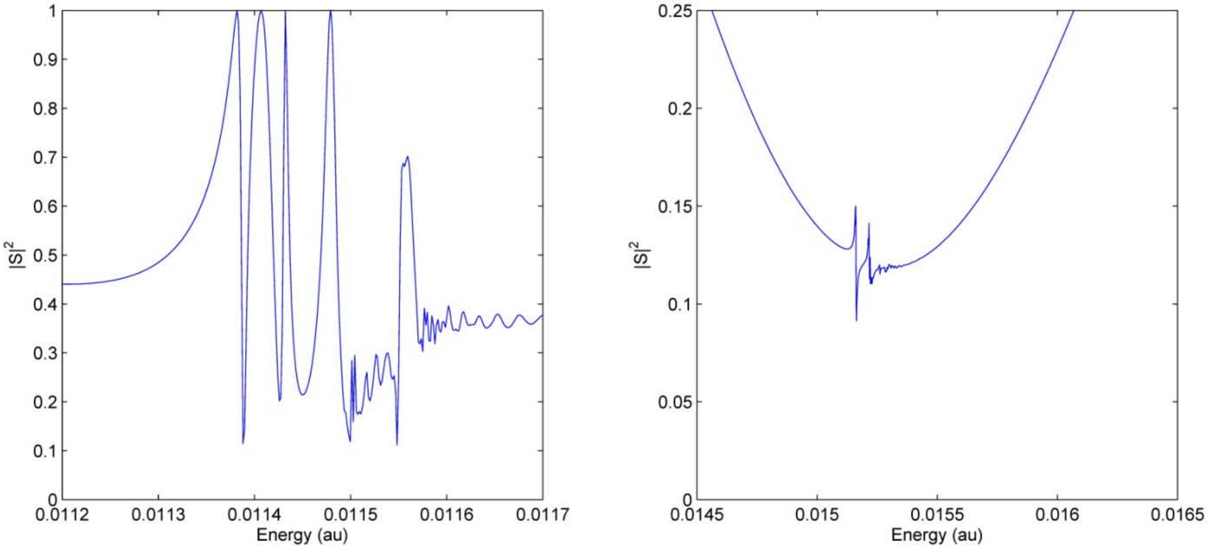

Figure 51. Detail of Feshbach Resonances in Reflection Scattering Matrix Element

These resonances span the energies of the $\left|\begin{matrix}2 & \frac{1}{2}\\ k & \omega\end{matrix}\right\rangle, \left|\begin{matrix}2 & \frac{3}{2}\\ k & \omega\end{matrix}\right\rangle$ states and $\left|\begin{matrix}4 & \frac{1}{2}\\ k & \omega\end{matrix}\right\rangle, \left|\begin{matrix}4 & \frac{3}{2}\\ k & \omega\end{matrix}\right\rangle$, and are offset from the internal energies of those states by a small amount associated with the energy of the shallow potential wells.

Although smaller in magnitude, the $\left|\begin{matrix}0 & \frac{1}{2}\\ 0 & \frac{1}{2}\end{matrix}, v=0\right\rangle \rightarrow \left|\begin{matrix}0 & \frac{1}{2}\\ 0 & \frac{1}{2}\end{matrix}, v=1\right\rangle, \left|\begin{matrix}0 & \frac{3}{2}\\ 0 & \frac{1}{2}\end{matrix}, v=1\right\rangle$ transitions also display Feshbach resonances at the energies associated with the $\left|\begin{matrix}2 & j_a\\ k & \omega\end{matrix}, v=1\right\rangle$ and $\left|\begin{matrix}4 & j_a\\ k & \omega\end{matrix}, v=1\right\rangle$ states (0.0304 au, 0.0339 au).

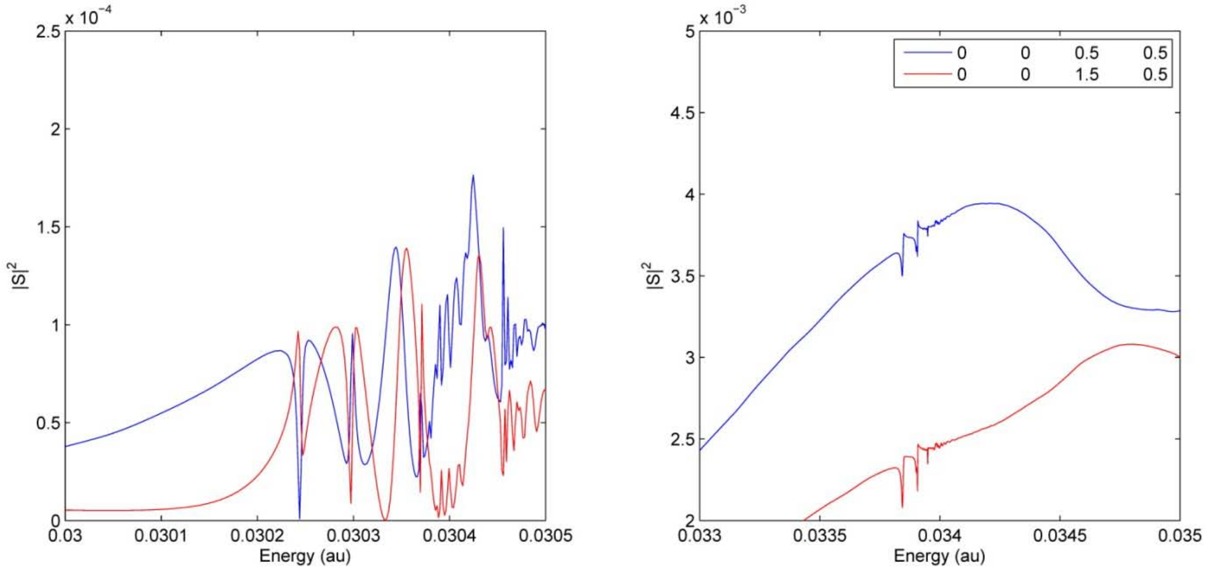

Figure 52. Feshbach Resonance Detail for Transition from $\left|\begin{matrix}0 & \frac{1}{2} \\ 0 & \frac{1}{2}\end{matrix},0\right\rangle$ **to** $\left|\begin{matrix}0 & \frac{1}{2} \\ 0 & \frac{1}{2}\end{matrix},1\right\rangle$ **and** $\left|\begin{matrix}0 & \frac{3}{2} \\ 0 & \frac{1}{2}\end{matrix},1\right\rangle$

Feshbach resonances are also observed in calculations utilizing a one-dimensional propagator. By including the *r* dimension, the resonances now occur at energies that are the eigenvalues of a two-dimensional well. In the region of the shallow potential wells in the *R*-dimension the *r* cross-section is approximately that of the asymptotic H_2 potential.

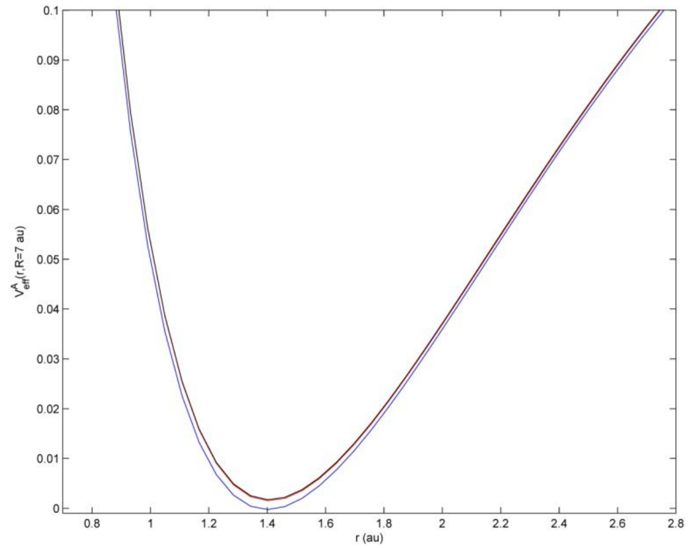

Figure 53. Cross-section of First Three Adiabatic Surfaces at $R = 7$ au

The steepness of the *r* cross-section (this may be quantified, for example, by representing it as a simple harmonic oscillator and examining the spring constant) is a factor of : 10^4 higher than in the *R*-direction. Because of this the two-dimensional well does not offer more quasi-stable states – they are simply offset from zero by approximately the energy of the vibrational ground state. Because of this relative steepness, and due to the fact that in the region of the shallow wells in the *R*-direction, the shape of the Feshbach resonances is not significantly different in the two-dimensional case compared to the one-dimensional case obtained by constraining the molecular bondlength to $r = 1.402$ au.

Because they have distinctive features and are associated with portions of the wavepacket that become trapped and exit the interaction region slowly, the Feshbach resonances provide a useful tool for determining convergence based on total propagation time. Figure 54 shows the Feshbach resonances observed in the scattering matrix element for reflection on the ground state as calculated using various total propatation times $T_{\max}$.

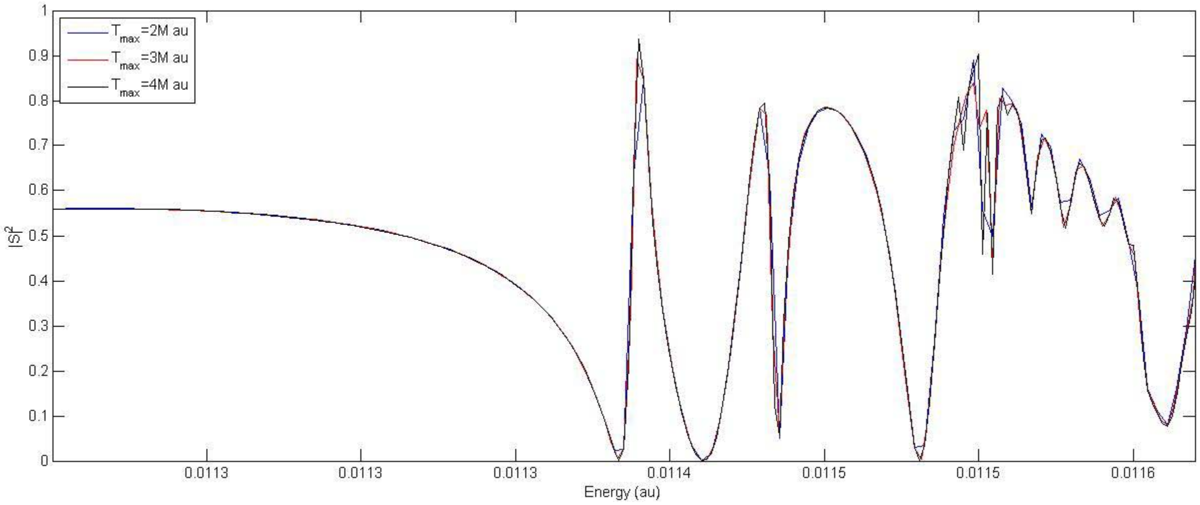

Figure 54. Detail of Feshbach Resonances for $T_{\max} = 2,3,4 \ \times 10^6$ au

Around the sharp peaks of the Feshbach resonances, the line corresponding to $T_{\max} = 2\times 10^6$ au deviates from the other lines. Because the correlation function has a shorter total time its Fourier transform does not have the resolution necessary to capture these features. The agreement between the calculation using $T_{\max} = 3\times 10^6$ au and $T_{\max} = 4\times 10^6$ au indicates the calculation has converged at that total propagation time.

Comparison to One Dimensional Calculation

Previous calculations of the $B+H_2$ scattering matrix elements were done by fixing the molecular bondlength to its equilibrium value $r = 1.402$ au and propagating on the resulting one dimensional potential energy surfaces. Including the *r* degree of freedom changes the scattering matrix elements in several ways. Figure 55 shows a comparison between the one dimensional and two dimensional results for the transitions from $\left|\begin{matrix}0 & \frac{1}{2} \\ 0 & \frac{1}{2}\end{matrix},0\right\rangle$ to $\left|\begin{matrix}0 & \frac{1}{2} \\ 0 & \frac{1}{2}\end{matrix},0\right\rangle$ and $\left|\begin{matrix}0 & \frac{3}{2} \\ 0 & \frac{1}{2}\end{matrix},0\right\rangle$. In these plots the two dimensional results are shifted by the energy of the ground vibrational state in order to make the energy scales the same.

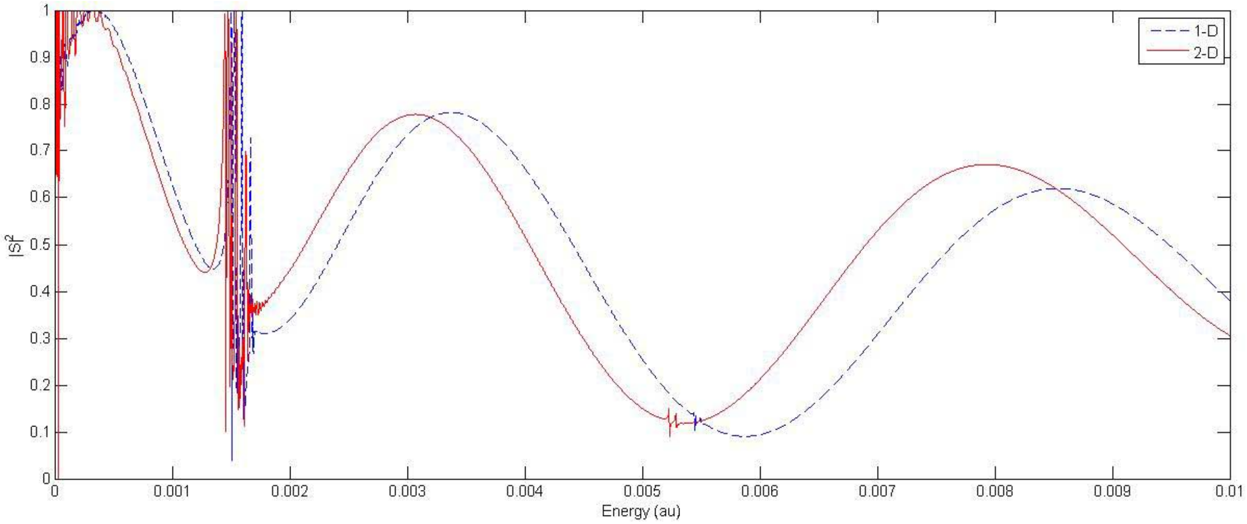

Figure 55. 1-D and 2-D Results for the Transition from $\left|\begin{matrix}0 & \frac{1}{2} \\ 0 & \frac{1}{2}\end{matrix},0\right\rangle$ to $\left|\begin{matrix}0 & \frac{1}{2} \\ 0 & \frac{1}{2}\end{matrix},0\right\rangle$

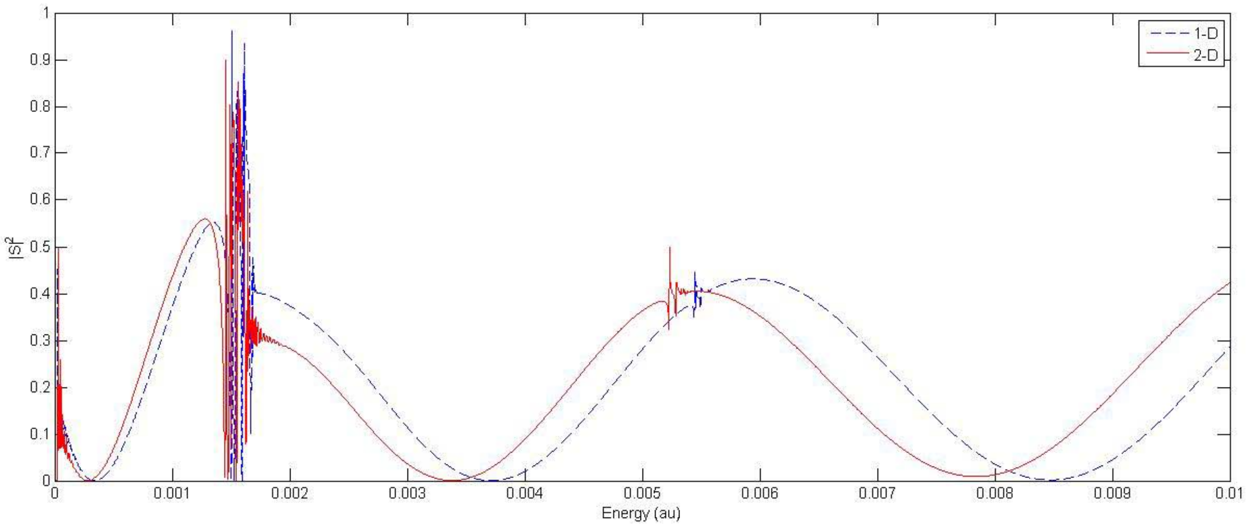

Figure 56. 1-D and 2-D Results for the Transition from $\left|\begin{matrix}0 & \frac{1}{2} \\ 0 & \frac{1}{2}\end{matrix},0\right\rangle$ **to** $\left|\begin{matrix}0 & \frac{3}{2} \\ 0 & \frac{1}{2}\end{matrix},0\right\rangle$

The scattering matrix elements for the one dimensional and two dimensional calculations are very similar with the primary difference being a shift towards lower energies in the two dimensional case. This shift grows larger at higher energies.

The two dimensional potential energy surfaces contain a $\frac{\hbar^2 j\left(j+1\right)}{2\mu_{H_2} r^2}$ term, as seen in eq. (31). Besides providing the rotor energy separation to the surfaces, this term also flattens out the *r*-cross section of the higher surfaces. As a result of this flattening, the ground vibrational energy is slightly lowered on surfaces with higher *j*. For example, the ground vibrational energy on the $j = 2$ surfaces is $\sim 5\times10^{-5}$ au lower than the ground vibrational energy on the $j = 0$ surfaces. This effectively makes the upper surfaces accessible at lower energies, resulting in a shift in the scattering matrix elements. This shift is examined at the first set of Feshbach resonances in the ground state transition.

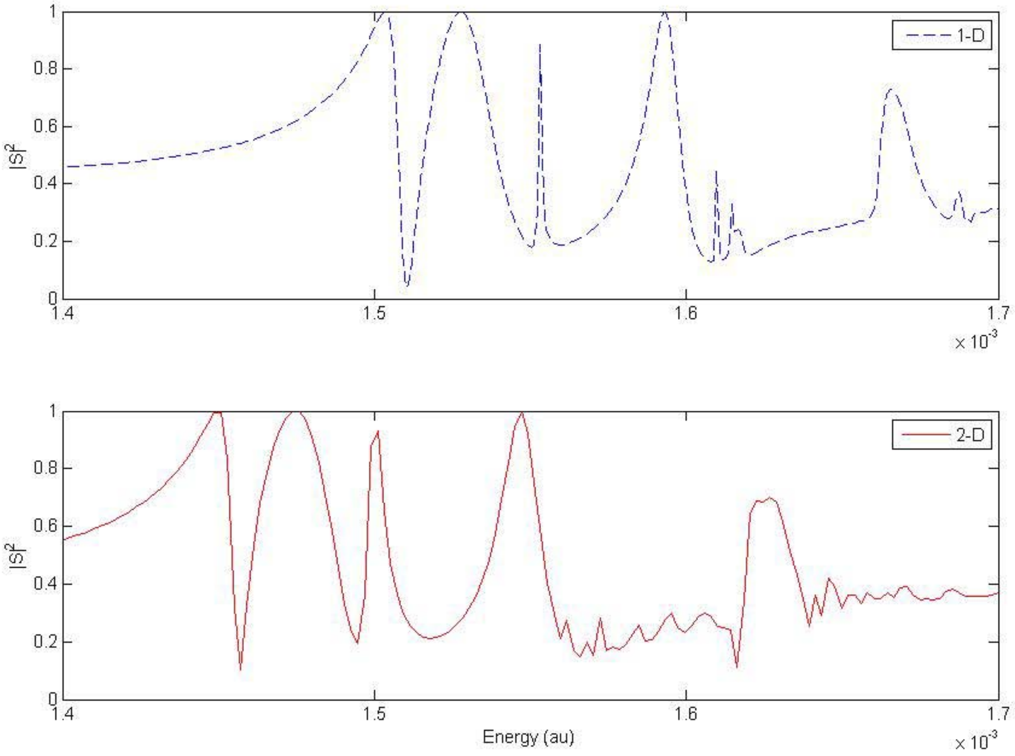

Figure 57. 1-D and 2-D Feshbach Resonances for the Transition from $\left|\begin{matrix}0 & \frac{1}{2} \\ 0 & \frac{1}{2}\end{matrix},0\right\rangle$ **to** $\left|\begin{matrix}0 & \frac{1}{2} \\ 0 & \frac{1}{2}\end{matrix},0\right\rangle$

The Feshbach resonances from the two dimensional calculation are shifted in energy by ∶ 5×10^{-5} au as predicted. While their structure is qualitatively the same, the two dimensional calculation yields additional low amplitude features. This is also seen in the Feshbach resonances in the fine structure transition.

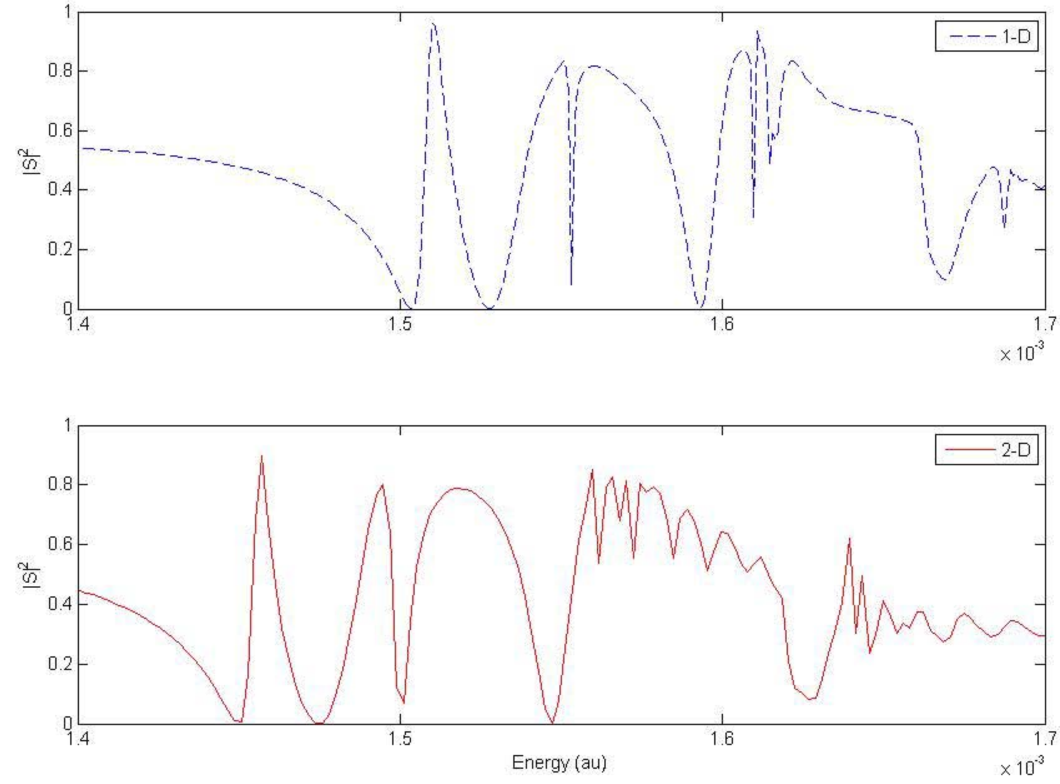

Figure 58. 1-D and 2-D Feshbach Resonances for the Transition from $\left|\begin{matrix}0 & \frac{1}{2},0\\ 0 & \frac{1}{2}\end{matrix}\right\rangle$ **to** $\left|\begin{matrix}0 & \frac{3}{2},0\\ 0 & \frac{1}{2}\end{matrix}\right\rangle$

IV. Conclusion

Coupling between different degrees of freedom presents a challenge when modeling the dynamics of atomic and molecular collisions. The collision of boron and molecular hydrogen is an example of a system in which this nonadiabatic behavior plays a key role. This work models the dynamics of $B+H_2$ as they collide and calculates for a range of energies the probability of changes to the molecule's rotational and vibrational state as well as the electronic fine-structure transition of the single open shell electron in boron.

Garvin [1] obtained the effective potential energy surfaces for $B+H_2$ by combining the system's rotational energy with the adiabatic electronic potential energy surfaces calculated by Yarkony and representing the result in an angular momentum basis. These effective PES are two-dimensional in *r*, the H_2 bondlength, and *R*, the distance from the boron atom to the H_2 center of mass. As a result of the angular momentum basis chosen these surfaces are labeled by the angular momentum quantum numbers. The PES are coupled, allowing a wavepacket initially on a single surfaces to transition to multiple surfaces. Since there are an infinite number of rotational states there are an infinite number of coupled PES. For practical considerations only those surfaces which are energetically accessible are considered. In this work only values of total angular momentum $J=1/2$ are considered, and the projection of *J* onto the body fixed *z*-axis, labeled *P*, is assumed to be constant under the centrifugal sudden approximation.

Wavepackets are propagated on these surfaces using a split-operator propagator which approximates the time-evolution operator for small time steps. Initially a wavepacket is located on a single PES. This wavepacket is chosen to be an eigenstate of the asymptotic Hamiltonian and is referred to as the reactant Møller state. As it is propagated forward in time it enters the interaction region and is coupled to the other surfaces so that it then exits the interaction region on all of the surfaces. At every point in time the correlation function is calculated between the evolving state and a product state located in the asymptotic limit of each PES. The Fourier transform of these correlation functions can be used to calculate scattering matrix elements using the channel packet method. The absolute value squared of the scattering matrix elements is the probability that as a result of the collision the system will transition from the state described by the reactant wavepacket to a state described by the product wavepacket.

Table 3. Summary of Steps for Calculating Scattering Matrix Elements

1.	Obtain electronic adiabatic PES for $B+H_2$ (Yarkony)
2.	Obtain effective diabatic PES for $B+H_2$ (Garvin)
3.	Numerically determine eigenstates and eigenvalues for each PES in asymptotic limit
4.	Define reactant Møller state on ground state and product Møller states (representing both the $v=0,1$ vibrational levels) on each PES
5.	Propagate reactant Møller state forward in time
6.	Calculate the correlation function between the reactant Møller state and each of the product Møller states (over all time for which it is nonzero)
7.	Calculate the scattering matrix elements using the channel packet method (eq. (89))

The scattering matrix elements exhibit broad oscillatory behavior with rapidly oscillating Feshbach resonances associated with energies of the quasi-stable states of the upper surfaces. Compared to a calculation requiring $r = 1.402$ au the scattering matrix elements are shifted towards lower energies consistent with the lowering of the vibrational energies as the rotational energy increases. Including the *r* degree of freedom also has the important result of allowing the reaction to $BH + H$, which is observed for energies beginning with 0.022 au. Finally, considering the *r* degree of freedom allows for calculation of scattering matrix elements for transitions involving changes to the vibrational eigenstate.

Summary of Key Contributions

This work extends the channel packet method to include treatment of nonadiabatic systems in which the reaction dynamics are described by potential energy surfaces that are two dimensional. This results in a calculation based on fewer unphysical constraints and allows for the consideration of changes of eigenstates associated with new degrees of freedom, as well as capturing important reaction dynamics which may not otherwise be predicted.

This work implements this methodology for the collision of $B + H_2$, resulting in transition probabilities for changes to the boron electronic fine structure and the rotational and vibrational eigenstates of the H_2 molecule as a result of the collision. It also allows a prediction that reaction $B + H_2 \rightarrow BH + H$ will begin to occur at a total energy of 0.022 au.

Recommendations for Future Work

By extending the effective potential energy surfaces to include values of total angular momentum *J* greater than 1/2 total scattering cross-sections may be calculated and used to predict reaction rates.

The potential energy surfaces could also be extended to include states for which there is a change in the projection of the total angular momentum onto the body fixed *z*-axis (*P*). This would allow the computation to be done without invoking the centrifugal sudden approximation.

Calculating the *BH* + *H* potential energy surfaces would allow propagation on these surfaces and allow for calculation of scattering events at higher energies without requiring the assumption that any portion of the wavepacket that crosses the barrier to reaction seen on the lowest adiabatic PES will react completely.

Bibliography

[1] M.B. Garvin, The Effective Potential Energy Surfaces of the Nonadiabatic Collision of Boron and Molecular Hydrogen, 2009, Doctoral Dissertation, Air Force Institute of Technology.

[2] D. E. Weeks and D. J. Tannor, "A time-dependent formulation of the scattering matrix using Møller operators," *Chemical Physics Letters*, pp. 301-308, 1993.

[3] M. E. Fajardo, S. Tam, T. L. Thompson, and M. E. Cordonnier, "Spectroscopy and reactive dynamics of atoms trapped in molecular hydrogen matricies," *Chemical Physics 189*, pp. 351-365, 1994.

[4] D.R. Yarkony, "Current Issues in Nonadiabatic Chemistry," *Journal of Chemical Physics*, vol. 100, 1996.

[5] T.J. Tague and L. Andrews, "Reactions of Pulsed-Laser Evaporated Boron Atoms with Hydrogen. Infrared Spectra of Boron Hydride Intermediate Species in Solid Argon," *J. Am. Chem. Soc.*, vol. 116, no. 11, pp. 4970-4976, 1994.

[6] M.H. Alexander, "Adiabatic and approximate diabatic potential energy surfaces for the B.H2 van der Waals molecule," *Journal of Chemical Physics*, vol. 99, no. 8, pp. 6014-6026, 1993.

[7] M.H. Alexander and M. Yang, "Theoretical investigation of weakly-bound complexes of B with H2," *Journal of Chemical Physics*, vol. 103, no. 18, 1995.

[8] W. F. Krupke, R. J. Beach, S. A. Payne, V. K. Kanz, and J. T. Early, "DPAL: A New Class of Lasers for CW Power Beaming at Ideal Photovoltaic Cell Wavelengths," , Sendai, Japan, 2003.

[9] A. Szabo and N. Ostlund, *Modern Quantum Chemistry: Introduction to Advanced Electronic Structure Theory*. New York: Dover, 1996.

[10] D. R. Yarkony, *Conical Intersections: Electron Structure, Dynamcis, & Spectroscopy*. Singapore: World Scientific, 2004.

[11] M.A. Morrison, T.L. Estle, and N.F. Lane, *Quantum States of Atoms, Molecules and Solids*.: Prentice-Hall, Inc., 1976.

[12] R. Cimiraglia and M. Persico, "The Evaluation of Nonadiabatic Matrix Elements," *Chemical Physics*, vol. 53, pp. 357-363, 1980.

[13] W. Lichten, "Resonant Charge Exchange in Atomic Collisions," *Physical Review*, vol. 131, pp. 229-238, 1963.

[14] F.T. Smith, "Diabatic and Adiabatic Representations for Atomic Collision Problems," *Physical Review*, vol. 179, pp. 111-123, 1969.

[15] M Baer, "Adiabatic and Diabatic Representations for Atom-Molecule Collisions: Treatment of the Colinear Arrangement," *Chemical Physics Letters*, vol. 35, pp. 112-118, 1975.

[16] D. E. Weeks, T. A. Niday, and S. H. Yang, "Inelastic scattering matrix elements for the nonadiabatic collision," *Journal of Chemical Physics*, vol. 125, no. 164301, 2006.

[17] M.L. Dubernet and J.M. Hutson, "Atom-molecule van der Waals complexes containing open-shell atoms," *Journal of Chemical Physics*, vol. 101, no. 3, pp.

1939-1958, 1994.

[18] R. T. Pack, "Space-fixed vs. body-fixed axes in atom-diatomic molecular scattering. Sudden approximations.," *Journal of Chemical Physics*, vol. 60, no. 2, 1974.

[19] R. L. Liboff, *Introductory Quantum Mechanics*. San Francisco: Addison Wesley, 2003.

[20] C. Leforestier et al., "A Comparison of Different Propagation Schemes for the Time-Dependent Schrödinger Equation," *Journal of Computational Physics*, pp. 59-80, 1991.

[21] J. Alvarellos and H. Metiu, "The evolution of the wave function in a curve crossing problem computed by a fast Fourier transform method," *Journal of Chemical Physics*, vol. 88, pp. 4957-4966, 1988.

[22] W. H. Press, B. P. Flannery, S. A. Teukolsky, and W. T. Vetterling, *Numerical Recipies in C*. Cambridge: Cambridge University Press, 1988.

[23] J. R. Taylor, *Scattering Theory: The Quantum Theory of Nonrelativistic Collisions*.: John Wiley & Sons, Inc., 1972.

[24] R.S. Calfas and D.E. Weeks, "A new application of absorbing boundary conditions for computing collinear quantum reactive scattering matrix elements," *Chemical Physics Letters 263*, pp. 292-296, 1996.

[25] P., Lui, B. Siegbahn, *The Journal of Chemical Physics*, vol. 68, p. 1794, 1978.

[26] D. G., Horowitz, C.J. Truhlar, *The Journal of Chemical Physics*, vol. 68, p. 2466.

[27] M.S. Child, *Atom-Molecule Collision Theory: A Guide for the Experimentalist*, R.B. Bernstein, Ed. New York: Plunum, 1979.

[28] M.S. Child, *Molecular Collision Theory*.: Dover Publications, 1974.

[29] M.H. Alexander, "Adiabatic and approximate diabatic potential energy surfaces for the B.H2 van der Waals molecule," vol. 99, no. 8, 1993.

[30] T.J. Tague and L. Andrews, "Reactions of Pulsed-Laser Evaporated Boron Atoms with," vol. 116, no. 11, 1994.

Vita

Capt Luke Barger graduated from Newbury Park Adventist Academy in 1996. He received a Bachelor of Science degree in mechanical engineering from Walla Walla College in 2000 and a Master of Science degree in Aeronautics and Astronautics from Stanford University in 2001.

After being commissioned in the United States Air Force in 2003 he was stationed at the Space and Missile Systems Center at Los Angeles Air Force Base. There he work on both the Titan and Delta launch vehicle programs performing booster/payload integration. Upon graduation he will be assigned to the National Reconnaissance Office.

REPORT DOCUMENTATION PAGE

Form Approved
OMB No. 074-0188

1. REPORT DATE *(DD-MM-YYYY)* 16-12-2010	**2. REPORT TYPE** Doctoral Dissertation	**3. DATES COVERED** *(From – To)* Sep 2007 – Sep 2010

4. TITLE AND SUBTITLE

The Scattering Matrix Elements of the Nonadiabatic Collision
$B\left({}^2P_{j_a}\right)+H_2\left({}^1\Sigma_g^+,\nu,j\right)\leftrightarrow B\left({}^2P_{j_a'}\right)+H_2\left({}^1\Sigma_g^+,\nu',j'\right)$.

5a. CONTRACT NUMBER

5b. GRANT NUMBER

5c. PROGRAM ELEMENT NUMBER

6. AUTHOR(S)

Barger, Luke A.
Captain, USAF

5d. PROJECT NUMBER

5e. TASK NUMBER

5f. WORK UNIT NUMBER

7. PERFORMING ORGANIZATION NAMES(S) AND ADDRESS(S)

Air Force Institute of Technology
Graduate School of Engineering and Management (AFIT/EN)
2950 Hobson Way
WPAFB OH 45433-7765

8. PERFORMING ORGANIZATION REPORT NUMBER

AFIT/DS/ENP/10-S02

9. SPONSORING/MONITORING AGENCY NAME(S) AND ADDRESS(ES)
AFSOR (AFMC)
ATTN: Dr. Michael R. Berman
875 North Randolph Street, Suite 325, Room 3112
Arlington, Va., 22203-1768 DSN: 426-7781

10. SPONSOR/MONITOR'S ACRONYM(S)

11. SPONSOR/MONITOR'S REPORT NUMBER(S)

12. DISTRIBUTION/AVAILABILITY STATEMENT
APPROVED FOR PUBLIC RELEASE; DISTRIBUTION UNLIMITED

13. SUPPLEMENTARY NOTES

14. ABSTRACT

Scattering matrix elements are calculated for the nonadiabatic inelastic collision $B\left({}^2P_{j_a}\right)+H_2\left({}^1\Sigma_g^+,\nu,j\right)\leftrightarrow B\left({}^2P_{j_a'}\right)+H_2\left({}^1\Sigma_g^+,\nu',j'\right)$. This calculation utilizes the effective potential energy surfaces for this collision generated by Garvin along with a correction to the asymptotic H_2 potential. Wavepackets are propagated on these surfaces using a split-operator propagator. This propagation yields correlation functions between reactant and product Møller states which are used to calculate the scattering matrix elements with the channel packet method. These scattering matrix elements represent probability amplitudes for the collision to result in changes to the electronic fine structure and to the rotational and vibrational eigenstates of the H_2 molecule over a range of energies, and are presented, discussed and compared to previous work in which the hydrogen bond length was fixed at its equilibrium value. A method for approximating probability for the reaction $B+H_2\rightarrow BH+H$ as a function of collisional energy is presented.

15. SUBJECT TERMS
Quantum Mechanics, Inelastic Scattering, Channel Packet Method, Nonadiabatic Collision

16. SECURITY CLASSIFICATION OF:			**17. LIMITATION OF ABSTRACT**	**18. NUMBER OF PAGES**	**19a. NAME OF RESPONSIBLE PERSON**
					Dr. David Weeks, AFIT/ENP
a. REPORT	**b. ABSTRACT**	**c. THIS PAGE**			**19b. TELEPHONE NUMBER** *(Include area code)*
U	U	U	UU	132	(937) 255-3636x4561 david.weeks@afit.edu